INTERNATIONAL ATOMIC ENERGY AGENCY
UNITED NATIONS EDUCATIONAL, SCIENTIFIC AND CULTURAL ORGANIZATION

INTERNATIONAL CENTRE FOR THEORETICAL PHYSICS
34100 TRIESTE (ITALY) - P.O.B. 586 - MIRAMARE - STRADA COSTIERA 11 - TELEPHONE: 9240-1
CABLE: CENTRATOM - TELEX 460392-1

SMR/459- 14

SPRING COLLEGE IN CONDENSED MATTER
ON
'PHYSICS OF LOW-DIMENSIONAL STRUCTURES'
(23 April - 15 June 1990)

ELECTRONS IN SUPERLATTICES

Gottried H. DÖHLER
Universität Erlangen-Numberg
Institut Für Technische Physik
Erwin-Rommel-Strasse 1
Erlangen 8520
Federal Republic of Germany

These are preliminary lecture notes, intended only for distribution to participants.

Electrons in Superlattices

1. Electronic band structure of s.l.'s
   a) in compositional superlattices
   b) in doping superlattices (n-i-p-i's)

2. Dynamics of electrons in s.l.'s
   Bloch oscillations
   Wannier-Stark ladder
   Intersubband transitions
   Interaction with phonons, impurities and photons
   Space charge effects

3) Interband transitions in s.l.'s
   Dipole matrix elements in typI, type II and nipi s.l.'s
   Franz-Keldysh-effect
   Quantum confined Stark effect

4) Magnetic field effects on electrons in superl.'s
   mainly wave function tuning by $B_{\parallel}$ and $B_{\perp}$

5) Impurity states and impurity bands in s.l.'s
   2-d imp. bands
   diagonal and off-diagonal disorder
   δ-doped n-i-p-i structures
   Metal-insulator transitions (Mott-Anderson, Mott-Hubb

compositional superlattice

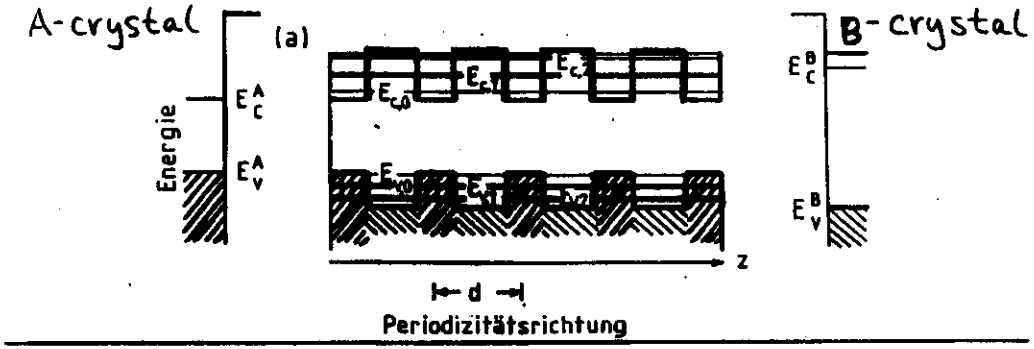

n-i-p-i doping superlattice

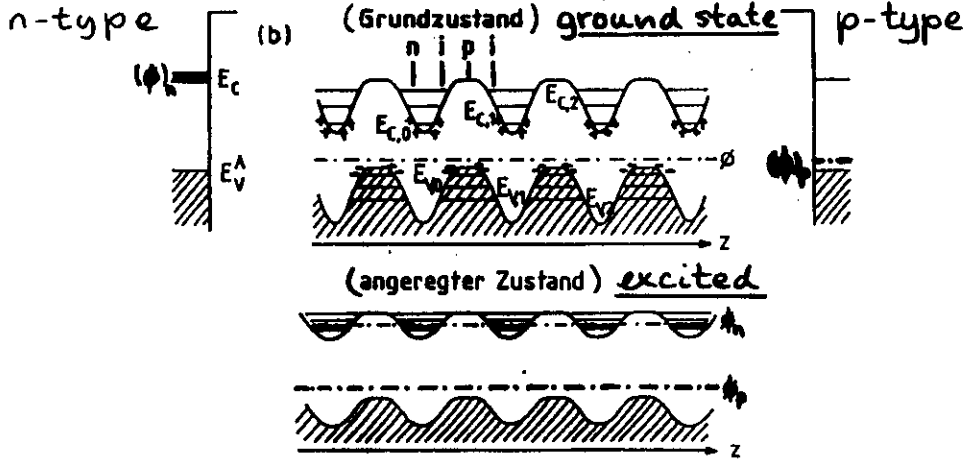

Effect of the Periodic Potential on the Electronic States in a Superlattice

a) NFE - Model

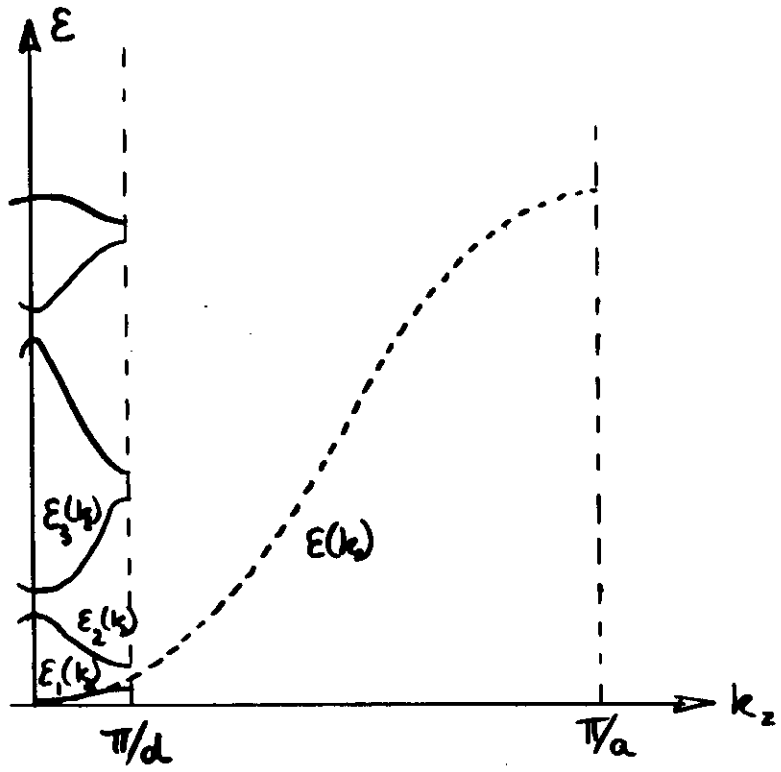

$-\pi/a < k_z \leq \pi/a \Longrightarrow \underbrace{-\pi/d < k_z \leq \pi/d}; \nu$

Reduction of B.Z.

Splitting into mini-bands

Electronic states in a superlattice

(Tight binding model)

I) Single potential well

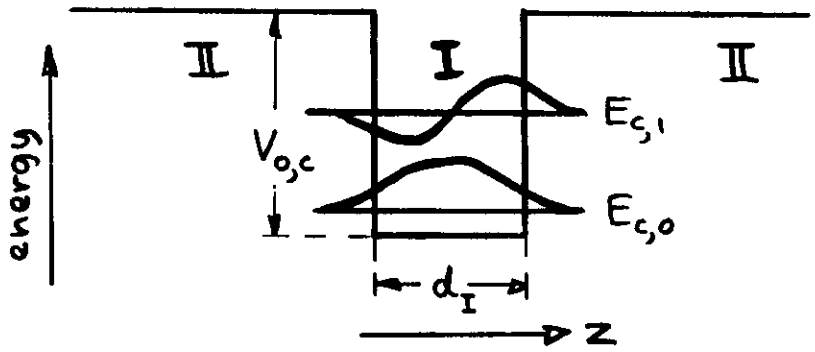

1) Quantization of motion in z direction $\rightarrow E_{c,\nu}$

2) Free motion parallel to the layer with kinetic energy $\approx \hbar^2 k_{\parallel}^2 / 2m_c$

$\Rightarrow$

2-D subbands : $\varepsilon_{c,\nu}(\vec{k}_{\parallel}) = E_{c,\nu} + \hbar^2 k_{\parallel}^2 / 2m_c$

position of $E_{c,\nu}$ depends on d_I and $V_{c,}$

Schrödinger equ. for semicond. Q.W.

$$\left(\underbrace{\frac{p^2}{2m}+V_0(\vec{r})}_{H_0(\vec{r})}+\underbrace{V(z)}_{\text{Q.W.}}\right)\phi_{c,\nu}(\vec{k}_{\parallel},\vec{r})=\mathcal{E}_{c,\nu}(\vec{k}_{\parallel})\phi_{c,\nu}(\vec{k}_{\parallel},\vec{r})$$

effective mass approximation:

$$\phi_{c,\nu}(\vec{k}_{\parallel},\vec{r})\simeq \xi_{c,\nu}(z)\,e^{i\vec{k}_{\parallel}\vec{r}}\,u_{c,\vec{k}=0}(\vec{r})$$

$$\mathcal{E}_{c,\nu}(\vec{k}_{\parallel})=E_{c,\nu}+\frac{\hbar^2}{2m_c}k_{\parallel}^2$$

$$\left(-\frac{\hbar^2}{2m_c}\frac{d^2}{dz^2}+V(z)\right)\xi_{c,\nu}(z)=E_{c,\nu}\,\xi_{c,\nu}(z)$$

$$V(z)=\begin{cases}0; & |z|<\frac{d_I}{2}\\ \Delta E_c; & |z|>\frac{d_I}{2}\end{cases}\Bigg\}\;\xi(z)=\begin{cases}a\cos kz; & \nu \text{ even}\\ b\sin kz; & \nu \text{ odd}\\ c\,e^{-\kappa|z|}\end{cases}$$

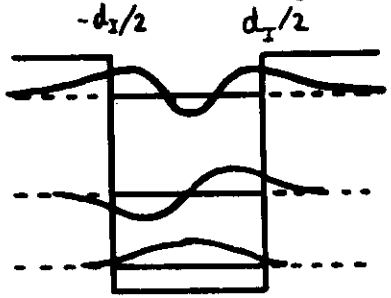

boundary conditions at $z=\pm d_I/2$:

$\xi(z)$ = continuous

$\frac{1}{m_c}\frac{\partial\varphi}{\partial z}$ = continuous

$$k^2=\frac{2m_I}{\hbar^2}E \qquad \kappa^2=\frac{2m_{II}}{\hbar^2}(\Delta E_c-E)$$

$\Delta E_c\to\infty$: $E_{c,\nu}^{\infty}=\frac{\hbar^2}{2m_I}\left(\frac{\pi}{d_I}\right)^2(\nu+1)^2$

Example: GaAs: $m_I=0.067\,m$

For $d_I=100\,\text{Å}$

$E_{c,\nu}^{\infty}\simeq 50\,\text{meV}\,(\nu+1)^2$ $\left(\leftrightarrow \Delta E_c^{Al_{0.3}Ga_{0.7}As/GaAs}\simeq 300\,\text{meV}\right)$

$$E=\frac{\hbar^2k_I^2}{2m_I}\;;\quad \Delta E_c=\frac{\hbar^2k_{I,II}^2}{2m_I}$$

$$\Delta E_c-E=\frac{\hbar^2\kappa_{II}^2}{2m_{II}}=\frac{\hbar^2}{2m_I}\left(k_{I,II}^2-k_I^2\right)$$

$$\left.\begin{array}{l}\frac{k_I}{m_I}\,\text{tg}(k_Id_I/2)\\ -\frac{k_I}{m_I}\,\text{ctg}(k_Id_I/2)\end{array}\right\}=\frac{\kappa_{II}}{m_{II}}=\frac{(k_{I,II}^2-k_I^2)^{1/2}}{(m_Im_{II})^{1/2}}$$

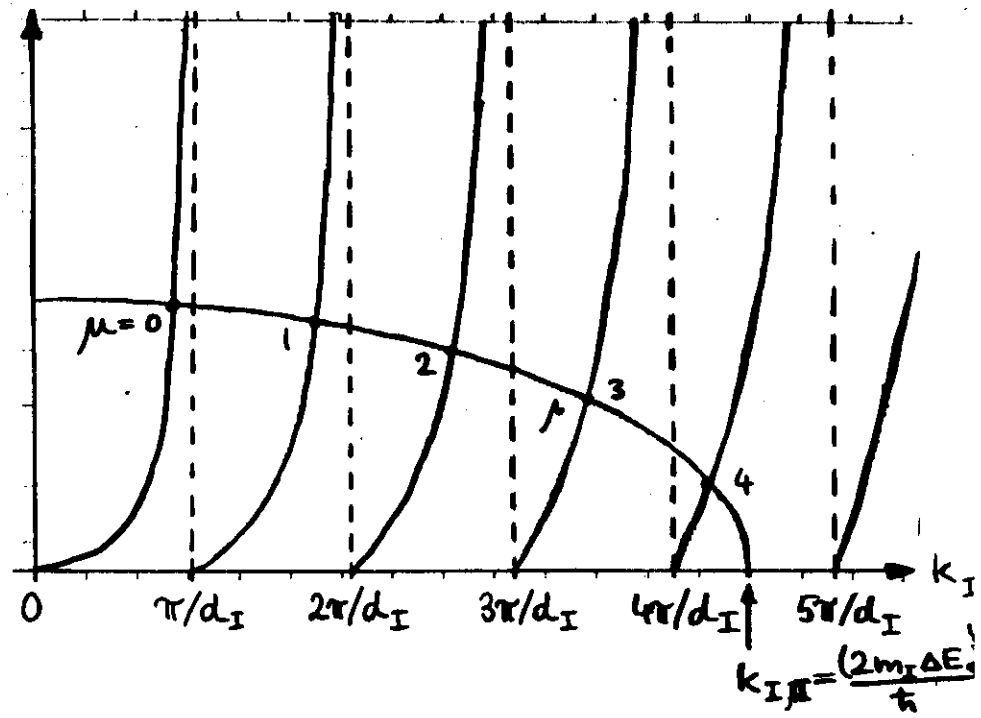

$$E_\mu=\frac{\hbar^2}{2m_I}k_{I,\mu}^2 \qquad \left(\to\frac{\hbar^2}{2m_I}\left((\mu+1)\pi/d_I\right)^2;\ \text{if } k_{I,II}\to\infty\right)$$

At least: one bound state for $k_{I,II}\to 0$

II) Superlattice

(periodic repetition of pot. wells)

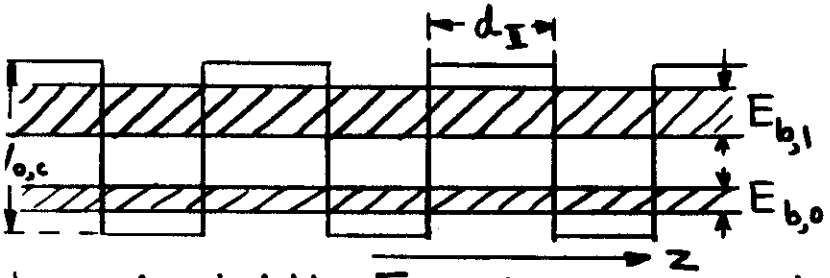

bandwidth $E_{b,\nu}$ depends on d_I and $V_{0,c}$

- **Electronic structure may be tailored**

Design parameters (Example $GaAs$-$Al_xGa_{1-x}As$)

x ⟶ barrier heights $V_{0,c}$

$d_{GaAs}, V_{0,c}$ ⟶ subband spacing

$d_{Al_xGa_{1-x}As}, V_{0,c}$ ⟶ subband width

"atom" (1-d)

$$\left(\frac{p^2}{2m_c} + v_a(z)\right) \varphi_{a\mu}(z) = E_\mu \varphi_{a\mu}(z)$$

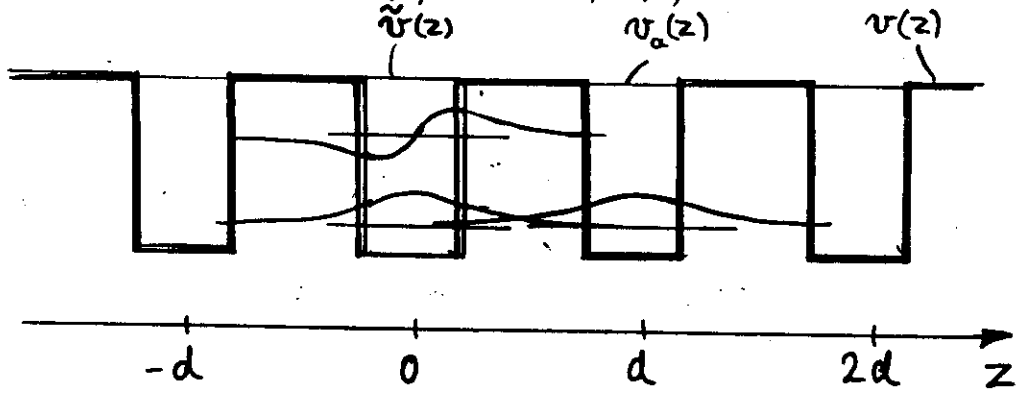

"crystal" (1-d)

$$v(z) = \sum_m v_a(z - md) = v_a(z) + \underbrace{v(z) - v_a(z)}_{\tilde{v}(z)}$$

$$\left(\frac{p^2}{2m_c} + v(z)\right) \varphi_{m,k}(z) = \mathcal{E}_m(k) \varphi_{m,k}(z)$$

LCAO-ansatz:

$$\varphi_{m,k}(z) = \sum_{\nu=0}^{\infty} c_{m\nu}(k) \underbrace{\sum_{m=-N/2}^{N/2} e^{ikmd} \varphi_{a\nu}(z - md)}_{\chi_{\nu,k}(z)}$$

$\mathcal{E}_m(k)$, $c_{m\nu}(k)$ from:

$$\det \left| H_{\mu\nu,k} - \mathcal{E}\,\delta_{\mu\nu} \right| = 0 \; ; \; H_{\mu\nu,k} = \langle \chi_{\mu,k} | H | \chi_{\nu,k} \rangle$$

nearest neighbor tight bind. appr.: $\nu = m$; $m = -1, 0, 1$

$$\mathcal{E}_m(k) = E_m + 2E_{m,m} + 2V_{m,m} \cos kd$$

exact band width from "counting of modes"

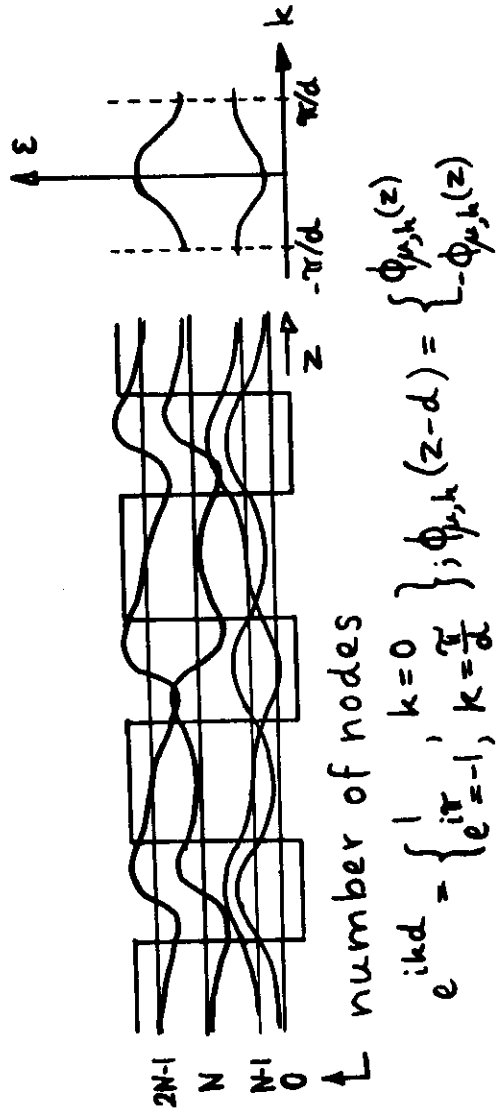

Numerical Solution for Quantum Wells and superlattices

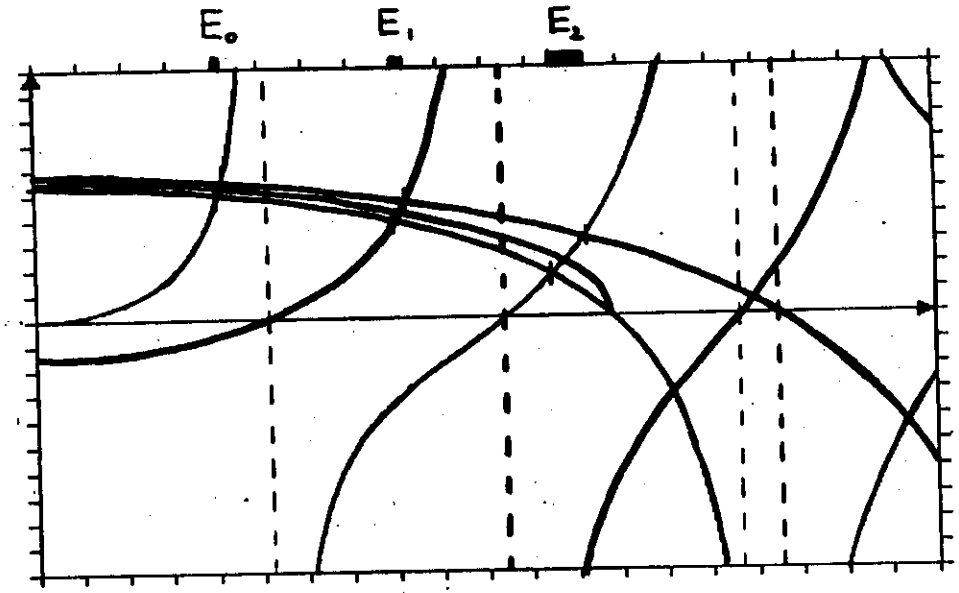

$$\left.\begin{matrix} \frac{k^A}{m^A}\,tg(k^A d^A/2) \\ -\frac{k^A}{m^A}\,ctg(k^A d^A/2) \end{matrix}\right\} = \begin{cases} \begin{cases} \frac{k^B}{m^B}\,th\,\frac{k^B d^B}{2}; & \varepsilon<0 \\ -\frac{k^B}{m^B}\,tg\,\frac{k^B d^B}{2}; & \varepsilon>0 \end{cases} & \text{upper band edge} \\ \begin{cases} \frac{k^B}{m^B}\,ctg\,\frac{k^B d^B}{2}; & \varepsilon<0 \\ \frac{k^B}{m^B}\,ctg\,\frac{k^B d^B}{2}; & \varepsilon>0 \end{cases} & \text{lower band edge} \end{cases}$$

$$\frac{k^B}{m^B} = \frac{(k_0^2 - k^{A2})^{1/2}}{(m_A m_B)^{1/2}} = \frac{ik^B}{m^B}$$

$$E = -\Delta E + \frac{\hbar^2}{2m_A}(k^A)^2$$

Compositional Superlattice

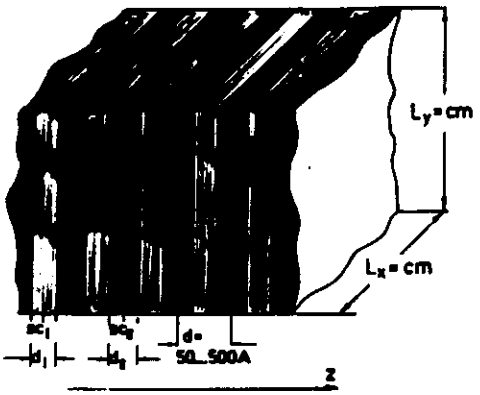

Superlattice Potential

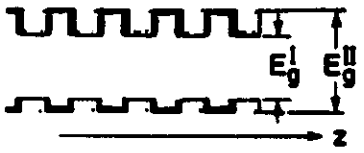

Doping Superl. ("n-i-p-i")

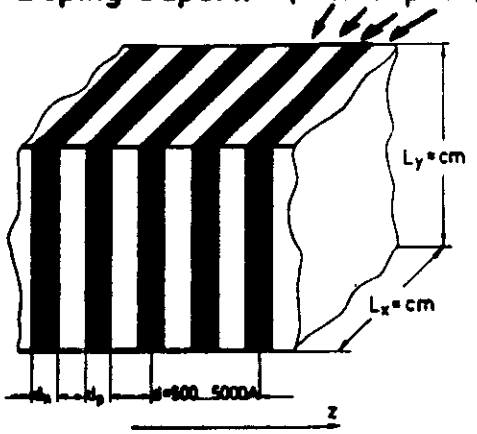

homogeneous semicond.

$(n_D, n_A) < 10^{-4} n_{at.}$

Superlattice potential

doping profile

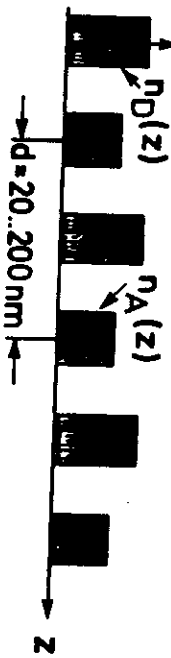

band scheme

a) neutral impurities

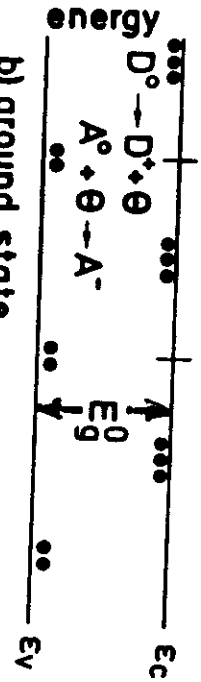

b) ground state

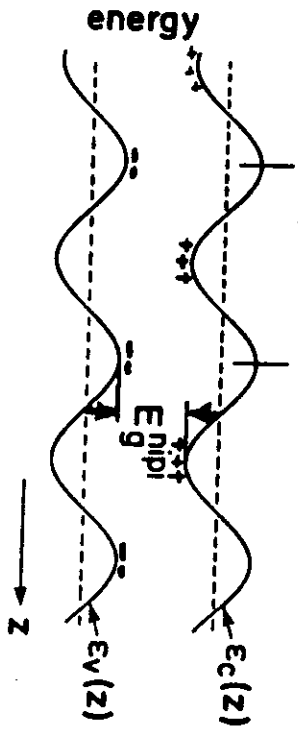

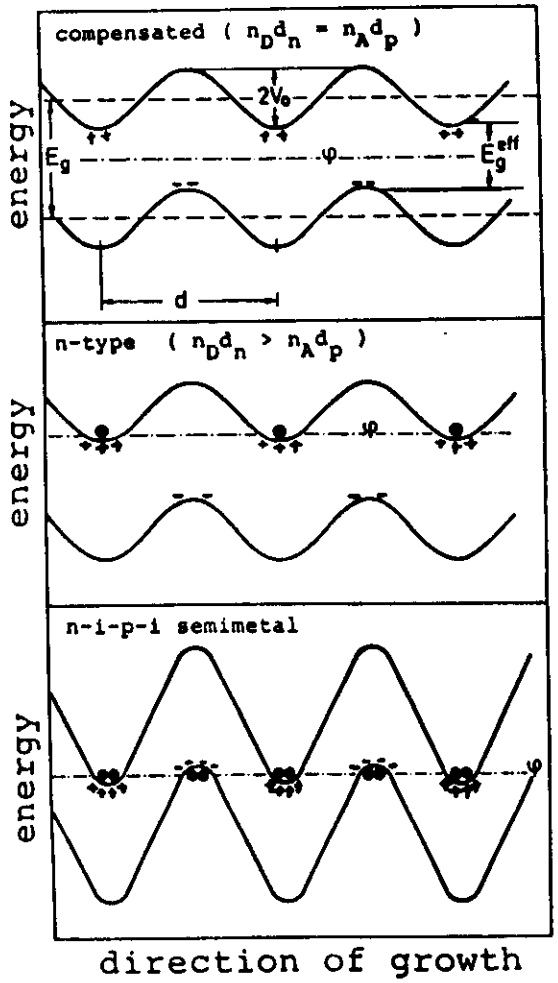

Electronic Subband Structure

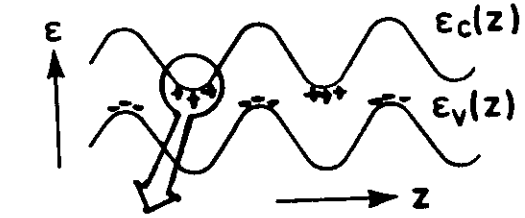

real space momentum space

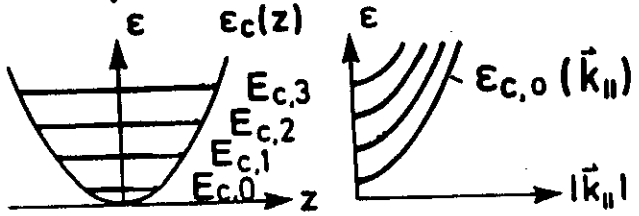

1) Quantization in z-direction

2) Free motion in (x,y)-direction

1)+2) Subbands:

$$\varepsilon_{c,\mu}(\vec{k}_{\parallel}) = E_{c,\mu} + \hbar^2 k_{\parallel}^2 / 2m_c$$

$$\varepsilon_{v,\mu}(\vec{k}_{\parallel}) = E_{v,\mu} + \hbar^2 k_{\parallel}^2 / 2m_v \quad (v = \{^{lh}_{hh})$$

Compositional Superlattice

($Al_xGa_{1-x}As$ - GaAs, e.g.)

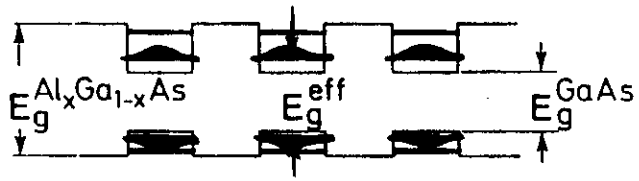

"direct gap in real space"

Doping Superlattice (n-i-p-i)

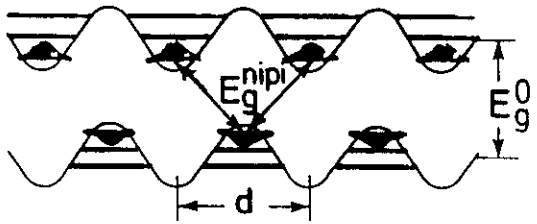

"indirect gap in real space"

ELECTRONIC STRUCTURE

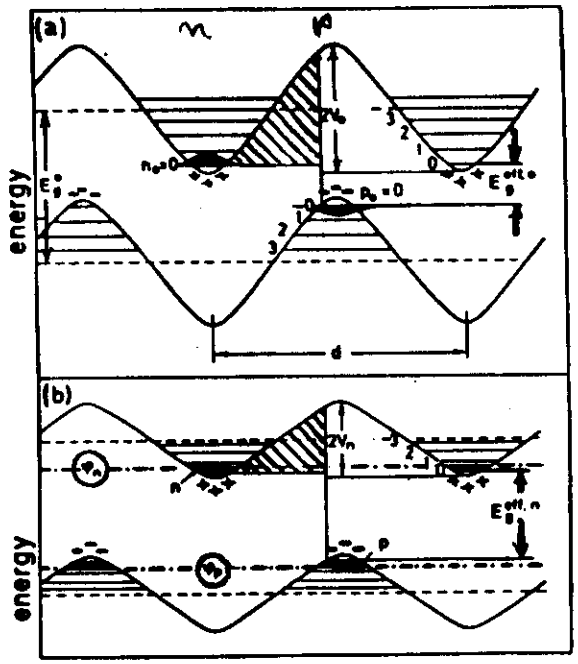

DIRECTION OF PERIODICITY

"Tailoring": $V_0 \propto (n_D, n_A)\, d^2$

"Tuning" of:

carrier concentration: $\Delta n = \Delta p$

band gap $E_g^{eff}(\Delta n)$

lifetimes $\tau^{nipi}(V_n)$

$$\left[\frac{p^2}{2m_c} + v_{sc}(z)\right]\xi_{c,\mu,k_z}(z) = E_{c,\mu,k_z}\,\xi_{c,\mu,k_z}(z)$$

self-consistent potential

$$v_{sc}(z) = v_{imp}(z) + v_H(z) + v_{xc}(z)$$

$$v_{imp}(z) = \frac{4\pi e^2}{\varepsilon_0}\int_0^z dz' \int_0^{z'} dz''\,(n_{D^+}(z'') - n_{A^-}(z''))$$

$$v_H(z) = \frac{4\pi e^2}{\varepsilon_0}\int_0^z dz' \int_0^{z'} dz''\,(p(z'') - n(z''))$$

$$v_{xc}(z) \simeq c\,[n(z)]^{1/3}$$

Solutions for $k_z = 0$ and $k_z = \pi/d \Rightarrow$

boundary conditions:

μ	even	odd
$k = 0$	$\left(\frac{\partial \xi}{\partial z}\right)_{z=\frac{d}{2}} = 0$	$\xi\left(z=\frac{d}{2}\right) = 0$
$k = \frac{\pi}{d}$	$\xi\left(z=\frac{d}{2}\right) = 0$	$\left(\frac{\partial \xi}{\partial z}\right)_{z=\frac{d}{2}} = 0$

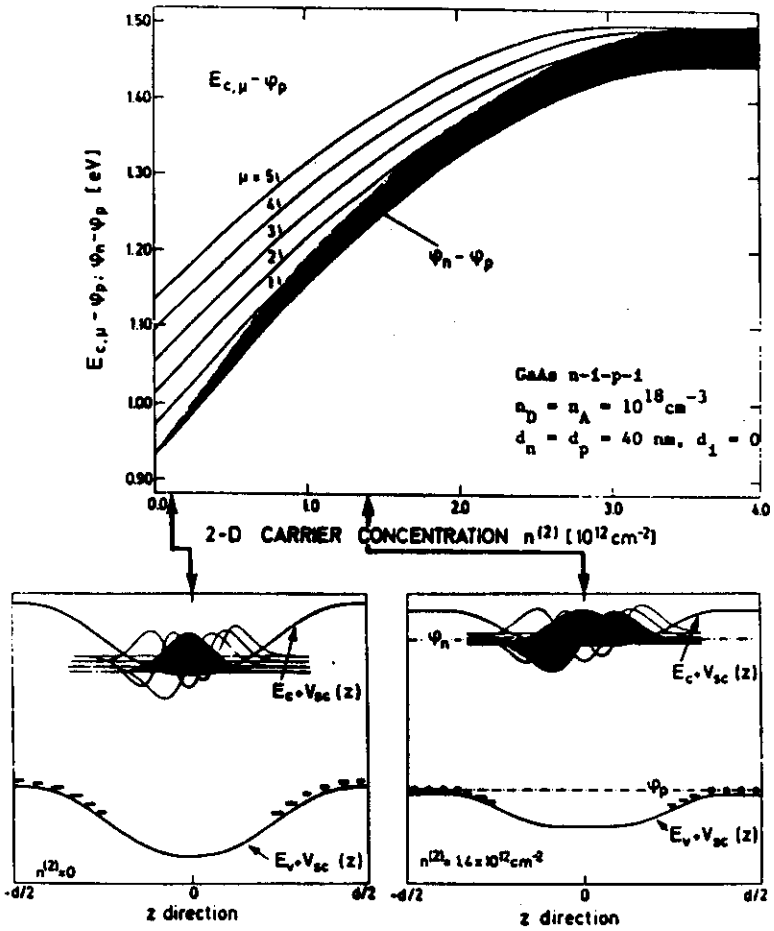

P. Ruden G. D. PRB 27 3538 ('83

npurity bands in (typical) n-i-p-i's?

Donors ($E_D \simeq 5$ meV, e.g.)

$E_D \ll$ { fluctuations of $\sum_i \frac{-e^2/\varepsilon_0}{|\vec{r}-\vec{r}_{D_i}|}$; if $n^{(2)}$ small
$\varepsilon_F(n^{(2)}) = (\hbar^2/2m_c)\,2\pi n^{(2)}$; if $n^{(2)}$ not too small

$\Rightarrow$ imp. band effects negligible

Acceptors ($E_A \simeq 30$ meV, e.g.)

E_A { $>$ fluctuations of $\sum_j \frac{e^2/\varepsilon_0}{|\vec{r}-\vec{r}_{A_j}|}$ } if $p^{(2)}$ is not extremely high
{ $>$ $\varepsilon_F(p^{(2)}) \simeq (\hbar^2/2m_{hh})(2\pi p^{(2)})$ }

$\Rightarrow$ At low temperatures holes are in the acceptor impurity band

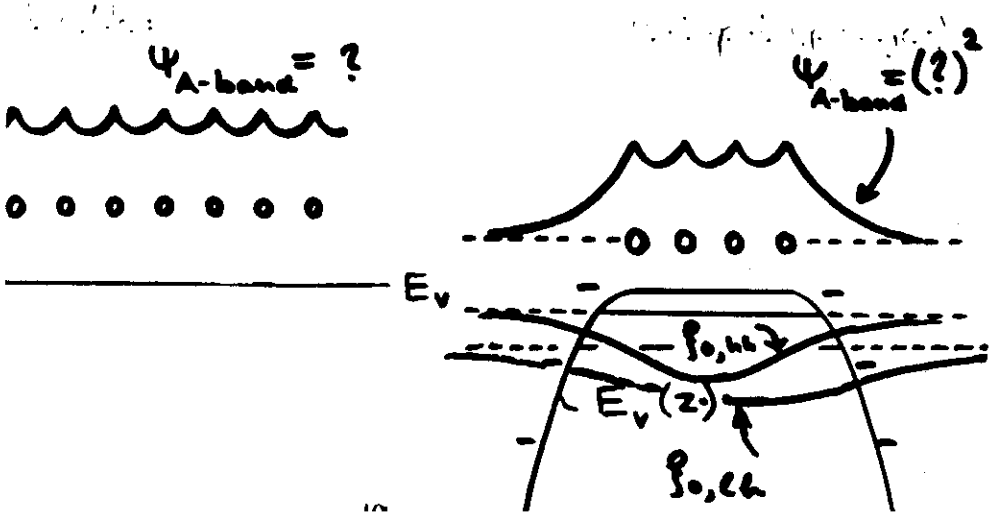

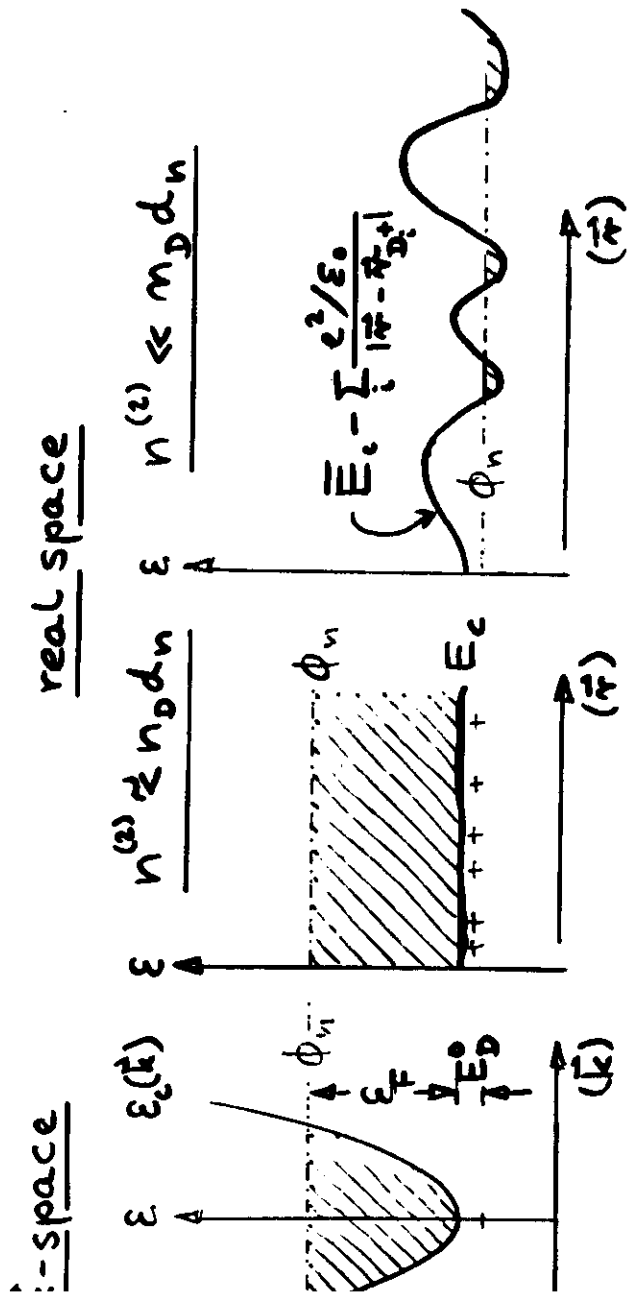

crystal 1,2 ⇒ amorphous 1,2

bulk crystal superlattice X-tal

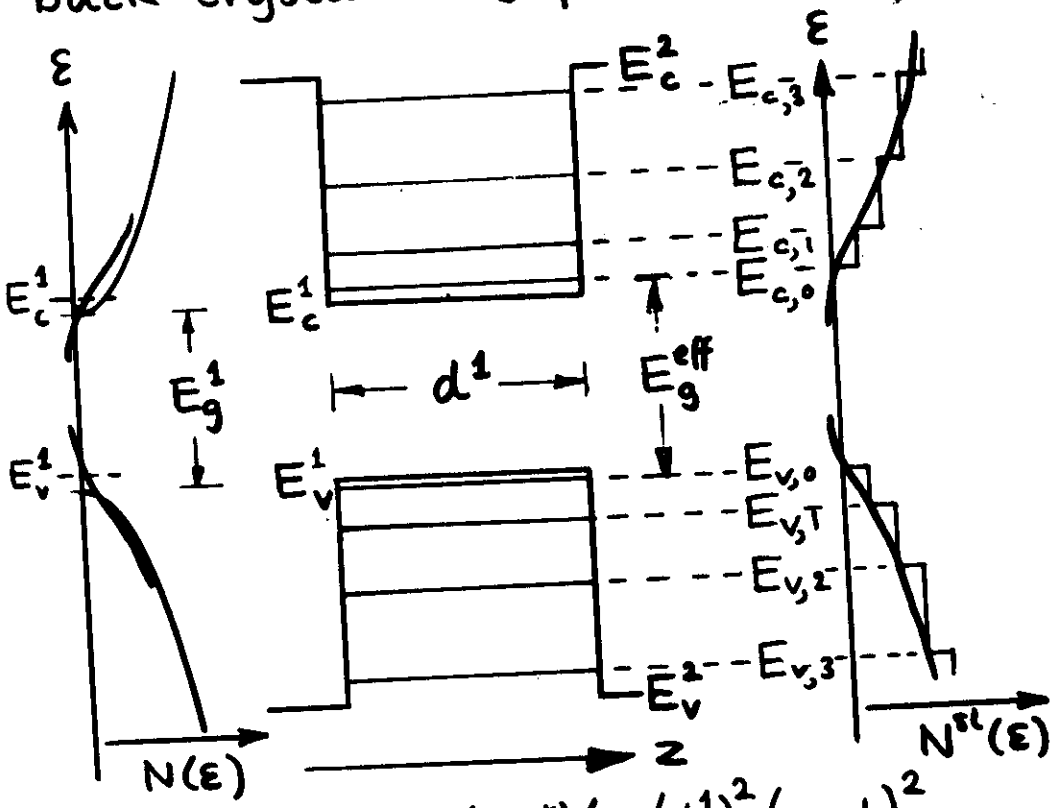

$$E_n \simeq (\hbar^2/2m^*)(\pi/d^1)^2 (n+1)^2$$

assume: no fluctuations of d^1

- $E_g^{eff} > E_g^1$ (mobility gap) $\xrightarrow{(?)}$ m_c^*, m_v^* Abeles+Tiedje PRL 51, 2003 (83)
- "subbands" in am. MLS ?

  homog. ↔ inhomog.

  inter-subband correlations ?

High-field phenomena - real space pic

familiar s.c.

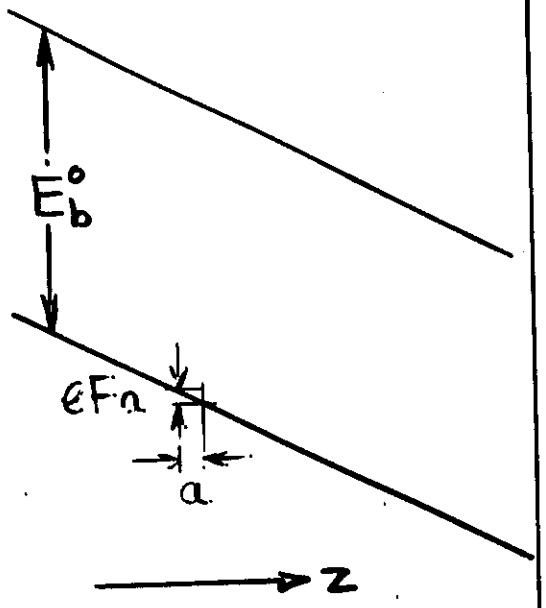

$eFa \ll E_b^0$

unless $F \gtrsim 10^7 Vcm^{-1}$

s.c. superlattice

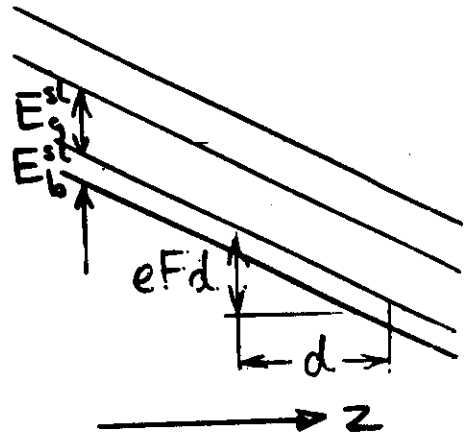

$eFd \begin{cases} > E_b^{sl} \\ \lesssim E_g^{sl} \end{cases}$ possi

if $F \simeq 10^4 Vcm^{-1}$

Transport in z-direction (if barrier thickness d_{II} small

Dynamics of charge carriers in momentum space

normal semicond.

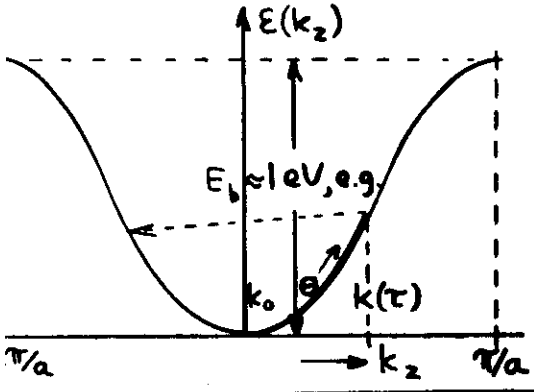

semicond. superlattic

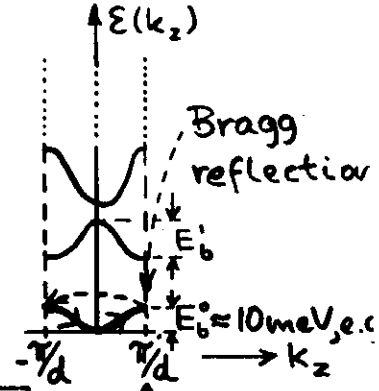

equ. of motion: $k(t) = k_0 + \frac{eF}{\hbar} t$

real space

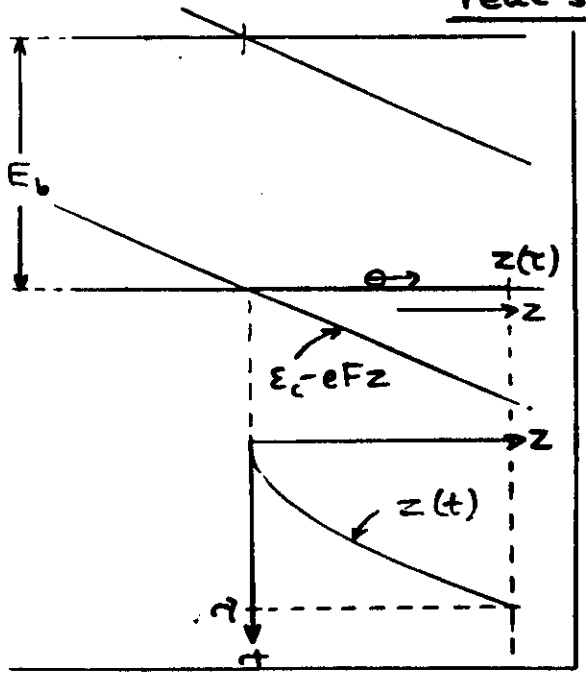

Bloch oscillation

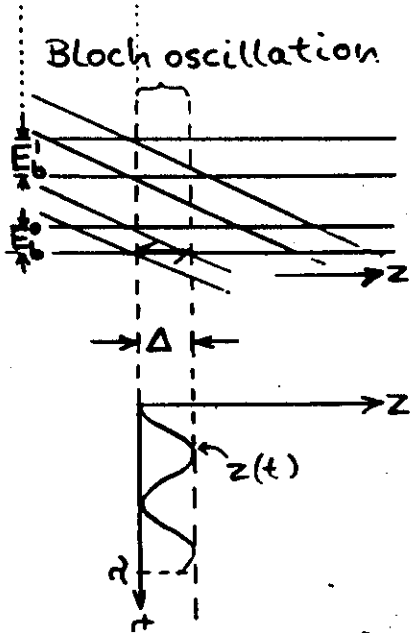

Amplitude of Bloch oscillations $\Delta \approx \frac{E_b^*}{eF}$

Negative differential conductivity by Blochoscillating electrons

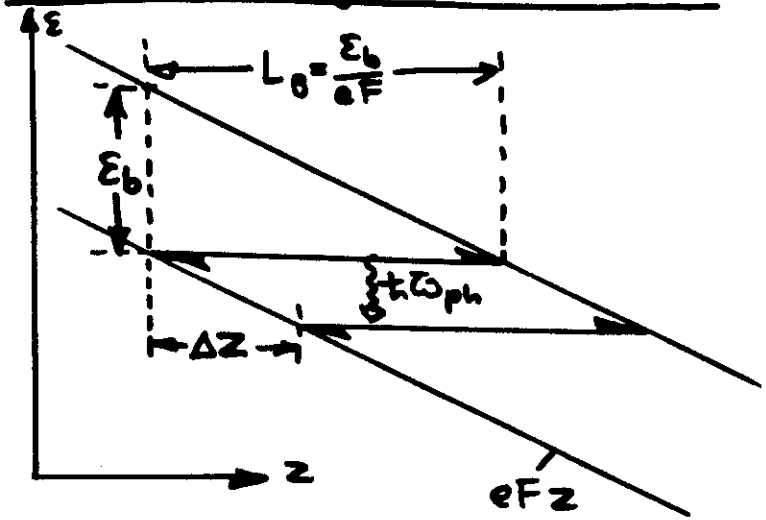

$\langle z \rangle$ changes only beg inelastic scattering

Average of $\Delta\langle z \rangle$ given by:

$eF\,\Delta\langle z \rangle = \hbar\bar{\omega}_{ph}$

Drift velocity:

$$v_{dr} = \frac{\Delta\langle z \rangle}{\tau} = \frac{\hbar\bar{\omega}_{ph}}{eF\tau}$$

Current:

$$j = e n_0 v_{dr} = e n_0 \frac{\hbar\bar{\omega}_{ph}}{eF\tau} \propto \frac{1}{eF}; \quad \frac{\partial j}{\partial F} \propto -F^{-2}$$

if $\hbar\bar{\omega}_{ph}$ and τ at high field constant

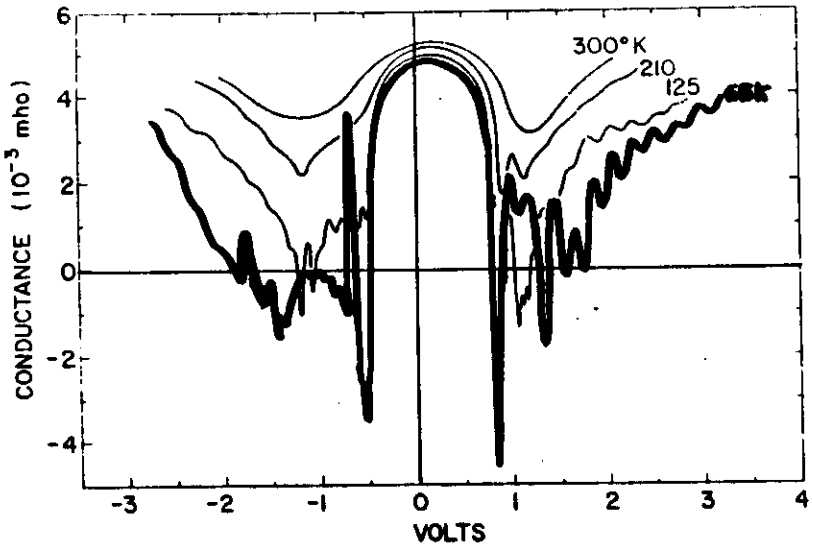

Fig. 7 Differential conductance versus applied voltage in a superlattice at four specified temperatures.

L. Esaki
L.L. Chang } PRL, 1974
R. Tsu

Blochoscillation → { Kane-States / Stark-Ladder

$\phi^m(x)$; W^m

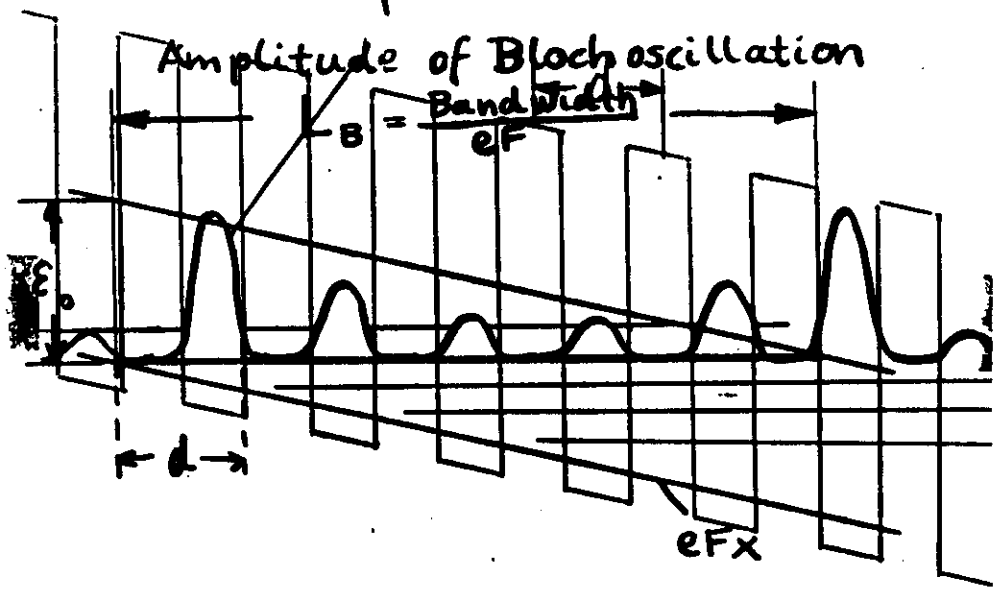

Translational Symmetry ⇒

$\phi^{m+1}(x) = \phi^m(x-d)$; $W^{m+1} = W^m + eFd$

eFd ≳ Bandwidth

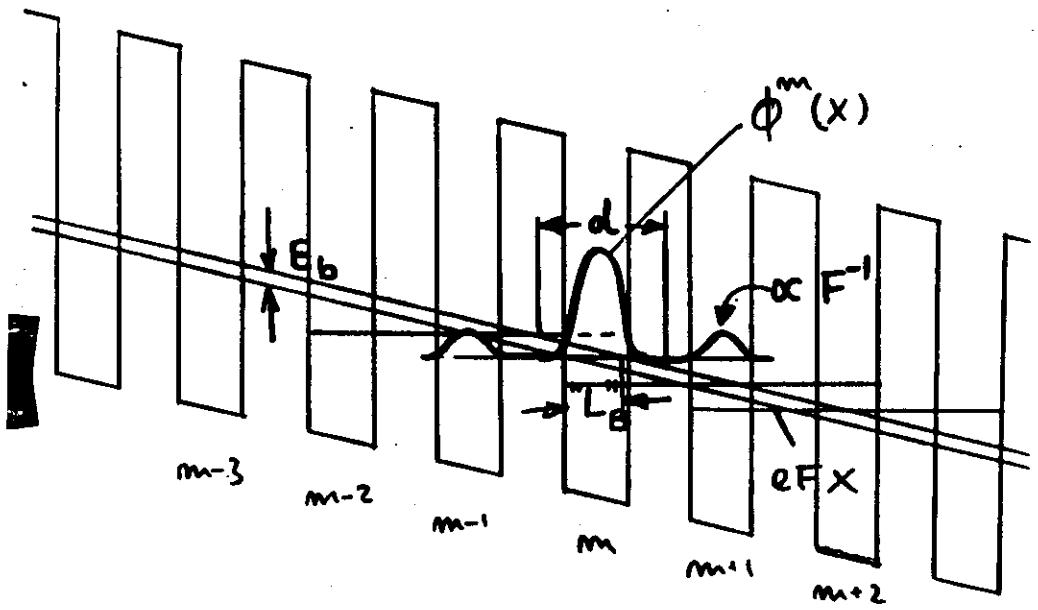

$$w_{m,m+1} \propto \underbrace{|\langle m+1|H^{ep}|m\rangle|^2}_{\propto F^{-2},\ \text{for } eFd > \varepsilon_b}$$

Ohne el. Feld: Blochzustände

$$\underbrace{H_0}_{\frac{\vec{p}^2}{2m}+\underbrace{v(\vec{r})}_{\text{Gitter}}+\underbrace{V(z)}_{\text{Übergitter}}} |\nu,\vec{k}\rangle = \varepsilon_\nu(\vec{k})\underbrace{|\nu,\vec{k}\rangle}; \; -\tfrac{\pi}{a}<k_x,k_y<\tfrac{\pi}{a}; \; -\tfrac{\pi}{d}<k_z<\tfrac{\pi}{d}$$

$$\langle\vec{r}|\nu,\vec{k}\rangle = e^{i\vec{k}\vec{r}}\underbrace{u_{\nu,\vec{k}}(\vec{r})}_{\tilde{u}_\nu(z)\,u_{c,\vec{k}=0}(\vec{r})}$$

Mit el. Feld in z-Richtung:

Kane Zustände, Wannier-Starkleiter

$$(H_0 - eFz)|\nu,m,\vec{k}_\parallel\rangle = W_\nu^m(\vec{k}_\parallel)|\nu,m,\vec{k}_\parallel\rangle$$

mit

$$W_\nu^m(\vec{k}_\parallel) = E_\nu - eFd\,m + \frac{\hbar^2 k_\parallel^2}{2m_c^*}; \quad m = 0,\pm1,\pm2\ldots$$

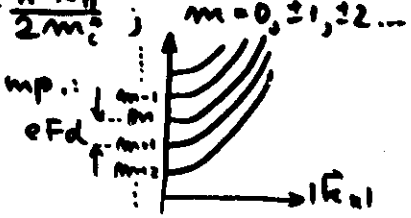

Quantisierung der k_z-Komp.: $k_z \longrightarrow m$

und

$$\langle\vec{r}|\nu,m,\vec{k}_\parallel\rangle = \underbrace{\frac{1}{a\sqrt{\nu}}\int_{-\pi/d}^{\pi/d} dk_z\, e^{i\frac{\varepsilon_\nu}{eFd}\sin k_z d - k_z m d}}_{J_{m-\frac{\varepsilon_\nu}{eFd}}\left(\frac{\varepsilon_\nu}{eFd}\right),\ \text{in z-Richtung lokalisiert}} e^{ik_z z} e^{i\vec{k}_\parallel\vec{r}_\parallel}\tilde{u}_\nu(z)\,u_{c,\vec{k}=0}(\vec{r})$$

Translationssymmetrie

Für eFd > ε_ν

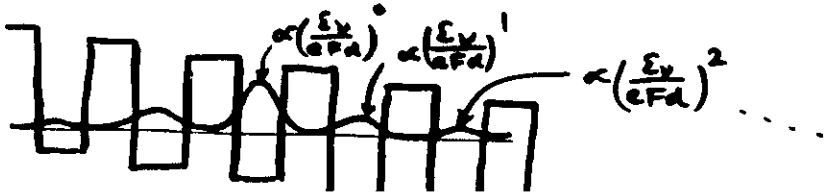

Strom durch Hopping zwischen lokalisierten Zuständen.

(G.H. Döhler, R. Tsu, L. Esaki, Sol. State Commun. 17, 317 (1975); R. Tsu, G.H. Döhler, Phys. Rev. B. 12, 680 (1975)

$$j = e \sum_{\substack{m \\ \vec{k}_\parallel \\ \vec{k}'_\parallel}} n d \left\{ w_{m,\vec{k}_\parallel;m+1,\vec{k}'_\parallel}(F) f_m(\vec{k}_\parallel)\left[1 - f_{m+1}(\vec{k}'_\parallel)\right] - w_{m+1,\vec{k}'_\parallel;m,\vec{k}_\parallel}(F) f_{m+1}(\vec{k}'_\parallel)\left[1 - f_m(\vec{k}_\parallel)\right] \right\}$$

mit

$$w_{m,\vec{k}_\parallel;m+1,\vec{k}'_\parallel} = \frac{2\pi}{\hbar} |\langle m+1,\vec{k}'_\parallel;F | H^{int} | m,\vec{k}_\parallel;F\rangle|^2 \times \delta(W_m(\vec{k}_\parallel) - W_{m+1}(\vec{k}'_\parallel) - \varepsilon^{int}(\vec{k}_\parallel - \vec{k}'_\parallel))$$

Nach thermischer Mittelung

$$j = e \sum_{m=1} n d \langle w_{m,m+1}(F)\rangle \underbrace{\left[1 - e^{-meFd/kT}\right]}_{\text{det. Gleichgew.}}$$

Nur Übergänge zwischen benachbarten Zuständen

$$j = ed \langle w_{m,m+1}(F)\rangle \left[1 - e^{-eFd/kT}\right]$$

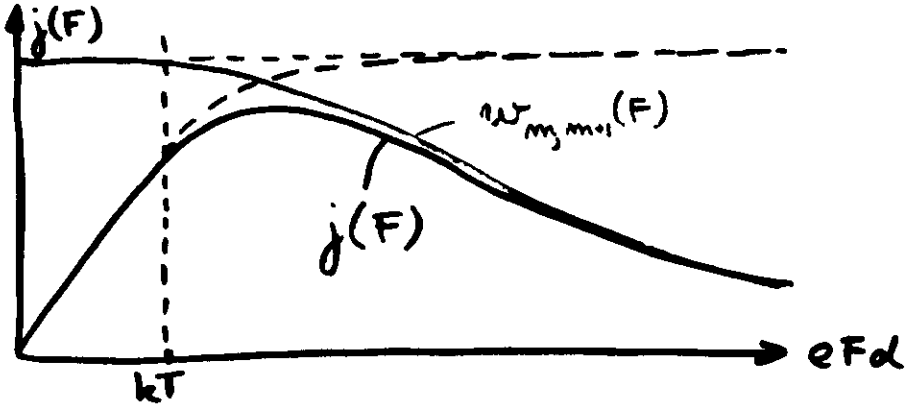

N.D.C., wenn $\frac{\partial \langle w_{m,m+1}\rangle}{\partial F} < 0$ für $eFd > kT$

$$w_{m,\vec{k}_\parallel;m+1,\vec{k}'_\parallel} = \sum_{\vec{q}} \frac{2\pi}{\hbar} |\langle m+1,\vec{k}'_\parallel | e^{i\vec{q}\vec{r}} | m,\vec{k}_\parallel\rangle|^2 |C(\vec{q})|^2 \delta(W_m(\vec{k}_\parallel) - W_{m+1}(\vec{k}'_\parallel) - \varepsilon^{int}(\vec{k}_\parallel - \vec{k}'_\parallel))$$

$\propto F^{-1}$ for $eFd > \varepsilon_b$

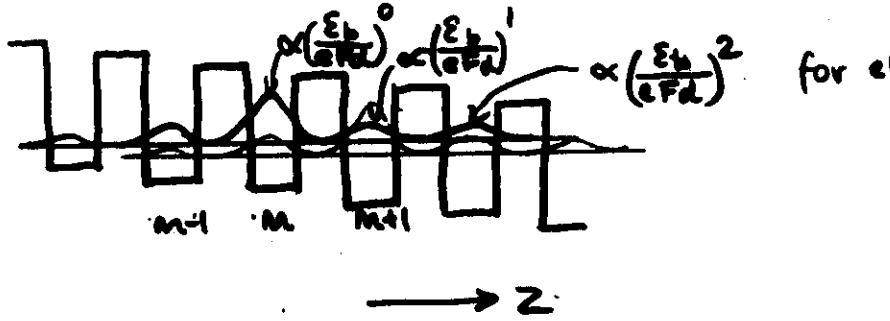

thermal average

$$\langle w_{m,m+1}\rangle = \sum_{\vec{k}_\parallel,\vec{k}'_\parallel} w_{m,\vec{k}_\parallel;m+1,\vec{k}'_\parallel} f_m(W_m(\vec{k}_\parallel))\left[1 - f_{m+1}(W_{m+1}(\right.$$

$$\propto \frac{1}{F^2} \cdot \underbrace{\phi(F)}_{\text{increases less than } \propto F^2}$$

Hopping probability

$$w_{m,\vec{k}_\parallel;\,m+n,\vec{k}'_\parallel} = \frac{2\pi}{\hbar}\left|\langle m+n,\vec{k}'_\parallel|H^{int}|m,\vec{k}_\parallel\rangle\right|^2 \delta\left(W_m(\vec{k}_\parallel) - W_{m+n}(\vec{k}'_\parallel) - \varepsilon^{int}(\vec{k}_\parallel - \vec{k}'_\parallel)\right)$$

H^{int}, for instance

a) acoustic phonons : $\hbar\omega_{\vec{q}} \simeq \hbar c_s \underbrace{|\vec{q}|}_{((\vec{q}_\parallel)^2+q_z^2)^{1/2}}$

$$H^{eaph}_{\vec{q}} = \underbrace{C(q)}_{\propto q^{1/2}}\, e^{i\vec{q}\vec{r}} \;;\; \varepsilon^{int}(\vec{k}_\parallel - \vec{k}'_\parallel = \vec{q}_\parallel, q_z) = \hbar\omega_{\vec{q}} = \text{small}$$

b) charged impurity (donor, acceptor)

$$H^{e\,imp} = \pm\frac{e^2/\varepsilon_0}{|\vec{r}-\vec{r}_{imp}|} = \pm\frac{4\pi e^2}{\varepsilon_0}\sum_{\vec{q}_\parallel} e^{i\vec{q}_\parallel(\vec{r}_\parallel - \vec{r}_{\parallel imp})} \sum_{q_z}\frac{e^{iq_z(z-z_{imp})}}{q_\parallel^2+q_z^2}$$

elastic scattering : $\varepsilon^{int}(\vec{k}_\parallel - \vec{k}'_\parallel) = 0$

el. current in a s.c. superl.

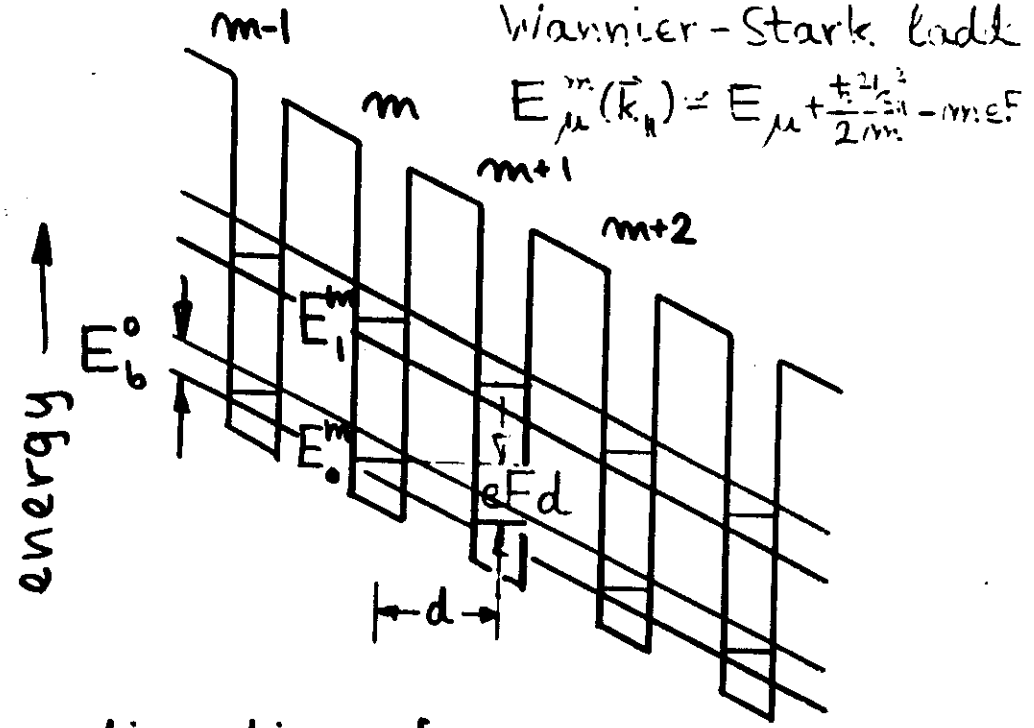

$j_{m,m+1}(F) = e\,n^{(2)} v_d(F)\,1/d$

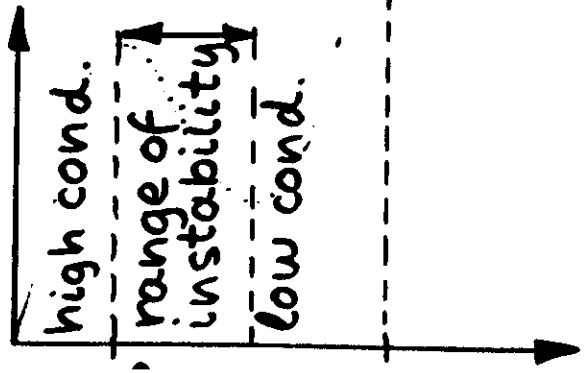

energy

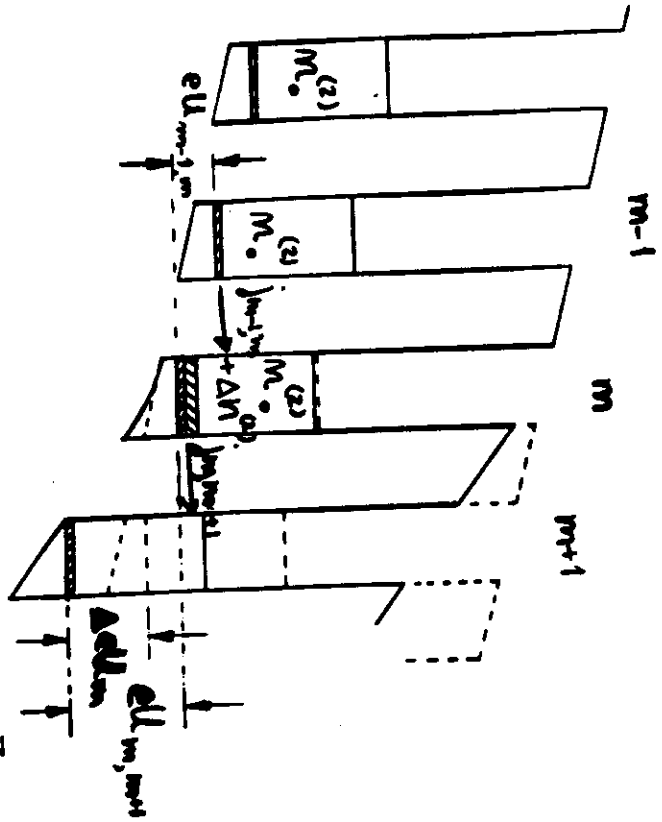

continuity cond. for steady state:

$$j_{m,m+1} = j_{m+1,m}$$

$$e n_0^{(2)} v_{dr}(U_{m,m+1})/d$$

$\Rightarrow$ no NDC-ox if $n_0^{(2)} \ll \Delta n^{(2)}$

Wannier-Stark Leiter: Sprossen abstand eFd

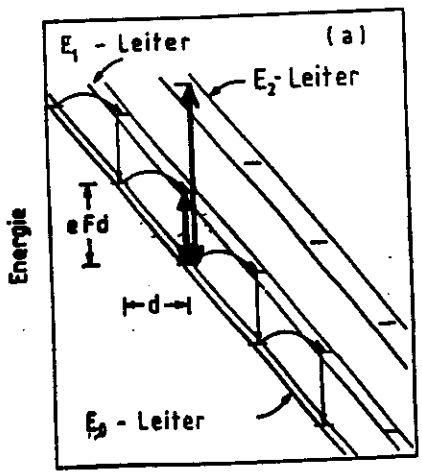

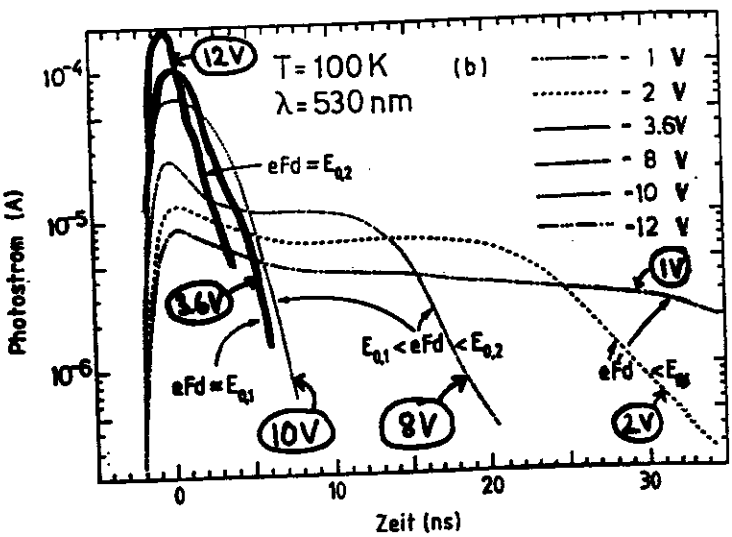

H. Scheider, K. von Klitzing, K. Ploog
Europhys Lett. 8, 575 (1989)

Emission und Absorption von Photonen mit $\hbar\omega = (n)eFd$ im unendl. äquidist. System (Intra Minibandübergänge)

Wegen Translationssymmetrie gilt für Dipolmatrixelement

$$|\vec{p}_{m,m+n}(\vec{k}_\parallel)|^2 = |\vec{p}_{m,m-n}(\vec{k}_\parallel)|^2$$

und für Übergang mit $\hbar\omega = neFd$

$$w^{(em)}_{m,m+n}(\vec{k}_\parallel,\vec{K}) = \cdots K\,|\,|\,K\rangle^2 \delta(neFd - \hbar\omega_K)\,(n_{\vec{K}}+1)$$

ind. Em. ↑ sp. Em.

$$w^{(abs)}_{m,m-n}(\vec{k}_\parallel,\vec{K}) = -K\,|\,|\,K\rangle^2 \delta(-neFd + \hbar\omega_K)\; n_{\vec{K}}$$

Im stationären Zustand Verteilungsfkt. von m unabh.

$$f_m(\vec{k}_\parallel) = f_{m\pm n}(\vec{k}_\parallel)$$

$\Rightarrow$ Thermische Mittelung (wegen $\vec{k}_\parallel$-Erhaltung!)

$$\langle w^{em}(\vec{K})\rangle = \sum_{\vec{k}_\parallel} f_m(\vec{k}_\parallel)\,[1 - f_{m+n}(\vec{k}_\parallel)]\, w_{m,m+n}(\vec{k}_\parallel,\vec{K})$$

$$= \underbrace{\langle w^{ind.em}(\vec{K})\rangle}_{\equiv w^{abs}(\vec{K})} + \langle w^{sp.}(\vec{K})\rangle$$

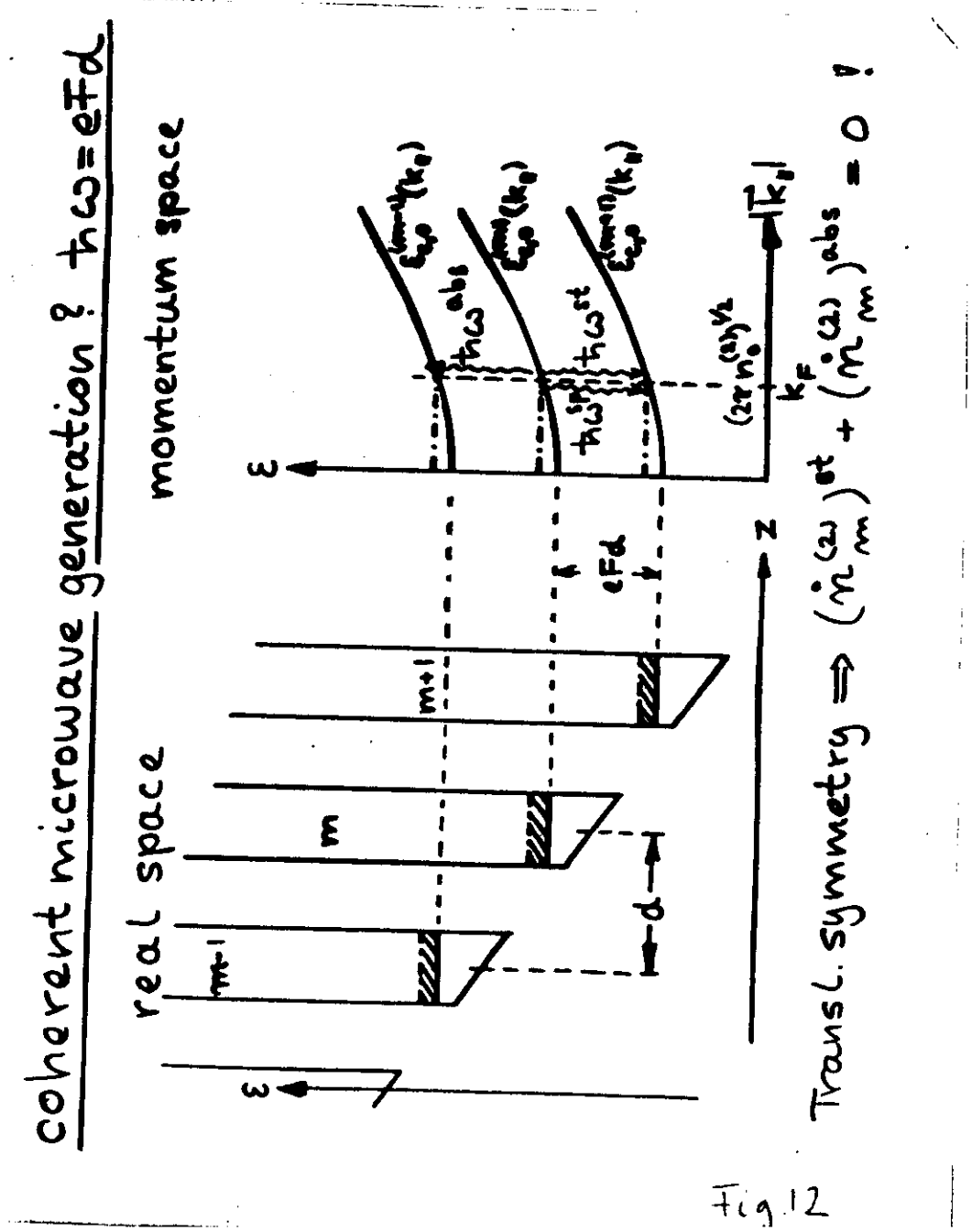

Fig. 12

Interband transitions in MQW's

$$w_{c,\mu,\vec{k}_{\parallel}';v,\nu,\vec{k}_{\parallel}} \propto \left|\langle c,\mu,\vec{k}_{\parallel}'|e^{i\vec{q}\vec{r}}\vec{p}|v,\nu,\vec{k}_{\parallel}\rangle\right|^2;\ v=$$

$$\langle c,\mu,\vec{k}_{\parallel}'|e^{i\vec{q}\vec{r}}\vec{p}|v,\nu,\vec{k}_{\parallel}\rangle =$$

$$\int d^2r_{\parallel}\int_{-d/2}^{d/2} dz\, \xi^*_{c,\mu}(z)e^{-i\vec{k}_{\parallel}'\vec{r}_{\parallel}}u^*_{c,\vec{k}_0}(\vec{r})\, e^{i\vec{q}\vec{r}}\underbrace{\vec{p}}_{\frac{\hbar}{i}\vec{\nabla}}\xi_{v,\nu}(z)e^{i\vec{k}_{\parallel}\vec{r}_{\parallel}}u$$

$$\simeq \delta_{\vec{k}_{\parallel}',\vec{k}_{\parallel}+\vec{q}_{\parallel}}\int dz\, \xi^*_{c,\mu}(z)e^{iq_z z}\xi_{v,\nu}(z)\underbrace{\int_0^{a_x}\int_0^{a_y}\int_0^{a_z} d^3r\, u^*_{c,\vec{k}_0}(\vec{r})\vec{p}\,u_{v,\vec{k}}}_{\vec{p}_{cv}(\vec{k}_0)}$$

bulk interband ma
element of $\vec{p}$

$$q_z = \frac{2\pi}{\lambda} = \frac{2\pi}{\underbrace{\lambda_0/n_{opt}}_{800nm/3.4=235nm}}$$

$(\lambda/n_{opt})/2 \gtrsim d$ in n-i-p-i's!

other terms:

$$\int dz\, \xi^*_{c,\mu}(z)\tfrac{\hbar}{i}\left(\tfrac{\partial}{\partial z}\xi_{v,\nu}(z)\right)\underbrace{\int_0^{a_x}\int_0^{a_y}\int_0^{a_z} d^3r\, u^*_{c,\vec{k}_0}(\vec{r})\,u_{v,\vec{k}_0}(\vec{r})}_{0}$$

(orthogonality of bulk Bloch

$$\langle c,\mu,\vec{k}_{\parallel}|\vec{p}|v,\nu,\vec{k}_{\parallel}\rangle \simeq \underbrace{\langle c,\mu|v\nu\rangle}_{\int_{-d/2}^{d/2} dz\, \xi^*_{c,\mu}(z)\,\xi_{v,\nu}(z)}\vec{p}_{cv}(\vec{k}_0)$$

Superlattice Maser (tunable: $\hbar\omega = c(\ldots)$ eV!
(Superlattice with superstructure)

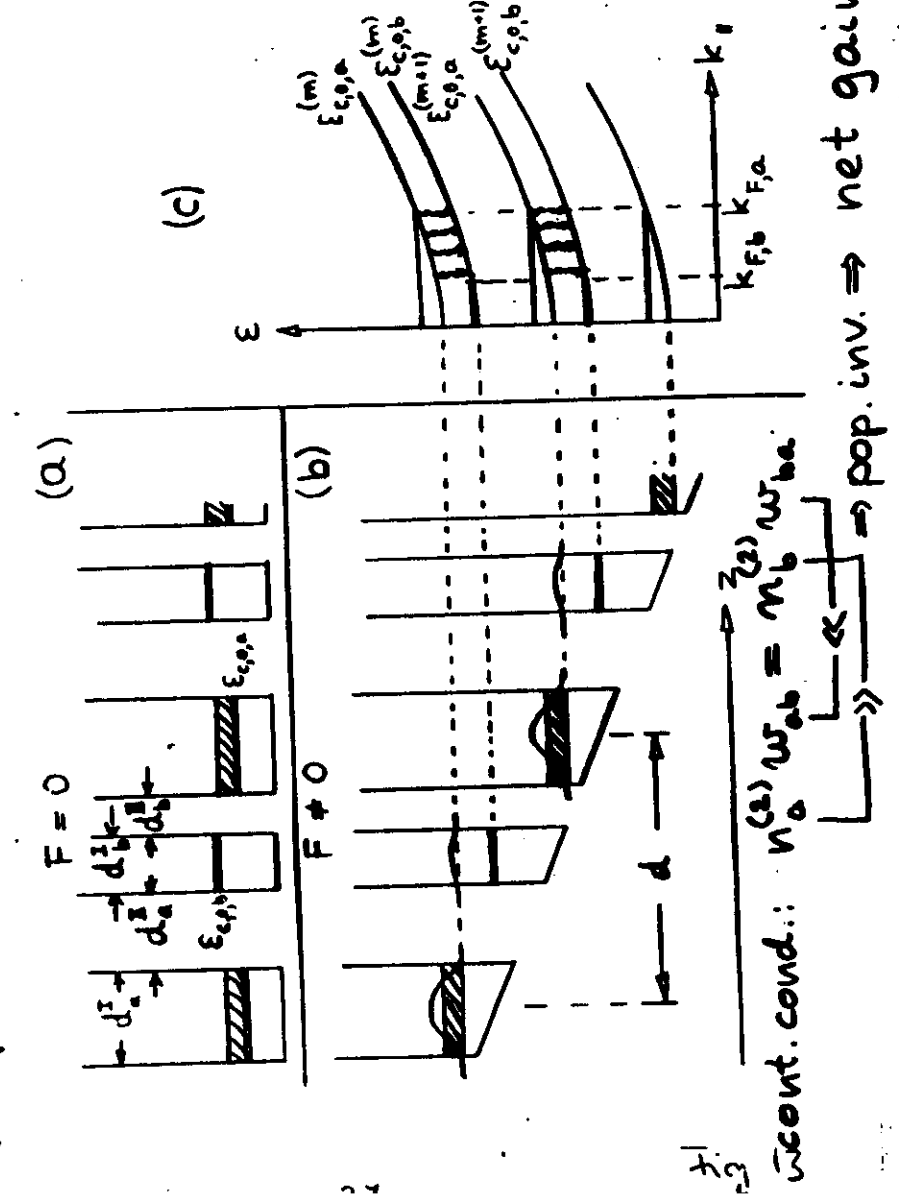

Fig

interband transitions

type-I compositional s.l.

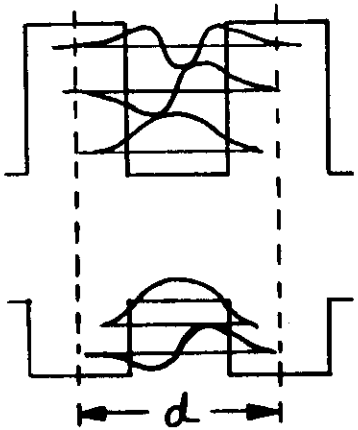

$$w_{c\mu,v\nu}(\vec{k}_\parallel) \propto \underbrace{|\langle c,\mu|v,\nu\rangle|^2}_{\simeq \delta_{\mu\nu}} |\vec{p}_{cv}|^2$$

(quasi selection rule)

type-II compositional s.l.

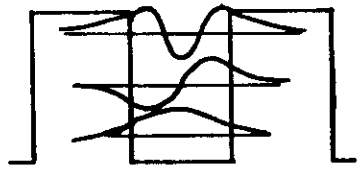

$$w_{c\mu,v\nu}(\vec{k}_\parallel) \propto \underbrace{|\langle c\mu|v,\nu\rangle|^2}_{\text{usually: } \ll 1} |\vec{p}_{cv}|^2$$

(no selection rule)

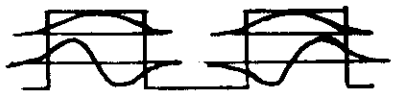

interband trasitions in n-i-p-i X-tal

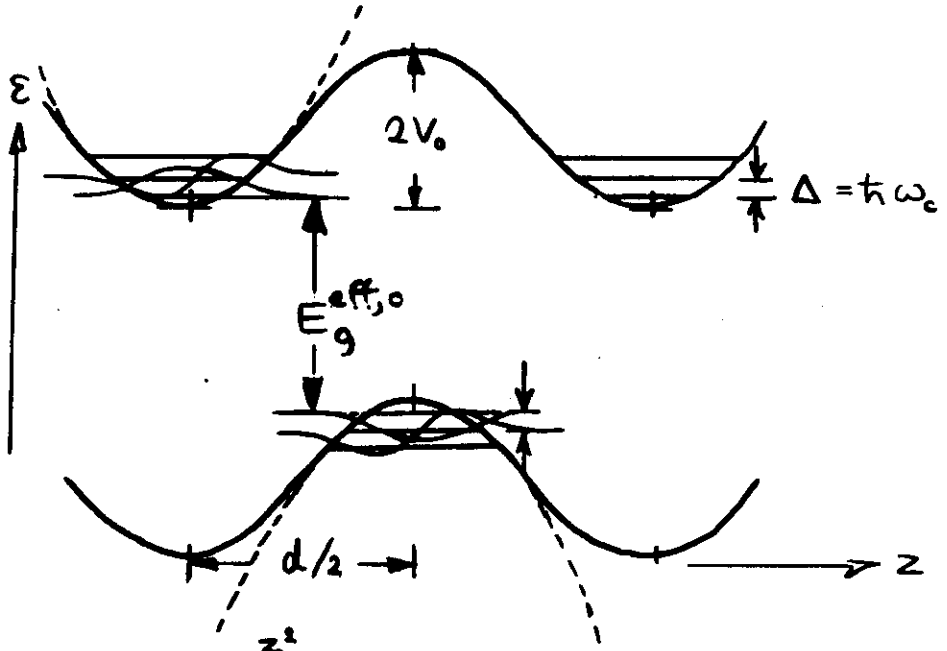

$$\xi_{c,\mu}(z) = c_\mu e^{-\frac{z^2}{2\alpha_c^2}} H_\mu(z/\alpha_c)$$

$$\alpha_c^2 = \hbar/m_c\omega_c \; ; \; \omega_c^2 = 4\pi e^2 n_D/\varepsilon_0 m_c$$

$$\xi_{v,\nu}(z) = v_\nu e^{-\frac{(z\pm d/2)^2}{2\alpha_v^2}} H_\nu((z\pm d/2)/\alpha_v) \; ; \; \nu = h,l$$

$$\alpha_v^2 = \hbar/m_v\omega_v \; ; \; \omega_v^2 = 4\pi e^2 n_A/\varepsilon_0 m_v \; ; \; \nu = h,l$$

$$|\langle c,\mu|v,\nu\rangle|^2 = \underbrace{e^{-\frac{(d/2)^2}{\alpha_c^2+\alpha_v^2}}}_{e^{-\frac{2\cdot 2V_0}{\hbar\omega_c}}, \text{ if } \omega_c=\omega_v} \underbrace{I_{\mu\nu}}_{\simeq 1 \text{ for } \mu=\nu=0,\; \gg 1 \text{ for } \mu,\nu\neq 0}$$

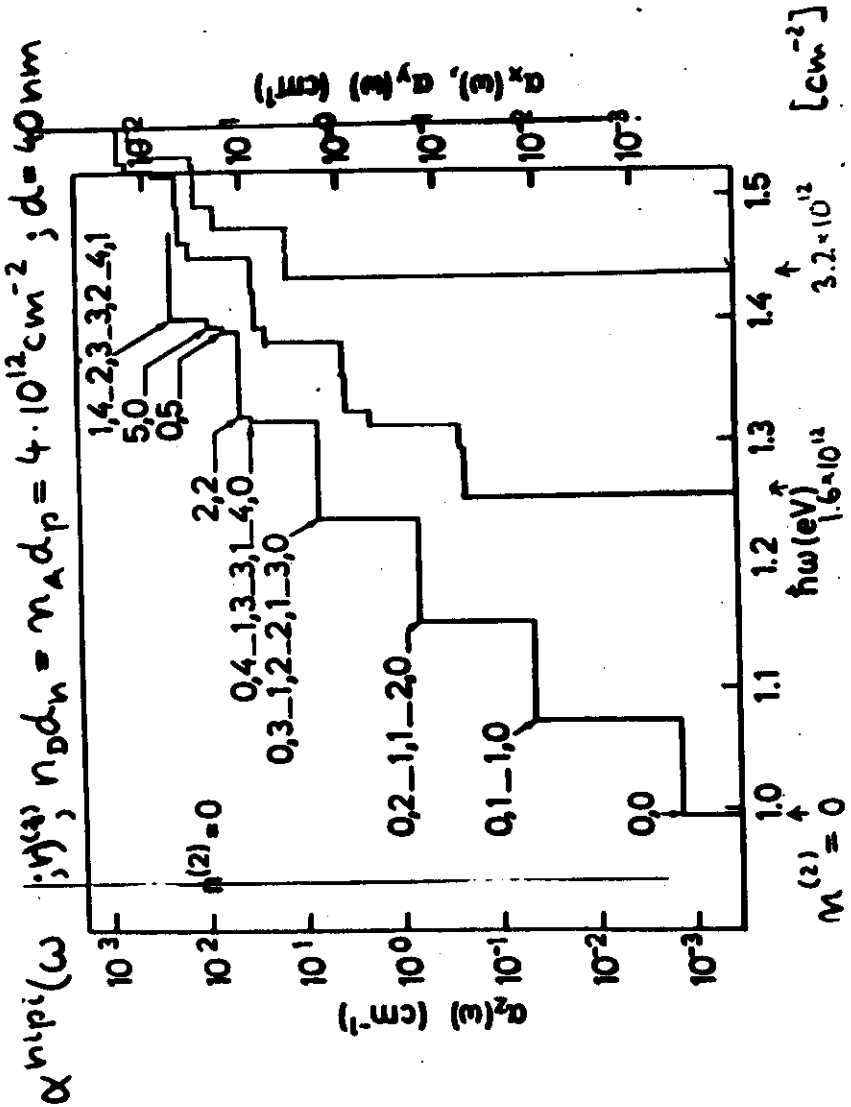

Ideal nipi
(G.H.D. 1972)

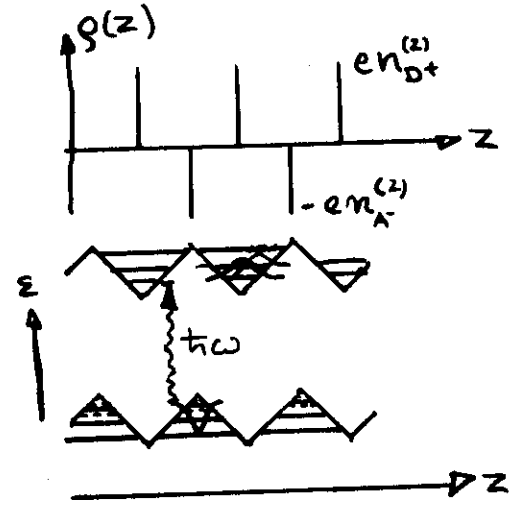

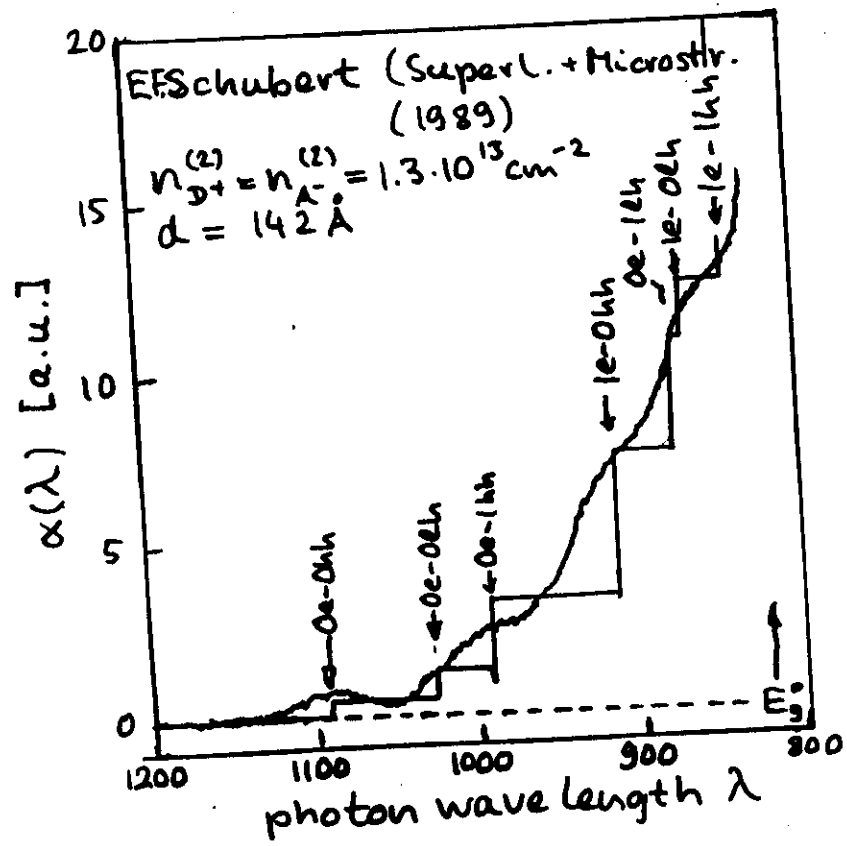

absorption in a n-i-p-i X-tal (semiclassical model; Franz-Keldysh

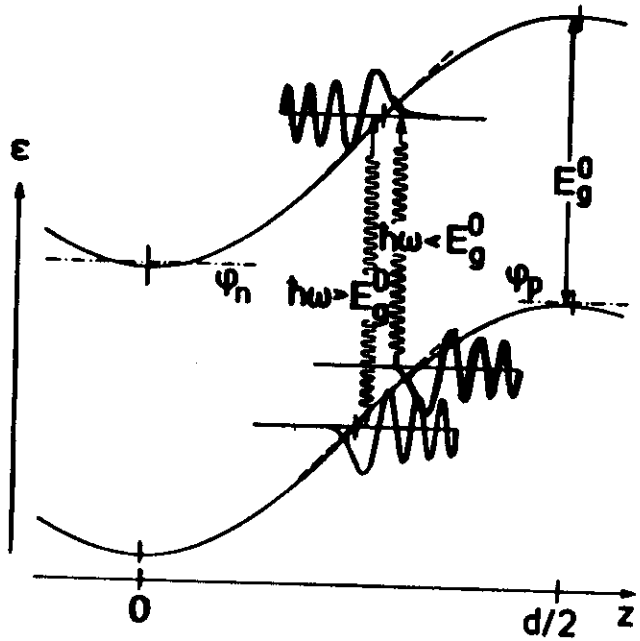

(absorption from subband trans. see G.H. Döhler + P.P. Ruden, PRB 30, 5932 (1984))

paper: 1286-32

FK - Modulator

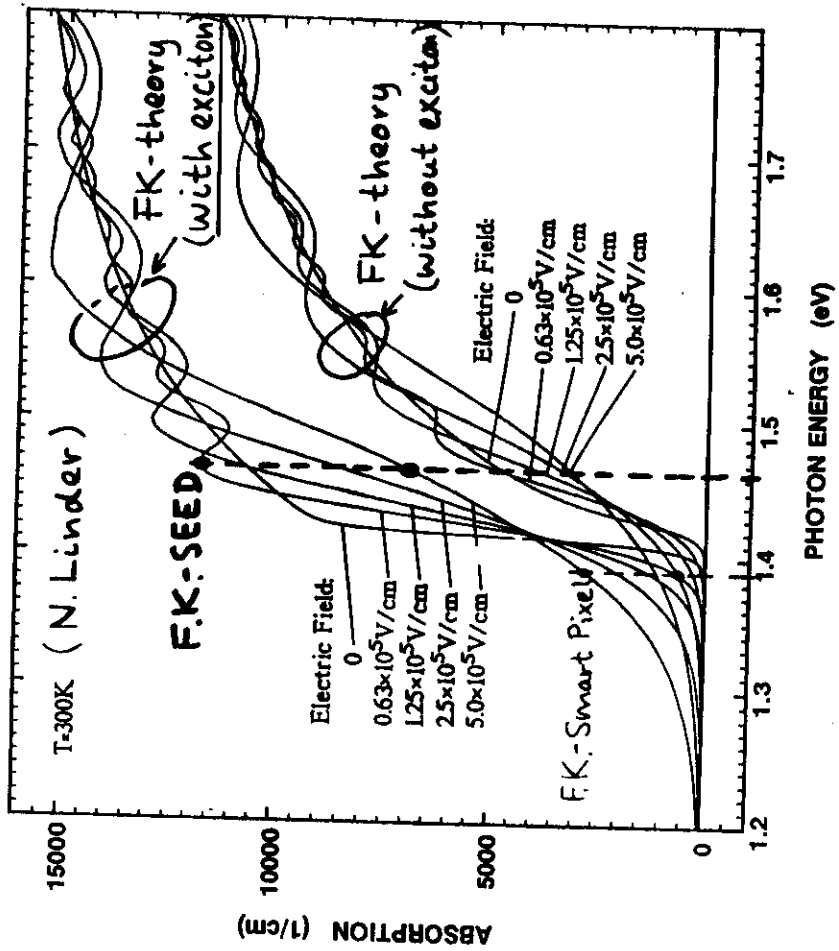

$\alpha(\omega; \Delta\varphi_{np} = eV_{np})$ for n-i-p-i semimetal

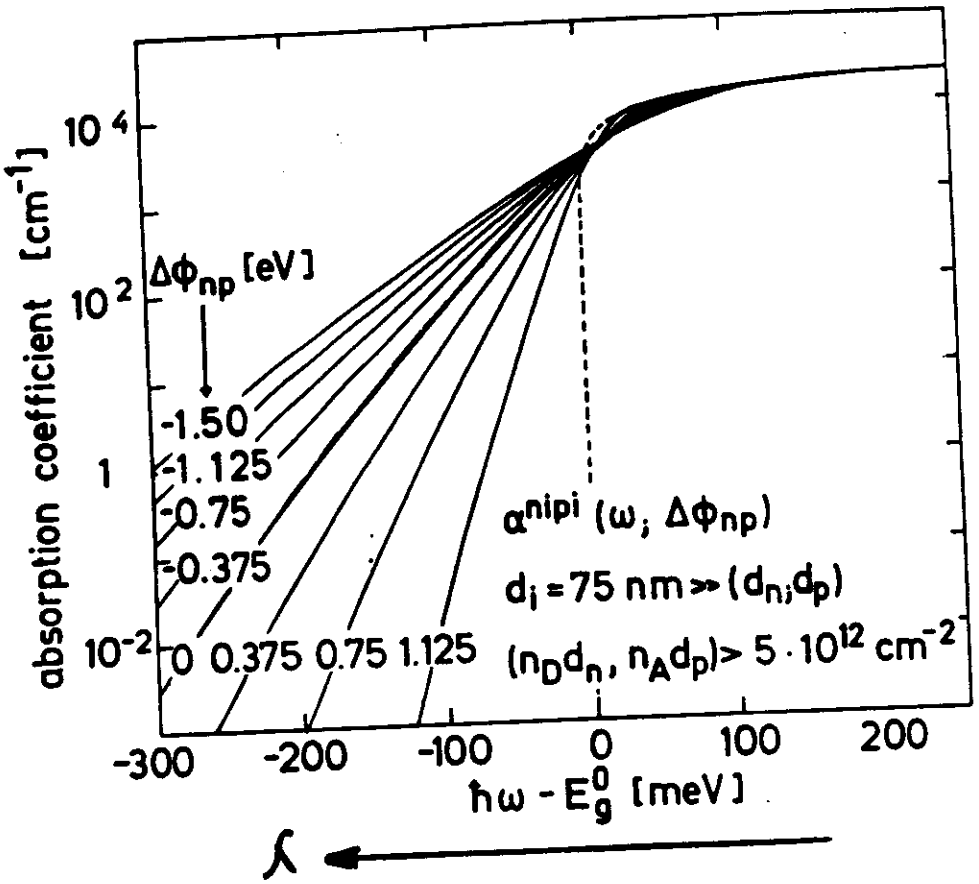

Absorption in a δ- n-i-p-i

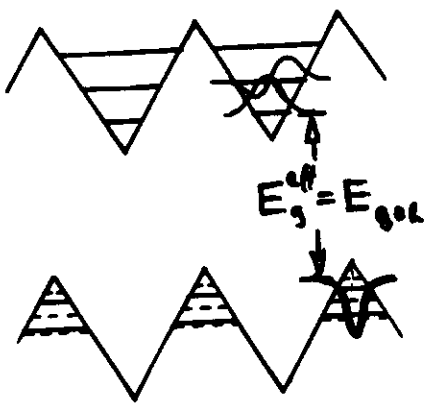

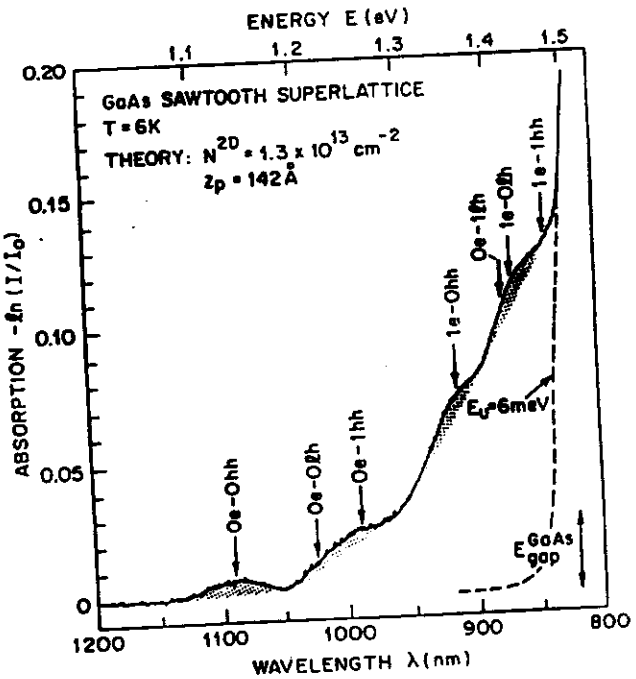

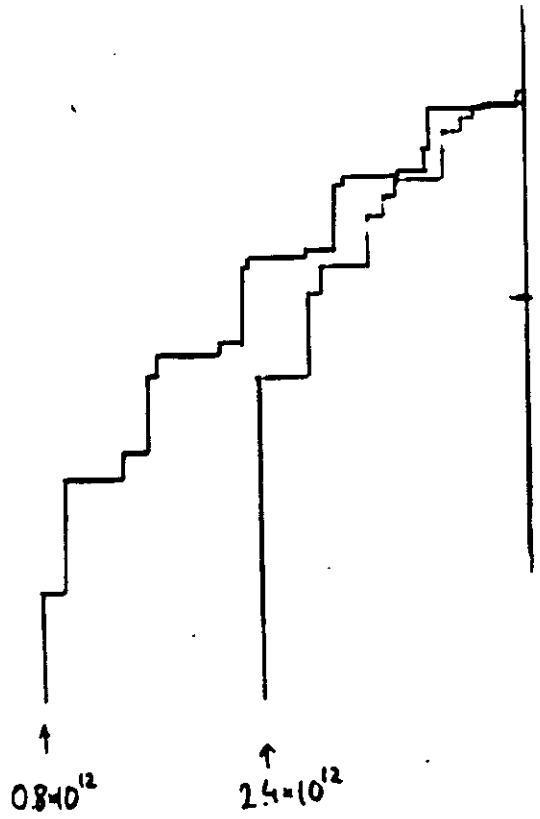

$\Delta\alpha(\omega; V_{ph})$ from change of transmission

$$\frac{\Delta I_\omega^{tr}(\Delta V_{ph})}{I_\omega^{tr}} = e^{-\Delta\alpha(\omega;\Delta V_{ph})\, L_z}$$ *

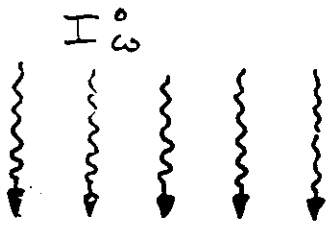

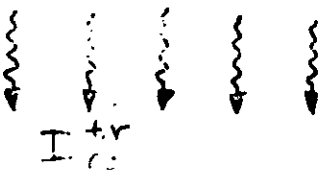

* Fine layer extinction ratio : waveguide str. !

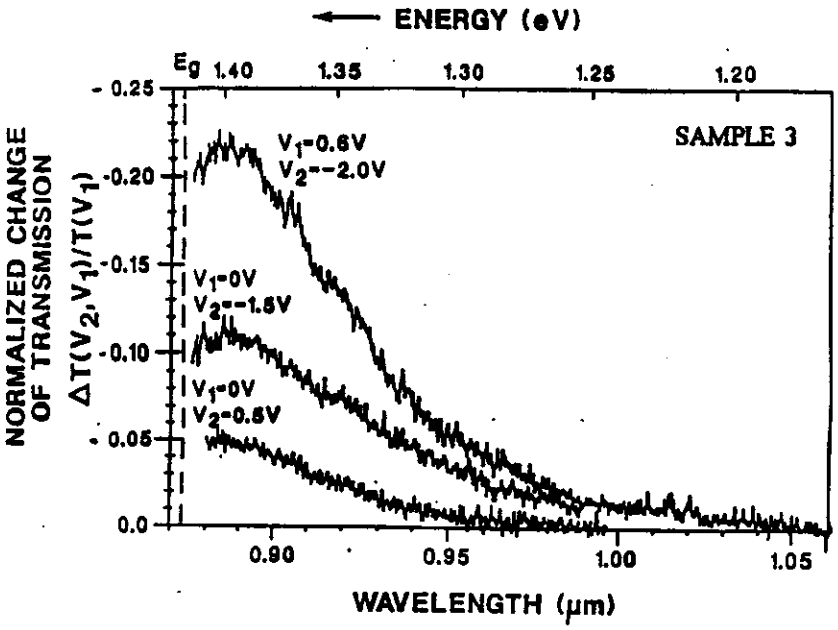

Chang-Hasnain et. al., APL 50, 915 (1987)

$n_p = n_A = 2 \cdot 10^{18} cm^{-3}$

$d_n = d_p = d_i = 50nm$

10 periods

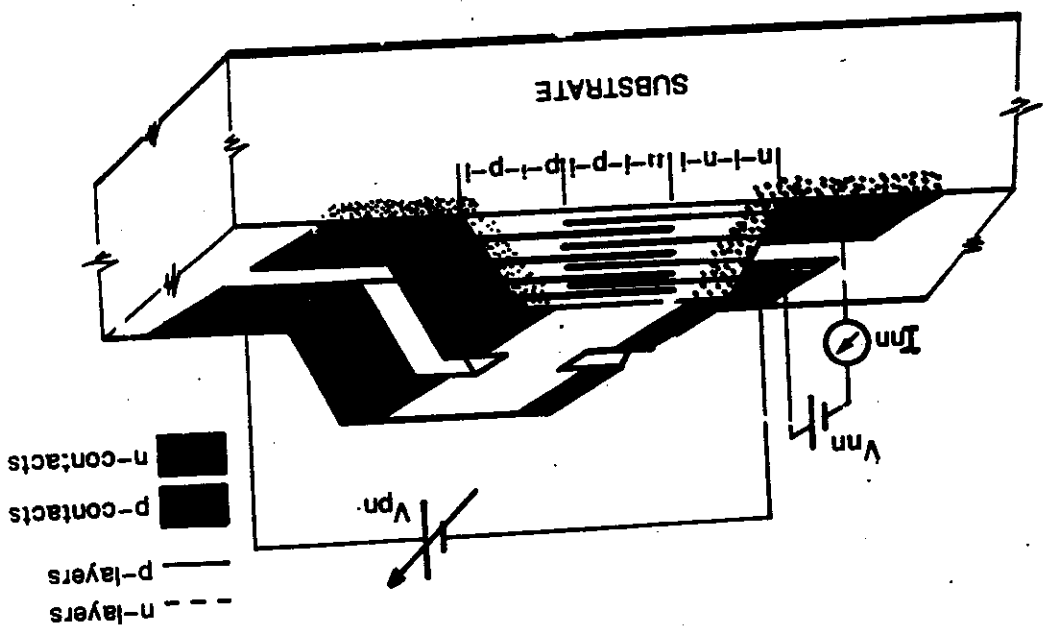

49

N. Linder
(paper 1286-32!

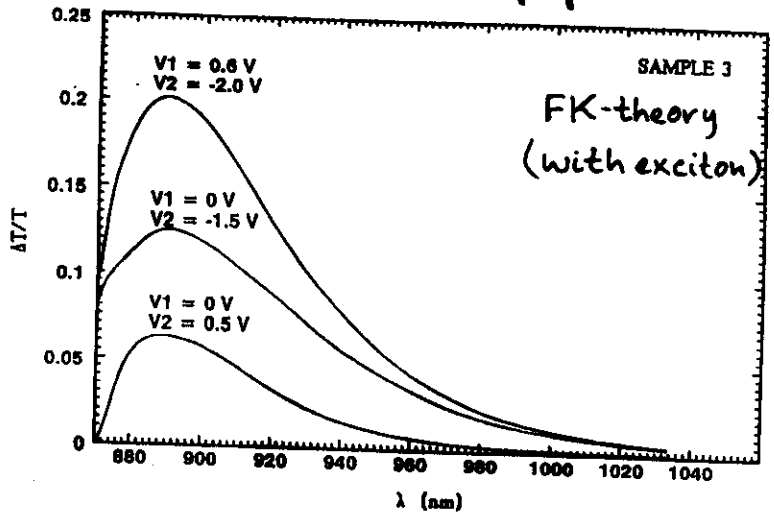

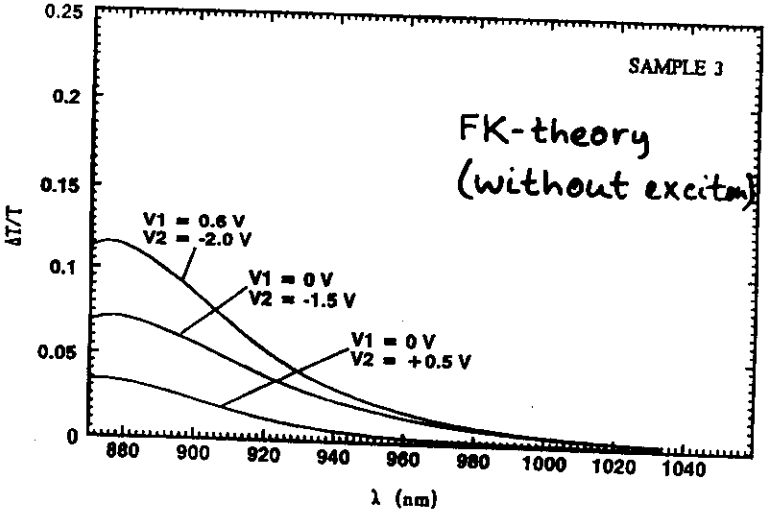

TUNNELING VS. THERM. ACTIVATED RECOMBINATION

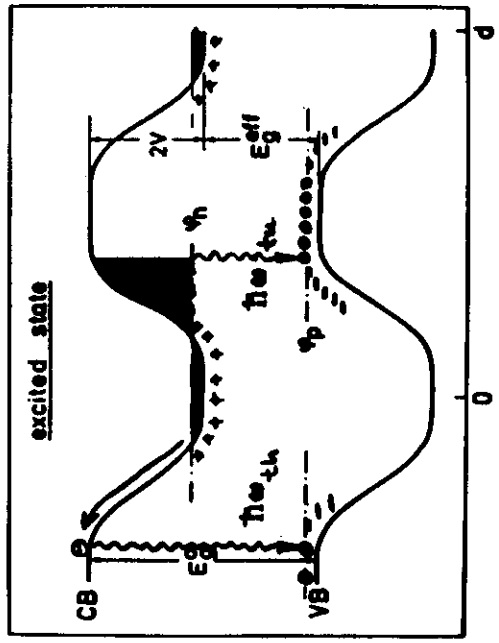

$$\frac{\tau^{nipi}_{thermal}}{\tau^{bulk}} \approx \exp[(E_0 - E_g^{eff})/kT]$$

$$\frac{\tau^{nipi}_{tunnel}}{\tau^{bulk}} \approx \exp[(E_0 - E_g^{eff})/\Delta]$$

$$\Delta \propto (n_D^{1/2}, n_A^{1/2})$$

⇒ tunneling recombination dominates, if $\Delta > kT$

St. Malzer
G. Mantel
M. Renn

$n_D = 4 \times 10^{18}\,cm^{-3}$; $d_n = 25\,nm$ $(d_i = 0)$
$n_A = 1 \times 10^{19}\,cm^{-3}$; $d_p = 35\,nm$

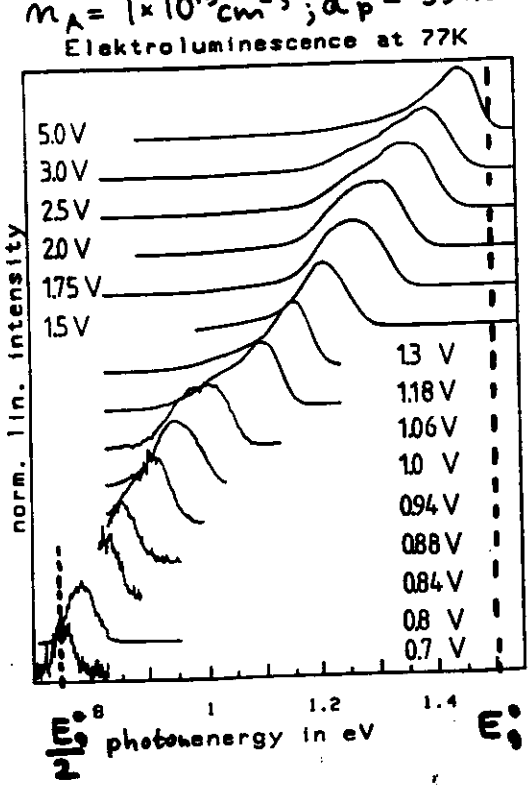

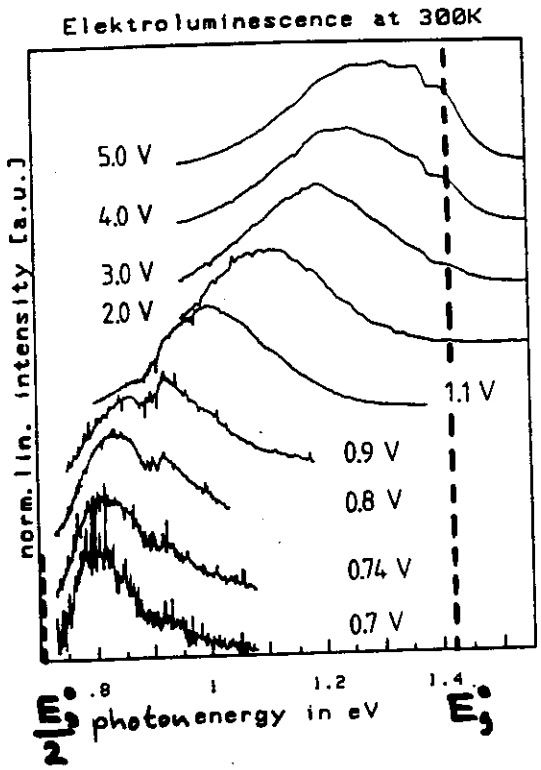

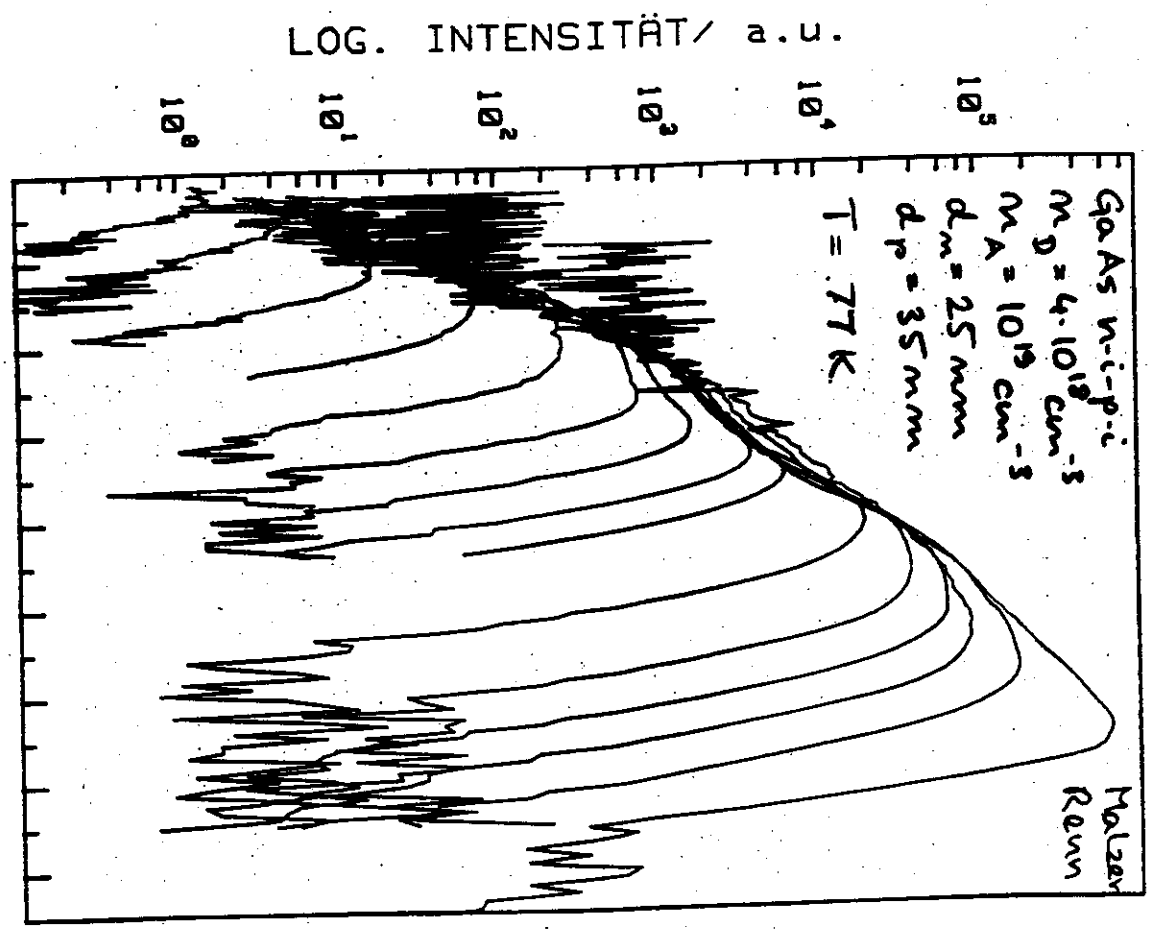

Electroluminescence

Type II hetero n-i-p-i

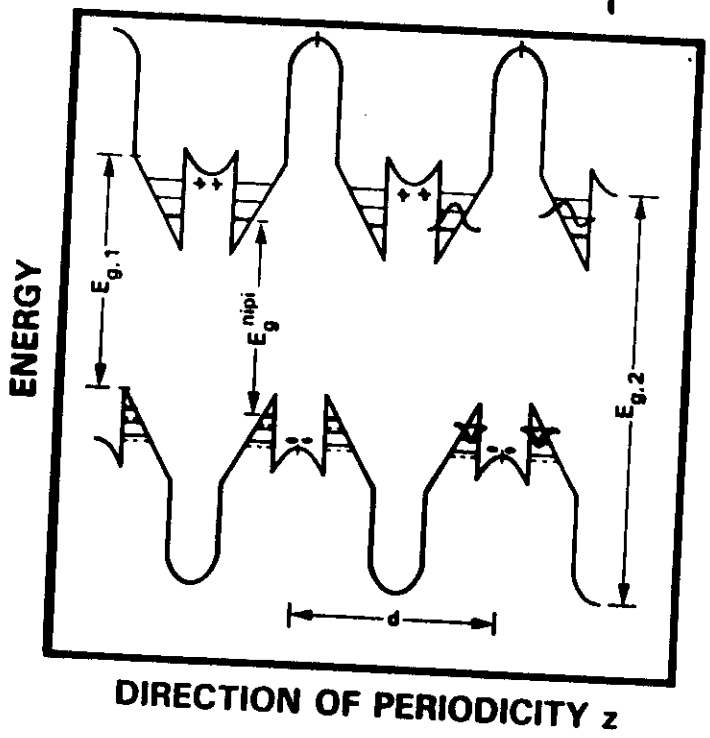

finite T:

$$\frac{I_{1;k0}}{I_{0;k0}} \propto \frac{N_c^{(i)} kT e^{-\frac{E_{c,1}-\varphi_n}{kT}} w_{1;k0}}{n^{(i)} w_{0;k0}}$$

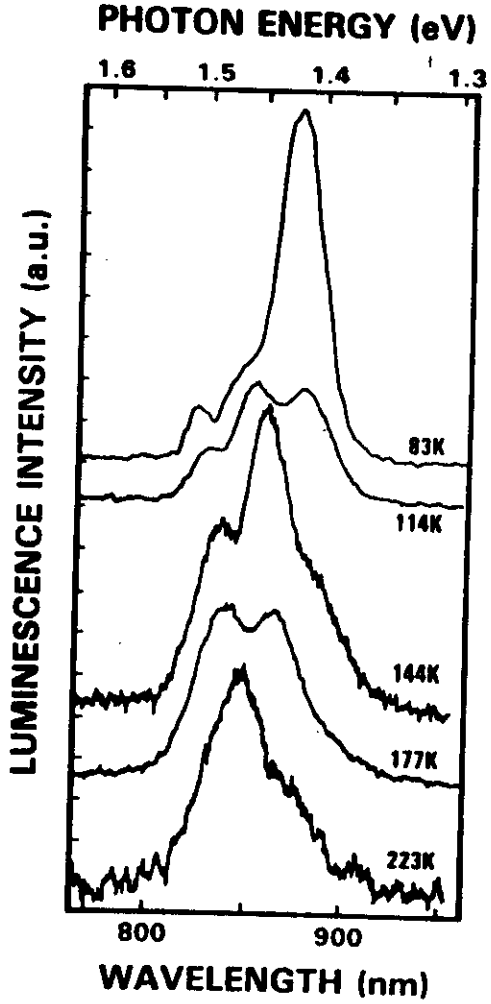

R.A. Street (Xerox), J.N. Miller, G.H.D.

opt. trans. prob. in Si-nipi

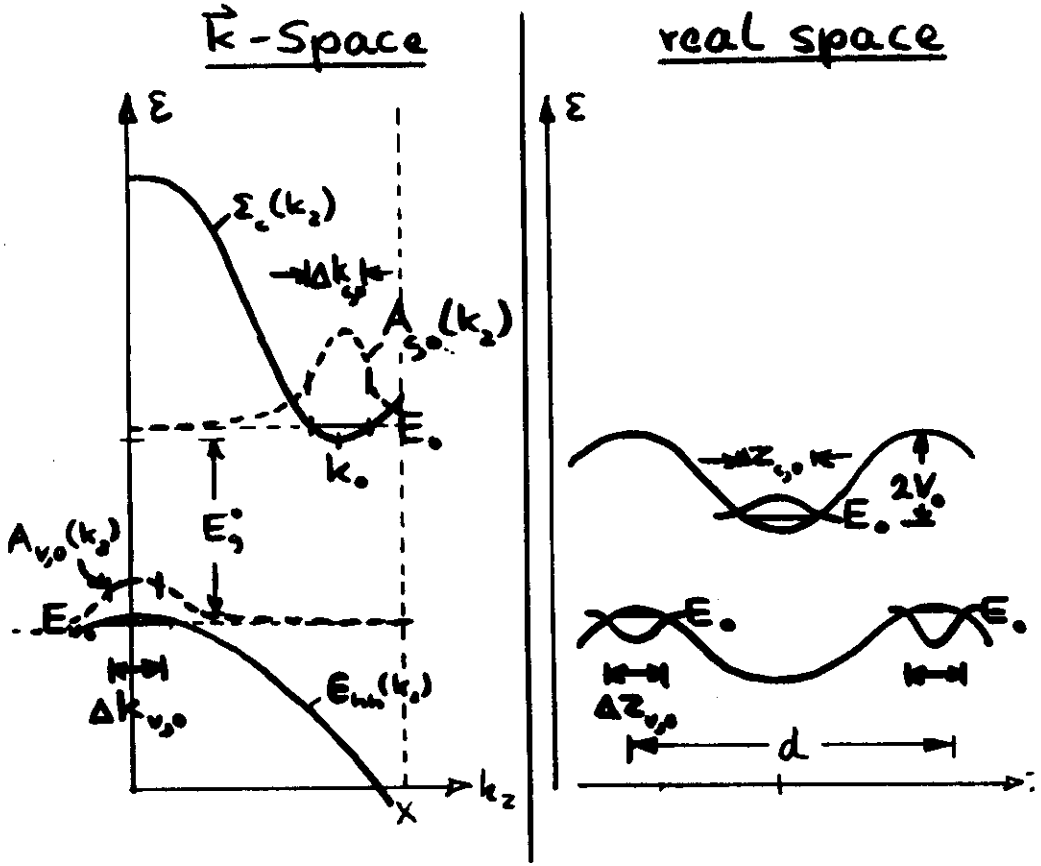

Effect of increasing doping level:

E_0 incr.

E_0 incr.

for $2V_0 \propto n_s d^2 = \text{const.}$

d decr.

$\Delta k_{c,0}, \Delta k_{v,0}$ incr.

overlap incr.

⇒ helps in k- and real space (no trade off!)

Luminescence intensity $\propto |\langle | \vec{p} | \rangle|^2$

In our case:

$$\langle c,\mu',\vec{k}_\parallel | \vec{p} | v,\mu,\vec{k}_\parallel \rangle$$

v-Block fct.

$$= \frac{1}{2\pi}\int dk_z A_{v,\mu}(\vec{k}) \varphi_{v,\vec{k}}(\vec{r})$$

$$\left[\frac{1}{2\pi}\int dk'_z A^*_{c,\mu'}(k'_z) \varphi^*_{c,\vec{k}}(\vec{r})\right]$$

c-Block-fct.

$$= \int dk'_z A^*_{c,\mu'}(k'_z) \int dk_z A_{v,\mu}(k_z) \underbrace{\langle c,\vec{k} | \vec{p} | v,\vec{k} \rangle}_{\text{bulk interband dipol matr. elem}} \delta(\vec{k}-\vec{k}$$

W1

n-i-p-i Doping Superlattices under High Magnetic Fields

Topic of this talk:

1) talked about for many years
2) barely worked on (J.C. Maan et al. ≃'8:
3) planned to think about more seriously for many years
4) started to think about more seriously just recently (perhaps too recently! (see workbook))
5) experiments planned
6) interesting:
   very large effects
   information on wave functions
   localized vs extended state
   metal-insulator transition in 2D
   Mott-Anderson
   Mott-Hubbard

W2

Effect of High Magnetic Fields on 2-D Systems

Without B-field:

3-D bulk $\Rightarrow$ 2-D QW

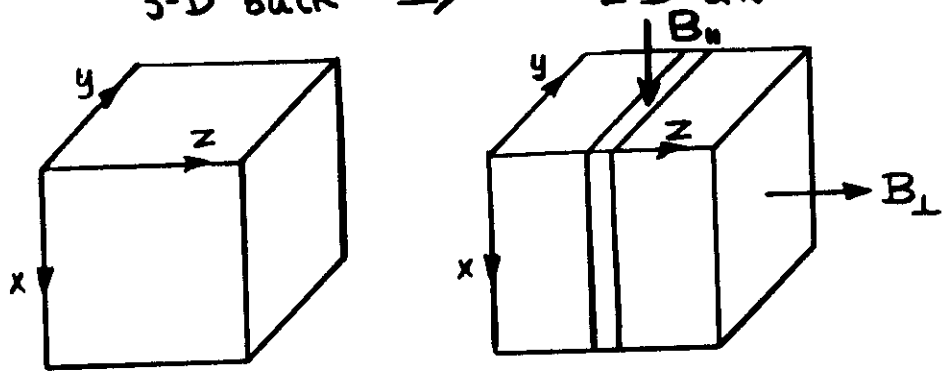

$\varepsilon(\vec{k}) \simeq \hbar^2 k^2/2m^* \Rightarrow \varepsilon_\mu(\vec{k}_\parallel) \simeq E_\mu + \hbar^2 k_\parallel^2/2m^*$

$\varphi_{\vec{k}}(\vec{r}) \simeq e^{i\vec{k}\vec{r}}\, u_0(\vec{r}) \Rightarrow \phi_{\mu,\vec{k}_\parallel}(\vec{r}) \simeq \xi_\mu(z) e^{i\vec{k}_\parallel \vec{r}_\parallel} u_0(\vec{r})$

With B-field:

$B_\perp$: fully quantized system

$$\left.\begin{matrix}\varepsilon_\mu(\vec{k}_\parallel) \\ \phi_{\mu,\vec{k}_\parallel}(\vec{r})\end{matrix}\right\} \Rightarrow \begin{cases}\varepsilon_{\mu m} \simeq E_\mu + \hbar\omega_c\left(m+\frac{1}{2}\right) \\ \phi_{\mu,m}(\vec{r}) \simeq \xi_\mu(z)\,\eta_m(x;k_y)\, e^{ik_y y} u_0(\vec{r})\end{cases}$$

$B_\parallel$: renormalization

$$\left.\begin{matrix}\varepsilon_\mu(\vec{k}_\parallel) \\ \phi_{\mu,\vec{k}_\parallel}(\vec{r})\end{matrix}\right\} \Rightarrow \begin{cases}\varepsilon^B_\mu(k_\parallel) \simeq E^B_\mu + \hbar^2 k_x^2/2m^* + \varepsilon(k_y) \\ \phi^B_{\mu,\vec{k}_\parallel}(\vec{r}) \simeq \xi^B_\mu(z;k_y)\, e^{i\vec{k}_\parallel \vec{r}_\parallel} u_0(\vec{r})\end{cases}$$

What is different in nipi's ?

W3
W7

B-field changes:

1) energies
2) wave functions

usually:
energy changes more important than changes of wave functions (unless: forbidden ⇒ allowed)

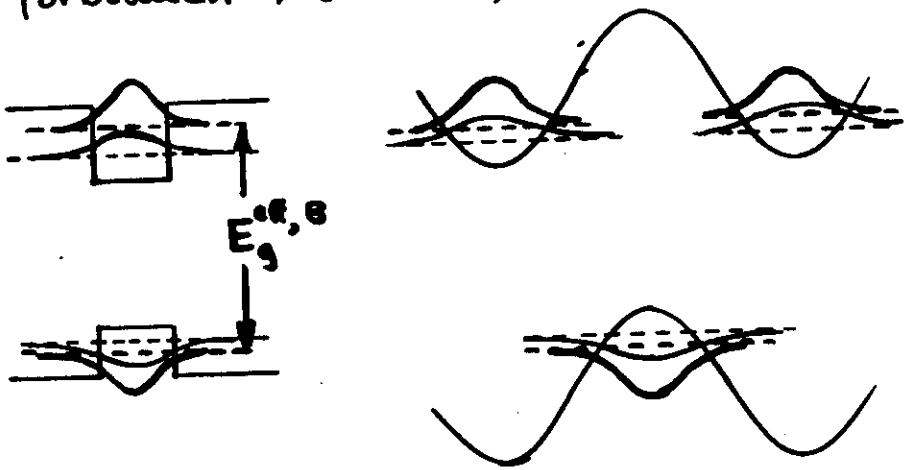

minor changes of matrix elements for interband trans.

huge changes of matrix elements for interband trans.

⇒ nipi = very sensitive tool to detect B-field induced changes of the wave fct.s

Example:

$n_D = n_A = 4\times10^{17}\,cm^{-3}$; $d_n = d_p = 25\,nm$ $\quad d_i = 0$

$\vec{B} = (B,0,0)$; $\vec{A} = (0,-zB,0)$; $k_y \neq 0$

$B = 15\,T$

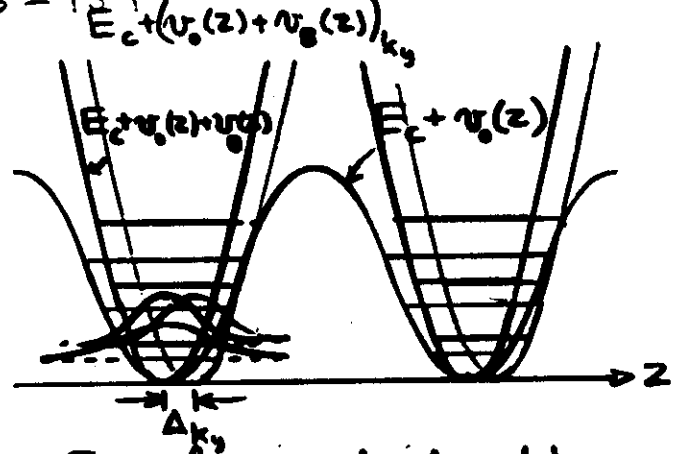

Schr. Equ. for conduct. subb. envel. fct.

$$\left\{\frac{p^2}{2m_e} + \underbrace{V_e(z)}_{\uparrow} + \underbrace{\frac{e^2B^2}{2m_e c^2}(z-\Delta_{k_y})^2}_{\frac{1}{2}m_e\omega_{c,e}^2}\right\} f_{c,\mu}(z) = E_{c,\mu}\, f_{c,\mu}$$

$$(2\pi e^2 n_D/\kappa_0)\, z^2 = \frac{m_e\omega_{p,e}^2}{2}(z\pm\Delta_{k_y})^2 \quad |z| <$$

$$\mathcal{E}_{c,\mu}(\vec{k}_{\parallel}) = E_c + \hbar\omega_e^B(\mu+\tfrac{1}{2}) + \frac{\hbar^2k_x^2}{2m_e} + \frac{\hbar^2k_y^2}{2m_e}\left(\frac{\omega_{p,e}}{\omega_e^B}\right)$$

$$\omega_e^{B2} = \frac{4\pi e^2 n_D}{\kappa_0 m_e} + \left(\frac{eB}{m_e c}\right)^2 = \omega_{p,e}^2 + \omega_{c,e}^2 = 2(2$$

$$f_{c,0}(z\ ) \propto e^{-\frac{m_e\omega_e^B}{2\hbar}(z-\Delta_{k_y})^2}$$

$$\Delta_{k_y} = \frac{\hbar k_y}{m_e}\frac{\omega_{c,e}}{(\omega_e^B)^2} = 4.5\,nm$$

$\uparrow k_y = k_{y,F}(n^{(2)} = 4\cdot10^{11}\,cm^{-2})$

interband Transition probability

$$w_{c\mu,v\nu} = w_{cv}^{bulk} \left| \int_0^d dz\, \xi_{c\mu}(z)\, \xi_{v\nu}(z) \right|^2$$

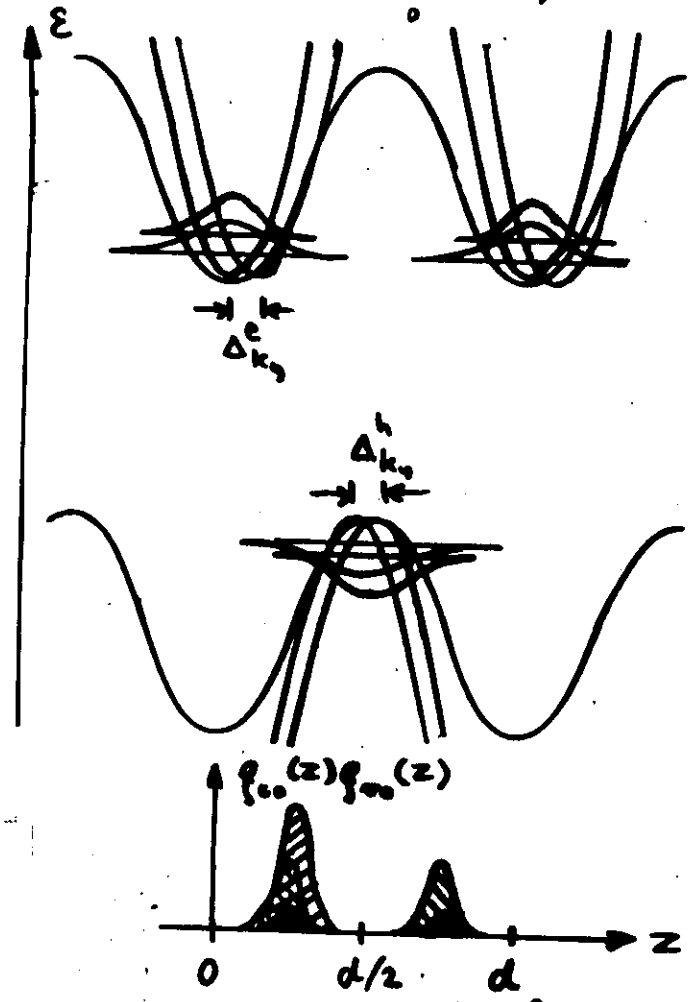

$$w_{c0,v0} = w_{cv}^{bulk}\, e^{-2(d/2)^2 m_e \omega_e/\hbar} = w_{cv}^{bulk} \cdot 5\times10^{-7}$$

$$w^B_{c0,v0} = w_{cv}^{bulk}\, e^{-2(d/2)^2 m_e \omega_e^B/\hbar} = w_{cv}^{bulk} \cdot 4\times10^{-9}$$

$$w^B_{c0,v0}(k_y) = w_{cv}^{bulk}/2\left[e^{-2(d/2-2\Delta_{k_y})\, m_e \omega_e^B/\hbar} + e^{-2(\quad+\quad)\cdots}\right.$$

$$= w_{cv}^{bulk} \cdot 1.5\cdot10^{-4} \;;\; k_\perp = k_\perp\,(n^{(2)} = 4\cdot10^{11}\,cm^{-2}$$

classical interpretation of Δ_{k_y}

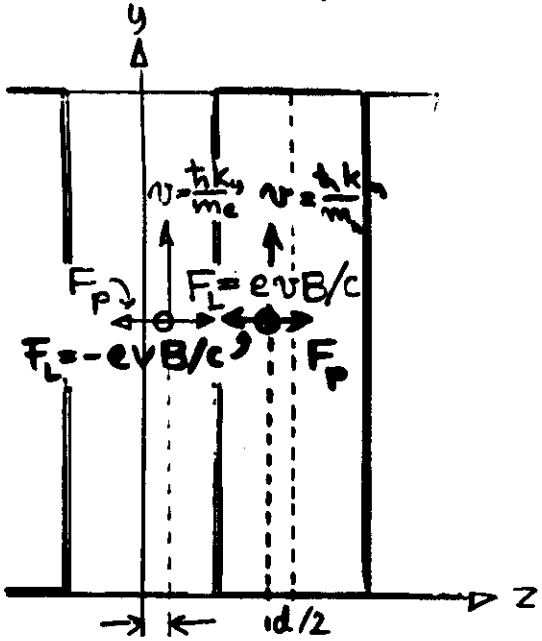

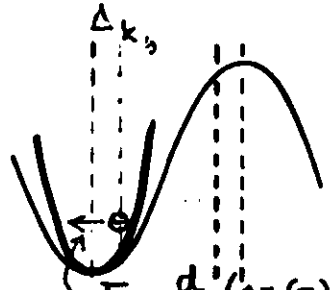

$$F_p = \frac{d}{dz}\left(v_0(z) + v_B(z)\right) = m_e(\omega_{p,e}^2 + \omega_{c,e}^2)\, z$$

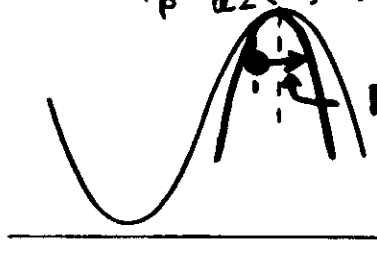

$$F_p = \frac{d}{dz}\left(v_0(z) + v_B(z)\right)$$

$$= m_e(\omega_{p,h}^2 + \omega_{c,h}^2)\, z$$

$$F_L = F_p \Rightarrow \begin{cases} \Delta_{k_y} = \dfrac{\hbar k_y}{m_e}\dfrac{\omega_{c,e}}{(\omega_e^B)^2} \\ \Delta_\perp = -\dfrac{\hbar k}{\quad}\dfrac{\omega_{c,h}}{\quad} \end{cases}$$

Dependence of interband transition probability on the momentum k_y

($d_n = d_p = 25\,nm$; $n_D = n_A = 4\cdot10^{17}\,cm^{-3}$; $B_x = 15\,T$)

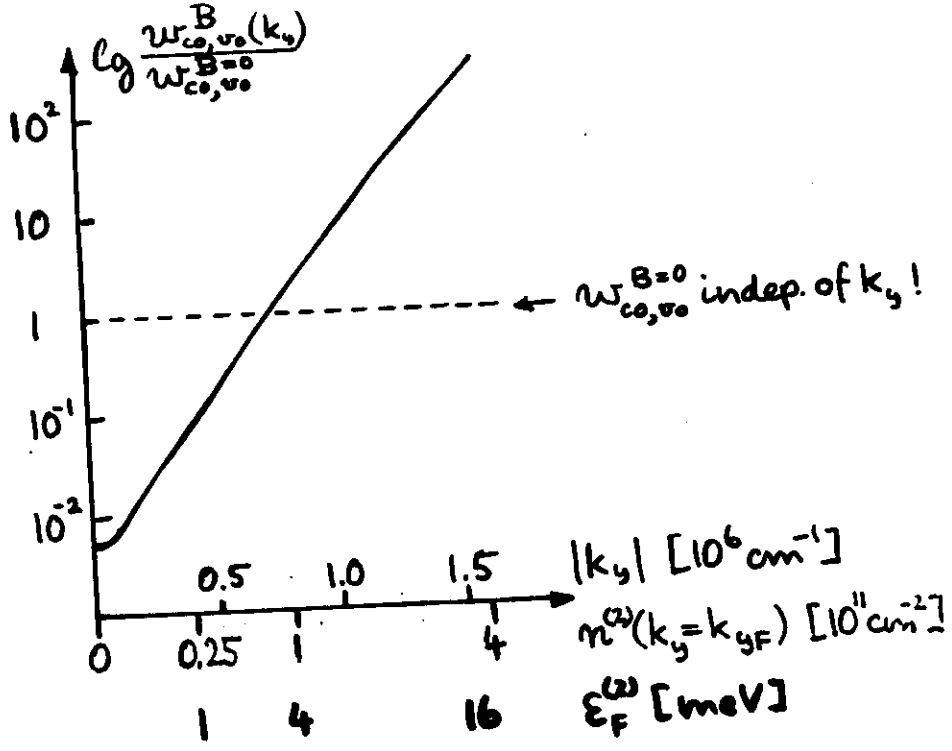

What happens to $\varphi_{c,\mu}(z)$ if k_y is no longer a good quantum number?

1) Disorder ⇒ Localized states in (xy)-plane

$$\phi^B_{c\mu,i}(\vec{r}) = \underbrace{\eta^B_{\mu i}(x,y)}_{\sum_{k_n} A^B_{\mu,i}(k_n)\, e^{i\vec{k}(\vec{r}_n - \vec{R}_i)}} \varphi^B_{c\mu}(z)\, u_c(\vec{r})$$

Question:

$\varphi^B_{c,0}(z) \simeq \varphi^B_{c,0}(z; k_y = 0)$ (no Lorentz force)

⇒ $w^B_{c_0,v_0}$ decreases strongly with B

or (?)

$\varphi^B_{c,0}(z)$ determined by the Fourier components $A^B_{\mu,i}(k_n)$ and, hence

$\varphi^B_{c\mu}(z) \Rightarrow \varphi^B_{c,\mu}(z; k_y)$

⇒ $w^B_{c_0,v_0}$ may even increase with B if the states are strongly localized

2) Due to additional $B_\perp$

Question:

$\varphi^B_{c,0}(z) \simeq \varphi^B_{c,0}(z; k_y = 0)$; for $m_z = 0$ (?)

$\varphi^B_{c,\mu}(z) \simeq$? ; for $m_z \neq 0$ (?)

$w^B_{c_0,v_0}$ decreases or increases (?)

Solid State Communications, Vol. 17, pp. 317–320, 1975. Pergamon Press. Printed in Great Britain

A NEW MECHANISM FOR NEGATIVE DIFFERENTIAL CONDUCTIVITY IN SUPERLATTICES*

G.H. Döhler,† R. Tsu, and L. Esaki

IBM Thomas J. Watson Research Center, Yorktown Heights, New York 10598, U.S.A.

(*Received* 10 *February* 1975 *by E. Burstein*)

Electrons in a superlattice at high fields are suitably described in terms of localized states related to the potential wells. Conduction is dominated by transitions between adjacent wells if the potential drop over a superlattice period exceeds the width of the lowest miniband. It is shown that the probability of these transitions, and consequently the current as well, decrease with increasing field. This effect originates from decreasing overlap between electron states of neighbouring wells, and it is found for the interaction with acoustic phonons and with impurities as well.

BY THE DEVELOPMENT of the computer-controlled molecular beam epitaxy it became possible to grow semiconductor crystals with one-dimensional superstructure having a period d of the order of 10^2 Å.[1] This large lattice constant and the resultant splitting of the bands into narrow minibands provide possibilities of observing a number of novel high field effects at moderate electric fields F:

(1) The Bloch frequency

$$\omega_B = eFd/\hbar \tag{1}$$

may exceed the inverse carrier relaxation time τ^{-1}, i.e.,

$$eFd/\hbar > \tau^{-1}. \tag{2}$$

Under this condition the average group velocity of the carriers decreases with increasing field and, consequently, negative differential conductivity (N.D.C.) appears.[2]

(2) When low multiples of the Bloch frequency coincide with the LO-phonon frequency ω_{LO}

$$neFd/\hbar = \omega_{LO},$$

there are peaks in the current due to electron phonon interaction with regions of N.D.C. in between.[3]

(3) The potential drop over a superlattice period can exceed the distance between the lowest and higher minibands $E^\nu - E^1$. Current peaks in interband tunneling[4,5] occur if

$$eFd \approx E^\nu - E^1. \tag{4}$$

In this paper we present a new mechanism for N.D.C. which results from another feature of superlattices. The potential drop over a lattice period eFd may exceed the bandwidth E_b of a miniband, i.e.

$$eFd > E_b. \tag{5}$$

Under this condition the current is dominated by transitions between localized states of adjacent wells. The current then decreases because of a decrease of the probability for these transitions whether phonon- or impurity-induced.

In the following we will assume E_b and eFd to be small compared with $\hbar\omega_{LO}$ and $E^2 - E^1$ thus excluding N.D.C. due to mechanisms (2) and (3). A description of the conduction in the momentum space, on which mechanism (1) is based, apparently becomes inappropriate (i) if the potential drop over a superlattice period exceeds the bandwidth, and / or (ii) if the mean free

* Research sponsored in part under ARO Contract, Durham, N.C.

† IBM World Trade Corporation Visiting Scientist, Permanent Address: Max-Planck-Institut für Festkörperforschung, Stuttgart, West Germany.

path Λ of a carrier without external field does not exceed appreciably the superlattice spacing d.

In these cases it is advantageous to describe the conduction in a local picture in terms of transitions between the localized states of neighbouring layers of the superlattice. The "free paths" in these cases are discrete, namely, low multiples of d. The expression for the current becomes[6]

$$|j| = n_0 ed \sum_{n=1}^{\infty} w_n(F, T)\{1 - \exp(-\beta n|eFd|)\}n. \quad (6)$$

$w_n(F, T)$ is the thermodynamically averaged probability for the transition of a carrier to the nth next potential well in field direction. n_0 is the carrier concentration in the miniband. The exponential term in (6) reflects the fact that motion against the field becomes negligible if $n|eFd| > kT$.

If the $w_n(F, T)$ were field independent, current would simply saturate for $F > kT/ed$. We will demonstrate, however, that the $w_n(F, T)$ decrease for $eFd > E_b$. This is sufficient for the appearance of N.D.C. In this high field case, condition (2) always holds. Hence, a description in terms of the proper electronic states at high fields, the so-called "Kane states"[7] $|m, \mathbf{k}_\perp\rangle$ is appropriate (m refers to the site $x = md$, $\mathbf{k}_\perp$ is the momentum perpendicular to the superstructure; see Fig. 1). The temperature averaged probability for transitions of electrons to the adjacent well by one phonon processes is given by[6]

$$w_1^{(ph)}(F, T) = \sum_{\mathbf{k}_\perp, \mathbf{k}'_\perp, q} f(\epsilon_{\mathbf{k}_\perp} - \mu)[1 - f(\epsilon_{\mathbf{k}'_\perp} - \mu)] \times \frac{2\pi}{\hbar} |\langle 1, \mathbf{k}'_\perp; n_q \pm 1|H_q^{e,ph}|0, \mathbf{k}_\perp; n_q\rangle|^2 \times \delta(\epsilon_{\mathbf{k}'_\perp} - \epsilon_{\mathbf{k}_\perp} - eFd \pm \hbar\omega_q) / \sum_{\mathbf{k}_\perp} f(\epsilon_{\mathbf{k}_\perp} - \mu). \quad (7)$$

The occupation probability f of the Kane states can be approximated by local equilibrium Fermi distributions

$$f(\epsilon_{\mathbf{k}_\perp} - \mu) = [\exp\{\beta(\hbar^2 \mathbf{k}_\perp^2/2m^* - \mu)\} + 1]^{-1} \quad (8)$$

if the energy relaxation by intralayer processes ($m' = m$) is fast compared to interlayer transitions ($m' \neq m$). This turns out to be justified always at high fields and sufficiently narrow minibands. Because of translational symmetry the distance between band edge and local Fermi level μ is independent of the site index.

Using a simple deformation potential approximation for the interaction with acoustic phonons[8]

$$H_q^{e,1a} = iC_1(|q|/2\rho c_s)^{1/2} \sum_{\mathbf{k},\mathbf{k}'} c_{\mathbf{k}'}^+ c_{\mathbf{k}}(a_q\langle \mathbf{k}'|e^{iqx}|\mathbf{k}\rangle - a_q^+\langle \mathbf{k}'|e^{-iqx}|\mathbf{k}\rangle), \quad (9)$$

one obtains for the matrix element in (7)[6]

$$\langle 1, \mathbf{k}'_\perp; n_q \pm 1|H_q^{e,1a}|0, \mathbf{k}_\perp; n_q\rangle = \frac{E_b}{eFd} \frac{iC_1|q|^{1/2}}{(2\rho c_s)^{1/2}} F(q_x)(n_q + \tfrac{1}{2} \pm \tfrac{1}{2})^{1/2} \delta_{\mathbf{k}'_\perp, \mathbf{k}_\perp \pm \mathbf{q}_\perp} \quad (10)$$

where $F(q_x)$ is an oscillating function with an amplitude decreasing $\propto (q_x d)^{-2}$ for $q_x \gg 2\pi/d$.

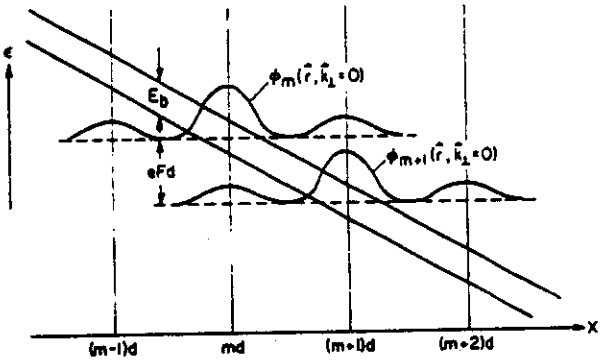

FIG. 1. Kane states $\phi_m(x, \mathbf{k}_\perp) = \langle x|m, \mathbf{k}_\perp\rangle$ at high fields, schematically. The probability for transitions between adjacent wells decreases with increasing field since the amplitude of $\phi_m(x, \mathbf{k}_\perp)$ at neighbouring wells decreases $\propto F^{-1}$. For the sake of clarity only Kane states with zero kinetic energy $\epsilon_{\mathbf{k}_\perp} = \hbar^2 \mathbf{k}_\perp^2/2m^*$ are shown.

The crucial point for the appearance of N.D.C. is the factor E_b/eFd in (10). This factor results from the decrease in overlap between Kane functions of neighbouring superlattice sites with increasing field (see Fig. 1). This is similar to the well-known decrease of overlap between the upper and the lower level in a system of two interacting, spacially separated states if the energies of the isolated states differ by more than the resonance splitting. The corresponding energies in our case are eFd and E_b, respectively.

The field dependence of $w_1^{ph}(F, T)$ from (7) is mainly determined by the factor F^{-2} from the square of the matrix element (10). The reasons are as follow:

REFERENCES

1. CHANG L.L., ESAKI L., HOWARD W.E., LUDEKE R. and SCHUL G., *J. Vac. Sci. Technol.* **10**, 655 (1973).
2. ESAKI L. and TSU R., *IBM J. Res. Dev.* 14, 61 (1970).
3. HACKER K., *Phys. Status Solidi* 33, 607 (1969); SAITOH M., *J. Phys.* C5, 914 (1972).
4. KAZARINOV R.F., and SURIS R.A., *Sov. Phys., Semicond.* 6, 120 (1972); TSU R. and ESAKI L., *Appl. Phys. Lett.* 22, 562 (1973).
5. ESAKI L. and CHANG L.L., *Phys. Rev. Lett.* 33, 495 (1974).
6. TSU R. and DÖHLER G.H. *Phys. Rev.* ~~B[illegible] (to be published)~~ 12, 680 (1975)
7. KANE E.O., *J. Phys. Chem. Solids* 12, 181 (1959).
8. KITTEL C., *Quantum Theory of Solids*, Chapter 7. Wiley, New York, London (1963).

(i) $|F(q_x)|^2$ from (10) represents a field independent cutoff for the q_x-integration;

(ii) the density of states for the $k_\perp$ and the $k'_\perp$-integration is energy independent;

(iii) the transverse momentum of the participating phonons $q_\perp$ increases with F, but less than $|q_\perp| \propto F^{1/2}$.

So far interlayer transitions induced by scattering of electrons at defects of the superlattice have not yet been considered. Though these elastic processes alone would not give rise to d.c.-conduction at all, they may even cause the dominant contribution in combination with successive inelastic intralayer phonon processes. Similar to expression (7), we get for the averaged first order contribution to the next layer transitions

$$w_1^{(e,D)}(F,T) = \sum_{k'_\perp,k_\perp} f(\epsilon_{k_\perp}-\mu)[1-f(\epsilon_{k'_\perp}-\mu)] \times |\langle 1,k'_\perp|V_j(x)|0,k_\perp\rangle|^2\,\delta\left(\frac{\hbar^2}{2m^*}(k_\perp^2-k_\perp'^2)-eFd\right) \Big/ \sum_{k_\perp} f(\epsilon_{k_\perp}-\mu). \tag{11}$$

The fluctuating part of the real superlattice potential has been split up into a sum of n_i independent scatterers with potentials $V_j(x-x_j)$. Thus, multiple scattering is neglected. For Coulomb-potentials with exponential screening corresponding to the average impurity distance, i.e.,

$$V_j(x-x_j) = \frac{4\pi e^2}{\kappa}\sum_q \frac{e^{iq(x-x_j)}}{q^2+\lambda^2} \tag{12}$$

with $\lambda = (4\pi n_i/3)^{1/3}$, e.g., the calculation yields a field dependence of the matrix element in (11) which tends to a F^{-2}-dependence at high fields. One factor F^{-1}, again, originates from the decreasing overlap. In addition to that, another factor F^{-1} appears, since the increasing momentum transfer $|q_\perp| = |k_\perp - k'_\perp|$ required for elastic processes by the δ-function in (11) reduces the scattering intensity according to (12).

Thus the contribution from transitions between adjacent layers whether due to the interaction with acoustic phonons or with impurities, indeed, leads to N.D.C. for $eFd > E_b, kT$. The investigation of transitions to more distant wells ($n \geqslant 2$) shows that in this range of fields their intensity decreases even with a higher power of F. Hence, their contribution to the current can be neglected in the high field region.

It should be noted that expression (6) for the current can be evaluated in terms of Kane states according to (7) and (11) for $eFd < E_b$ as long as (2) is still fulfilled. In this range of fields, transitions to more distant wells will become dominant, and the current will increase with decreasing field. This result is in accordance with the semiclassical treatment in terms of electrons performing Bloch oscillations.[2]

A case of particular interest in the view of our formulation is a superlattice with very low mobility. Transitions to other than the adjacent layers can be completely neglected in expression (6) for the current at low and high fields as well, if the low field mobility corresponds to the minimum possible mean free path, namely, $\Lambda = d$. The transition probability $w_1(F,T)$ will then be roughly constant at low field. At fields $eFd > E_b$ $w_1(F,T)$ will decrease according to (7) and (11) and N.D.C. will appear. The characteristic field at which deviations from ohmic behaviour become important is given by

$$eFd \simeq kT \tag{13}$$

because of the factor $\{1-\exp(-\beta|eFd|)\}$ in (6) (provided that $w(F,T)$ does not change too much in this range of fields). In contrast, the corresponding condition in the case of negative differential conduction resulting from Bloch-oscillations of the electrons is not related to the temperature, but rather to the momentum relaxation time τ_{k_x} by condition (2).

It should be pointed out that the N.D.C. mechanism described in this paper likely occurs at moderate fields in "tight binding superlattices" with narrow minibands. With narrowing the bandwidth the necessary condition for Bloch oscillations, that is, a mean free path should be longer than a superlattice constant, is hardly met.

(i) The maximum group velocity v_{max} in a miniban decreases proportionally with the bandwidth. The relaxation time τ, however, being dominated by intralayer processes is essentially constant. The mean free path, certainly less than $v_{max}\tau$, finally becomes smaller than d, even for an ideal superlattice.

(ii) Fluctuations in the thickness of neighbouring layers, which may be inevitable in a man-made superlattice, will cause some fluctuations in the bound state energies of the potential wells. In actual "tight binding superlattices" these fluctuations may be of the same order as the bandwidth itself. Under these circumstanc Bloch states do not exist anymore and the "free path" will be reduced to d.

PHYSICAL REVIEW B VOLUME 27, NUMBER 6 15 MARCH 1983

Electronic structure of semiconductors with doping superlattices

P. Ruden and G. H. Döhler
Max-Planck-Institut für Festkörperforschung, Heisenbergstrasse 1, D-7000 Stuttgart 80, Federal Republic of Germany
(Received 6 August 1982)

The dynamically two-dimensional electronic subband structure and the effective energy gap are tunable quantities in semiconductors with a doping superlattice. We present self-consistent calculations of the electronic states, in the framework of the local-density approximation, as a function of the charge-carrier concentration. A discussion of several superlattices differing in their design parameters exemplifies the wide range of electronic subband structures which may be realized in this type of system.

I. INTRODUCTION

During the last two years a number of experimental investigations have been performed on a new type of artificial semiconductor superlattice consisting of ultrathin *n*- and *p*-type doped layers, which were in some cases separated by undoped (*i*-) intrinsic layers (*n-i-p-i-* crystals).[1–3] The experiments have confirmed the crucial predictions concerning the novel electronic properties of this new class of semiconductors made by one of the present authors (G.H.D.) a long time ago.[4–6] This author had pointed out that doping (or *p-n* junction) superlattices would differ qualitatively not only from homogeneous semiconductors but also from compositional superlattices[7–9] (or heterojunction superlattices) because of the different superlattice potentials. In doping superlattices the conduction and valence bands are modulated by the periodic space-charge potential of the impurities. As a consequence the electron states near the bottom of the conduction band are shifted in their position by half a superlattice period with respect to electron states near the top of the valence bands (*indirect gap in real space*). Compositional superlattices with opposite sign of the conduction- and valence-band—edge discontinuities of the components (type-I superlattices,[7–9]) such as the $Al_xGa_{1-x}As/GaAs$ system, in contrast, exhibit a *direct gap in real space.* Heterojunction superlattices with equal sign for conduction- and valence-band—edge discontinuities between the constituent materials such as the GaSb/InAs system (type-II superlattices[8,9]) also have an indirect gap in real space. The overlap between electron and hole states, however, is still quite large in those systems. Therefore, they do not possess the following basic features of doping superlattices, which result from a very small overlap between electron and hole states.

(1) Owing to extremely long excess-carrier lifetimes, large deviations of the carrier concentrations from the thermal equilibrium values can be induced by rather weak optical excitation or carrier injection from outside.

(2) Because of the spatial separation of electrons and holes the compensating charge of the excess carriers decreases the amplitude of the space-charge—induced superlattice potential and thus increases the effective energy gap drastically. The effective gap of doping superlattices is thus no longer a fixed parameter of the system, but a quantity which may be tuned by changing the nonequilibrium electron and hole concentrations.

The interesting quantum-size effects (quasi-two-dimensional subband formation) which have been the major point of interest in the study of compositional superlattices are present in doping superlattices also. It is evident that the tunability of the (two-dimensional) carrier concentration and of the effective band gap makes the latter kind of superlattice a more fascinating model substance for the study of two-dimensional many-body effects.

In a recent Letter[1] the soundness of the theoretical concept was demonstrated by the observation of a tunable band gap in photoluminescence measurements and of tunable subband separations in Raman scattering experiments. Moreover, excellent quantitative agreement with our self-consistent calculations of the electronic subband structure was found. The first purpose of this paper is to show a more detailed presentation of these calculations including a discussion of many-body effects. Secondly, we will illustrate by a few examples the wide variety of tunable subband structures obtained by different choices of design parameters including the case of a

 ©1983 The American Physical Society

n-i-p-i crystal in which the composition is also modulated periodically (*n-i-p-i* heterojunction superlattice). Finally, we want to provide a basis for our forthcoming discussion of absorption, luminescence, and inelastic light scattering.[10]

II. THEORY OF ELECTRONIC SUBBANDS IN *n-i-p-i* CRYSTALS

A *n-i-p-i* crystal consists of an arbitrary homogeneous semiconductor with a periodic variation of *n*- and *p*-type doping,

$$n_D(z+d)=n_D(z) \quad \text{and} \quad n_A(z+d)=n_A(z)\ , \tag{1}$$

where z is the direction of periodicity and d the superlattice period.

The ground state of the *n-i-p-i* crystal can be described quite easily if there are no other impurities present than the shallow donors and acceptors, if the crystal is "macroscopically compensated," i.e.,

$$\int_{-d/2}^{d/2} n_D(z)dz = \int_{-d/2}^{d/2} n_A(z)dz\ , \tag{2}$$

and if the superlattice period and the doping concentration do not exceed some limiting values to be discussed below. Under these conditions all the impurities will be ionized and the superlattice potential will be the space-charge potential of the impurity distribution,

$$\rho_0(z)=e[n_D(z)-n_A(z)]\ . \tag{3}$$

For the sake of simplicity we will restrict ourselves in the following to the case of homogeneous doping as shown in Fig. 1(a) with rectangular doping profiles which are symmetric with respect to the origin placed in the middle of an *n*-type doped layer.

The space-charge potential of the impurities $v_0(z)$ is obtained by integrating Poisson's equation,

$$\frac{\partial^2 v_0(z)}{\partial z^2}=4\pi e\rho_0(z)/\kappa_0\ , \tag{4}$$

subject to the boundary conditions,

$$\left.\frac{\partial v_0(z)}{\partial z}\right|_{z=0},\quad v_0(0)=0 \tag{5}$$

where κ_0 is the static dielectric constant of the semiconductor. $v_0(z)$ consists of parabolic parts in the doping layers,

$$v_0(z)=\begin{cases}(2\pi e^2 n_D/\kappa_0)z^2 & \text{for } |z|\le d_n/2\\ 2V_0-(2\pi e^2 n_A/\kappa_0)(d/2-|z|)^2 & \text{for } d/2-|z|\le d_p/2\ ,\end{cases} \tag{6}$$

and linear parts in the intrinsic regions,

$$v_0(z)=(2\pi e^2 n_D d_n/\kappa_0)(|z|-d_n/4) \quad \text{for } d_n/2\le|z|\le(d-d_p)/2\ . \tag{7}$$

The maximum height of $v_0(z)$ is $2V_0$, given by

$$2V_0=(2\pi e^2/\kappa_0)(n_D d_n^2/4+n_A d_p^2/4+n_D d_n d_i)\ . \tag{8}$$

For $|z|\ge d/2$, $v_0(z)$ is obtained from a periodic repetition of the expressions (6)—(8).

Figure 1(b) shows the important consequences of the superposition of $v_0(z)$ to the crystal potential. The effective band gap E_g^{eff}, i.e., the difference between the lowest conduction- and the uppermost valence-band states, is lowered by about $2V_0$ compared with the gap of the homogeneous bulk material E_g^0. (Deviations which result from quantum-size effects and from impurity-band formation will be discussed later.) The term *indirect gap in real space* which was used in the Introduction now becomes clear: The lowest conduction-band states are shifted by half a superlattice period with respect to the uppermost valence-band states.

It should be noted that the value of $2V_0$ may exceed the band gap E_g^0 of the unmodulated semiconductor. Such a situation implies the possibility of conduction subbands with energies lower than the upper valence subband edge, which would correspond to a negative effective band gap E_g^{eff}. Actually, under these conditions there will be a finite-electron and -hole concentration in the *n*- and *p*-type layers in the ground state. The compensating space charge of the charge carriers reduces the value of $2V_0$ and changes the shape of the space-charge potential in a self-consistent way to be calculated later. The ground state will then be characterized by electron and hole concentrations $n_0^{(2)}$ and $p_0^{(2)}$ per layer which make the Fermi level equal for both types of carriers (*n-i-p-i* semimetal).

Another case with a finite-carrier concentration in the ground state occurs whenever the *n-i-p-i* crystal is not compensated, i.e., condition (2) does not hold. The ground-state superlattice potential, evidently, has to be calculated self-consistently in such a situation also.

As mentioned in the Introduction, one of the

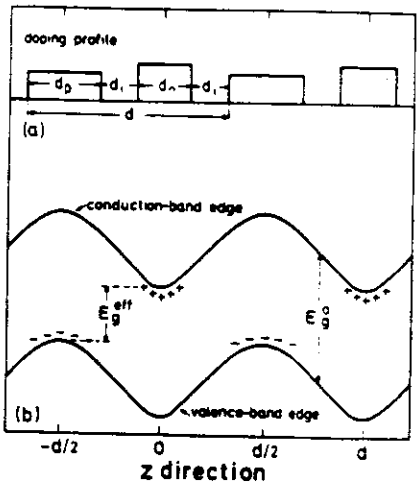

FIG. 1. *n-i-p-i* crystal with constant impurity concentration in the *n*- and *p*-type layers. (a) Periodic doping profile and (b) modulation of conduction- and valence-band edge by the periodic space-charge profile $v_0(z)$ from (6) and (7). Plus signs indicate ionized donor levels near the conduction-band edge and minus signs indicate the negatively charged acceptor levels above the valence-band edge. The effective gap E_g^{eff} is an indirect gap in real space. It differs from the gap of the homogeneous bulk material E_g^0 roughly by $2V_0$ as given by Eq. (8). Corrections to E_g^{eff} due to subband- and impurity-band formation are not shown in this schematic picture.

peculiarities of *n-i-p-i* superlattices is the possibility to induce metastable deviations from thermal equilibrium with different electron and hole quasi-Fermi-levels ϕ_n and ϕ_p, by varying of the electron and hole concentration in the layers. Thus the calculation of the electronic structure of a *n-i-p-i* crystal is not to be restricted to the ground state. The subband energies and wave functions are required as a function of the tunable-carrier concentration.

Before we solve the Schrödinger equation for a *n-i-p-i* crystal we will at least comment on some of the simplifying assumptions which we have made in our calculation of the impurity space-charge potential. So far, and also in the numerical calculations to be discussed, we have treated the space charge of the impurities as homogeneously smeared out in the respective doping regions. In doing so we have neglected the following:

(1) the spatial potential fluctuations which result from the random distribution of impurities in the doped regions and

(2) the point-charge character of the impurities which may lead to bound impurity states or to the formation of impurity bands.

These two points, indeed, limit the possibility to observe quantum-size effects in space-charge–induced potential wells and occasionally were used in the past as an argument against the existence of well-defined quasi-two-dimensional subbands in this kind of system.[11]

Without going into a detailed discussion of this rather complex problem we want to make plausible in the following that in GaAs doping superlattices,

(1) the influence of potential fluctuations is reasonably small,

(2) donor impurity bands may be neglected, and

(3) the formation of acceptor impurity bands must be considered within the typical range of values of design parameters of *n-i-p-i* crystals.

Long-range potential fluctuations are screened by a small concentration of free electrons in the *n*-type layers (holes in the *p*-type layers). Thus they will be unimportant if at least a certain fraction of the impurity space charge per layer is compensated by free carriers. The short-range potential fluctuations result mainly from the random nearest-neighbor impurity distances, which deviate from the mean value r_I (we use the subscripts I to indicate that the following is valid for donors as well as for acceptors). These fluctuations may be estimated by calculating the value of the unscreened Coulomb energy $e^2/\kappa_0 r_I$ of a point charge at distance $r_I \doteq [4\pi/(3n_I)]^{1/3}$. For any reasonable statistical distribution of the impurities the width of the distribution will have roughly the value of the average. The numerical value of $e^2/\kappa_0 r_I$ increases from 15 to 32 meV within the range $5\times10^{17}\ \text{cm}^{-3} \le n_I \le 5\times10^{18}\ \text{cm}^{-3}$ with $\kappa_0 = 12.5$ for GaAs, which is always smaller than the corresponding subband energies. It is clear that the screening by the charge carriers in the layers will actually reduce the potential fluctuation.

The importance of impurity bands may be estimated by the following argument. Let us consider a regular simple cubic array of n_I shallow impurities with ionization energy E_I, Bohr radius a_I, and nearest-neighbor distance $\bar{r}_I = n_I^{-1/3}$. The impurity bandwidth would be approximately $12E_I \exp(-\bar{r}_I/a_I)$ in a tight-binding picture.

A different approach would be based on the nearly-free-electron model. Here the kinetic energy at the Brillouin-zone boundary becomes

$$\epsilon(\pi/\bar{r}_I) \approx (\hbar^2/2m^*)\pi^2 n_I^{2/3} . \tag{9}$$

A rough estimate of the band splitting is

$$2V(2\pi/\bar{r}_I) \approx e^2/\kappa_0 \bar{r}_I = e^2 n_I^{1/3}/\kappa_0 . \tag{10}$$

The tight-binding picture is appropriate for $\bar{r}_I \gg a_I$ whereas the nearly-free-electron model suits the case $\epsilon(\pi/\bar{r}_I) \gg 2V(2\pi/\bar{r}_I)$. With an experimental value for the ionization energy of shallow donors in GaAs $E_D \simeq 6$ meV which corresponds to a Bohr radius, $a_D \simeq 10$ nm, and using $m^* = 0.067 m_0$ we get

$\epsilon(\pi/\bar{r}_D) > 2V(2\pi/\bar{r}_D)$ for $n_D > 10^{16}$ cm^{-3}. Thus even the unscreened impurity potentials act as a relatively small perturbation at donor concentrations which are typical for *n-i-p-i* crystals. Therefore impurity-band formation in the case of the conduction band can be neglected, and it is allowed to replace the actual donor space charge by a homogeneous space charge of density $en_D(z)$ for the calculation of $v_0(z)$ as given in Eqs. (6)—(8).

On the other hand, for the acceptors we find (because of the larger heavy-hole effective mass m^{hh}) a Bohr radius $a_A \simeq 1.8$ nm so that $\bar{r}_A > a_A$ for $n_A < 10^{20}$ cm^{-3} and $\epsilon(\pi/\bar{r}_A) > 2V(2\pi/\bar{r}_A)$ only if $n_A > 2\times 10^{19}$ cm^{-3} using $m^{hh} = 0.6m_0$. Thus we can expect an impurity band in the *p*-type layers of a *n-i-p-i* structure unless n_A is extremely high. This result does not signify that hole subbands do not exist in the *p*-type layers or that they are unimportant. The presence of an acceptor impurity band implies, however, important consequences for the calculation of the self-consistent potential. The population of the acceptor impurity band by holes is equivalent to a neutralization of the negatively charged acceptors. It is, therefore, a reasonably good approximation to consider the central part of width $d_p^0 = p^{(2)}/n_A$ in the *p*-type layers as neutral, if $p^{(2)}$ holes per layer are present in the sample.

We will now proceed by discussing the electronic subband structure in the *n*-type layers in the framework of the local-density-functional formalism of Hohenberg and Kohn[12] and Kohn and Sham.[3] Together with the effective-mass approximation[14] this formalism leads to a Schrödinger-type equation of the form

$$[-(\hbar^2/2m^e)\nabla^2 + v_0(z) + v_H(z) + v_{xc}(z)]\psi_{\mu\vec{k}}(\vec{r}) = \epsilon_{\mu\vec{k}}\psi_{\mu\vec{k}}(\vec{r}) . \quad (11)$$

Since the potential does not depend on x or y and is periodic in z with the periodicity d we can write for the wave functions

$$\psi_{\mu\vec{k}}(\vec{r}) = (1/\sqrt{A})\exp(i\vec{k}_{||}\cdot\vec{r}_{||})\xi_{\mu k_z}(z) , \quad (12)$$

where $\vec{k}_{||}$ is a wave vector parallel to the doping layers. A is the normalization area and $\xi_{\mu k_z}(z)$ is the superlattice Bloch function of subband μ and wave vector k_z $(-\pi/d \le k_z < \pi/d)$, with the lattice periodic part $u_{\vec{k}=0}(\vec{r})$ neglected. For the eigenvalues $\epsilon_{\mu\vec{k}}$ we thus get

$$\epsilon_{\mu\vec{k}} = \epsilon_{\mu k_z} + (\hbar^2 k_{||}^2/2m^e) , \quad (13)$$

and the Bloch functions $\xi_{\mu k_z}(z)$ and the eigenvalues $\epsilon_{\mu k_z}$ are to be determined self-consistently from

$$\left[-\left[\frac{\hbar^2}{2m^e}\right]\left[\frac{\partial^2}{\partial z^2}\right] + v_0(z) + v_H(z) + v_{xc}(z)\right]\xi_{\mu k_z}(z) = \epsilon_{\mu k_z}\xi_{\mu k_z}(z) . \quad (14)$$

The Hartree contribution of the electrons to the self-consistent potential is given by the solution of Poisson's equation

$$\frac{\partial^2 v_H(z)}{\partial z^2} = -\frac{4\pi e^2 n(z)}{\kappa_0} , \quad (15)$$

subject to the boundary conditions

$$\left.\frac{\partial v_H(z)}{\partial z}\right|_{z=0} = 0, \quad v_H(0) = 0 \quad (16)$$

with the electron density

$$n(z) = 2\sum_{\mu\vec{k}} |\xi_{\mu k_z}(z)|^2 \times \Theta(\phi_\mu - \epsilon_{\mu k_z} - (\hbar^2 k_{||}^2/2m^e) - E_c) . \quad (17)$$

E_c is the energy of the bottom of the conduction band at $z=0$.

The local exchange and correlation potential is obtained from

$$v_{xc}(z) = \epsilon_{xc}(n(z)) + n(z)(\delta\epsilon_{xc}/\delta n) , \quad (18)$$

where $\epsilon_{xc}(n)$ is the exchange and correlation energy per electron of a homogeneous electron gas of the (local) density n. Since the electronic densities of interest in *n-i-p-i* crystals are usually very high, i.e., the mean distance between two electrons is short compared to the effective-mass Bohr radius $a_D^{EMA} = a_B\kappa_0(m_0/m^e)$, we will take

$$-\epsilon_{xc} = -\epsilon_x = (0.916/r_s)(e^2/2\kappa_0 a_D^{EMA}) \quad (19)$$

with

$$r_s = [4\pi/(3n)]^{1/3}/a_D^{EMA} . \quad (20)$$

The inclusion of higher-order correlation terms does not affect the results appreciably. The contribution of the holes in the *p*-type layers to the self-consistent potential is not written explicitly since it can be incorporated into $v_0(z)$, as discussed above.

In most cases of interest only the lowest electronic subbands are partially occupied. For these low subbands and typical doping parameters an extreme tight-binding approach is correct, i.e., the subbands are flat in the k_z direction. The Bloch function can be written as

$$\xi_{\mu k_z}(z)=(1/\sqrt{N_{\mathrm{SL}}})\sum_m \exp(ik_z m_d)\Phi_\mu(z-md)\ , \tag{21}$$

where N_{SL} is the number of superlattice periods in the crystal and $\Phi_\mu(z-md)$ is the wave function of subband μ centered at the n-type layer with label m. Obviously, the square modulus of $\xi_{\mu k_z}(z)$ is in this case independent of k_z, and the electron density may be written as

$$n(z)=\sum_\mu n_\mu^{(2)}\,|\,\xi_{\mu 0}(z)\,|^2 N_{\mathrm{SL}} \tag{22}$$

$$=\sum_{\mu,m} n_\mu^{(2)}\,|\,\Phi_\mu(z-md)\,|^2\ , \tag{23}$$

where the population $n_\mu^{(2)}$ of the μth subband is determined by the requirement of equal Fermi levels in occupied subbands,[15]

$$\epsilon_\mu+(\hbar^2/2m^*)2\pi n_\mu^{(2)}=\epsilon_0+(\hbar^2/2m^*)2\pi n_0^{(2)} \tag{24}$$

with

$$\sum_{\mu_{\mathrm{occ}}} n_\mu^{(2)}=n^{(2)}\ . \tag{25}$$

We have solved Eq. (14) self-consistently by direct numerical integration at $k_z=0$ and $k_z=\pi/d$. The boundary conditions to be imposed are as follows: for $\mu=0,2,4,\ldots,$

$$\left.\frac{\partial\xi_{\mu 0}(z)}{\partial z}\right|_{z=0}=\left.\frac{\partial\xi_{\mu,\pi/d}(z)}{\partial z}\right|_{z=0}=0\ , \tag{26}$$

$$\left.\frac{\partial\xi_{\mu 0}(z)}{\partial z}\right|_{z=d/2}=0,\quad \xi_{\mu,\pi/d}(d/2)=0\ , \tag{27}$$

and for $\mu=1,3,5,\ldots,$

$$\xi_{\mu 0}(0)=\xi_{\mu,\pi/d}(0)=0\ , \tag{28}$$

$$\xi_{\mu 0}(d/2)=0,\quad \left.\frac{\partial\xi_{\mu,\pi/d}(z)}{\partial z}\right|_{z=0}=0\ . \tag{29}$$

Some n-i-p-i crystal subbands with a finite k_z dispersion may become occupied in the very highly excited state. It is then usually sufficient to calculate the potential once with the wave functions associated with $k_z=0$ and once with those at $k_z=\pi/d$ and then to average.

III. RESULTS AND DISCUSSION

We have solved the system of Eqs. (14)–(25) self-consistently, taking into account the boundary conditions (26)–(29) and averaging over occupied bands, if necessary as mentioned above, for different n-i-p-i crystals, including n-i-p-i heterojunction superlattices. To illustrate the variety of electronic structures obtainable with different design parameters of the system we present results for a structure without intrinsic layers (Figs. 2–4), for an extreme n-i-p-i structure with thin doping layers and rather wide intrinsic layers (Figs. 5–7) and, finally, for a n-i-p-i heterojunction superlattice composed of a periodic n-p-type doping structure with undoped layers of a smaller band-gap material interspersed in the middle of the n-type layers (Figs. 8 and 9). To facilitate the comparison of these systems we have kept one parameter fixed, namely, the superlattice constant d. We would like to emphasize the dependence of the subband structure on the shape of the doping profiles.

As the first structure we have chosen the sample for which we have compared quantitative results with experiments in Ref. 1. It is composed of 40-nm-thick GaAs layers with constant doping concentrations $n_D=n_A=10^{18}$ cm^{-3} and does not contain intrinsic layers. In Fig. 2 the solid lines represent the energies for the bottom of the various subbands referred to the position of the hole quasi-Fermi-level ϕ_p as a function of the two-dimensional carrier concentration per layer. We have assumed that ϕ_p coincides with the acceptor level in the central part of the p-type layers (acceptor ionization energy $E_A=28$ meV for Be acceptors).

It should be noted that the curve $\phi_n-\phi_p$ vs $n^{(2)}$ (dashed-dotted line) does not deviate appreciably from a parabola with a vertex at $n^{(2)}=n_D d_n=4\times10^{12}$ cm^{-2}. This behavior reflects the parabolic relation between injected carriers and the quasi-Fermi-level distance $\phi_n-\phi_p$ which would be obtained from a simple classical treatment of the problem.

At $n^{(2)}=0$ all the subbands shown are nearly equally spaced with

$$\epsilon_\mu-\epsilon_{\mu-1}=\hbar[4\pi e^2 n_D/(\kappa_0 m^*)]^{1/2}$$

since the bare potential $v_0(z)$ deviates appreciably from a harmonic potential only at higher energies. With increasing carrier concentration the subband distances decrease monotonously as the shape of the self-consistent potential

$$v_{\mathrm{sc}}(z)=v_0(z)+v_H(z)+v_{\mathrm{xc}}(z) \tag{30}$$

flattens and broadens due to screening of the fixed-impurity space charge (see Fig. 3). In order to show the behavior of the subbands, in particular the finite width of the upper bands at large carrier concentrations, the subband energies are displayed more clearly once more in Fig. 2 as an inset on an expanded energy scale and with the maximum of $v_{\mathrm{sc}}(z)$, i.e.,

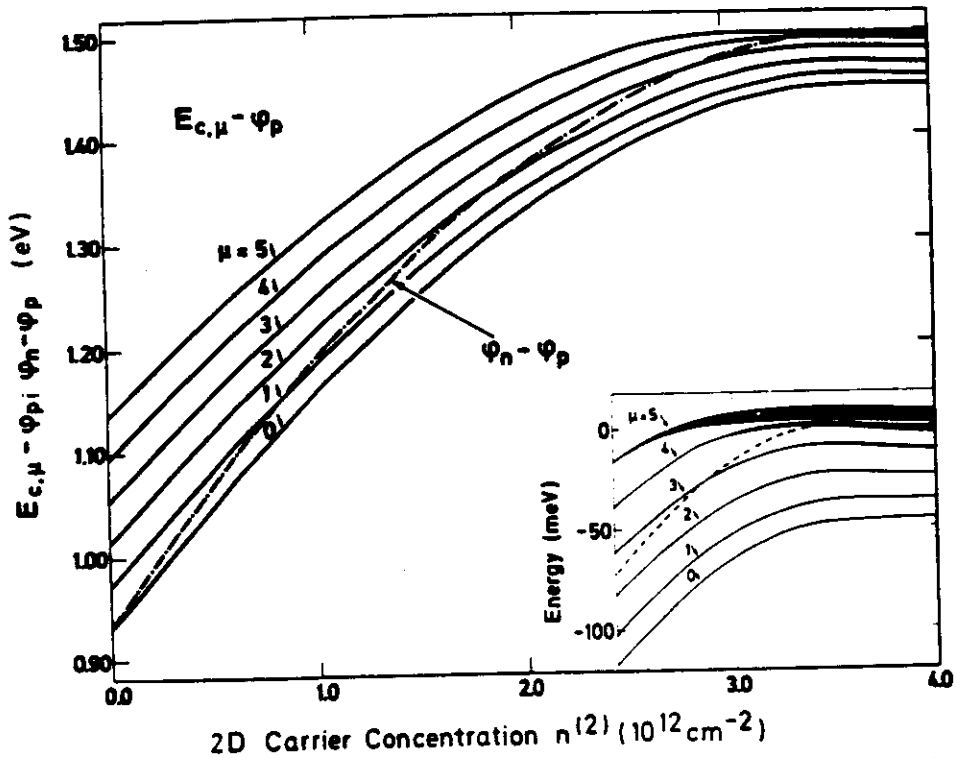

FIG. 2. Subband energies and a quasi-Fermi-level as a function of the electron concentration per period $n^{(2)}$ for a doping superlattice with constant doping $n_D=n_A=1\times10^{18}$ cm^{-3} in the n- and p-type layers, respectively, and with $d_n=d_p=40$ nm and $d_i=0$. $E_{c,\mu}=E_c+\epsilon_\mu$, the bottom of the μth conduction subband, and ϕ_n, the electron quasi-Fermi-level, are referred to the position of the hole quasi-Fermi-level ϕ_p in the acceptor impurity band. The inset shows the same subbands for large values on $n^{(2)}$ on an expanded energy scale and with the maximum of the self-consistent potential chosen as zero. The finite subband width due to the k_z dispersion becomes appreciable near zero energy, which corresponds to the classical free-particle threshold energy.

the classical free-particle threshold as the zero of energies. The band*width* becomes appreciable only when the energies nearly reach this threshold. For energies above the threshold, however, the subband *gap* becomes rather narrow. Thus the subbands

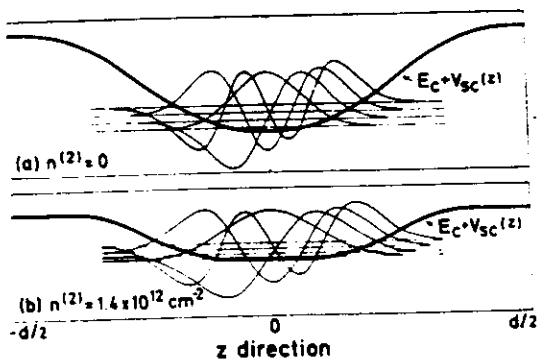

FIG. 3. Self-consistent potential $v_{xc}(z)$ (thick solid line), conduction-subband energies, and envelope wave functions for one period of a superlattice with the same design parameters as in Fig. 2. (a) Ground state ($n^{(2)}=0$) and (b) excited state ($n^{(2)}=1.4\times10^{12}$ cm^{-2}).

change their character from tight-binding to nearly-free-electron behavior within a few meV. This is to be expected because of the wide barrier between neighboring quantum wells. Another detail which should be noted is the position of ϕ_n at $n^{(2)}=4\times10^{12}$ cm^{-2} (which corresponds classically to a neutralization of all donors and acceptors by electrons and holes, respectively), which is found to be only slightly above the threshold energy. This means that the electrons almost exactly fill up to the top the self-consistent potential well formed by the impurity charges and the free carriers together.

Figure 4 demonstrates the influence of $v_{xc}(z)$ on the subband splitting. For $n^{(2)}>10^{11}$ cm^{-2} the difference between the results with $v_{xc}(z)$ taken into account (solid lines) and the Hartree energies (dotted lines) remains nearly constant and relatively small compared to exchange and correlation corrections in Si metal-oxide-semiconductor structures. The nearly constant exchange and correlation contribution is a consequence of the fact that the electron distribution $n(z)$ only widens with increasing $n^{(2)}$ but does not appreciably increase in height which is close to

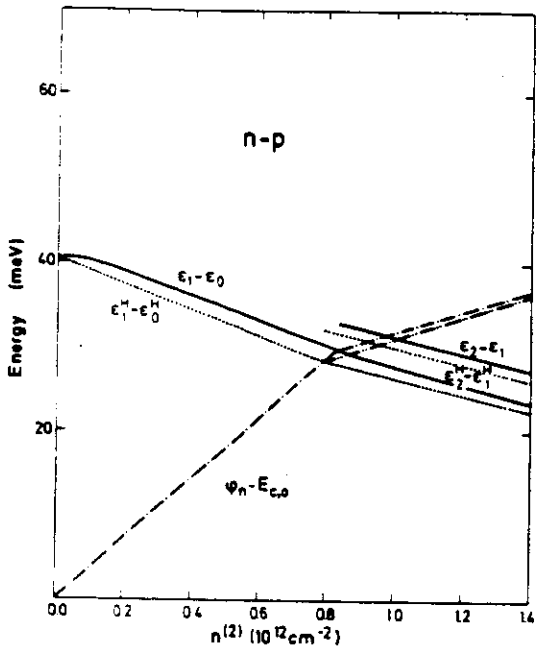

FIG. 4. Comparison of the subband splitting between occupied and the nearest-neighbor subbands for low carrier concentrations calculated with (solid lines) and without (dotted lines) exchange and correlation corrections. The dashed-dotted and dashed-double-dotted lines represent the Fermi energy of the lowest subband $\phi_n - E_{c,0}$ for the case with and without exchange and correlation corrections. The design parameters are those of Fig. 2.

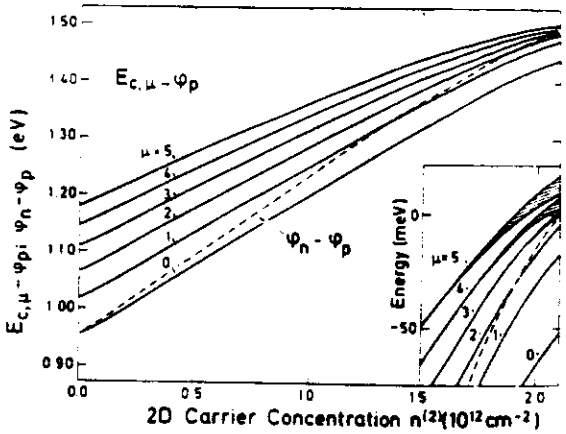

FIG. 5. Subband energies and a quasi-Fermi-level as a function of the electron concentration per period $n^{(2)}$ for a *n-i-p-i* superlattice with the design parameters $n_D = n_A = 5.25\times10^{18}$ cm^{-3} and $d_n = d_p = 4$ nm, $d_i = 36$ nm. $E_{c,\mu} = E_c + \epsilon_\mu$, the bottom of the μth conduction subband, and ϕ_n, the electron quasi-Fermi-level, are referred to the position of the hole quasi-Fermi-level ϕ_p in the acceptor impurity band. The inset shows the same subbands for large values of $n^{(2)}$ on an expanded energy scale and with the maximum of the self-consistent potential chosen as zero. The finite subband width due to the k_z dispersion becomes appreciable near zero energy which corresponds to the classical free-particle energy.

n_D over a layer of the width $n^{(2)}/n_D$.

The corresponding results for a *n-i-p-i* structure with very thin doping layers of only 4 nm and a thickness of 36 nm for the intrinsic layers are given in Figs. 5–7. The doping concentration $n_D = n_A = 5.25\times10^{18}$ cm^{-3} has been chosen such that the effective gap has approximately the same value for $n^{(2)}=0$ as in the former case. From Fig. 5 we see that the subband distances are now larger at small μ values and that they decrease at higher μ since the bare potential $v_0(z)$ has a triangular rather than a parabolic shape. The relation between $\phi_n - \phi_p$ and $n^{(2)}$ is quite close to a linear dependence because of the wide nearly constant field zones in the intrinsic layers. The subband spacing also decreases with increasing $n^{(2)}$. In contrast to the former case, however, the relative decrease is weaker and affects the higher subbands more than the lower ones: $\epsilon_1-\epsilon_0$ decreases only by 1/1.8 between $n^{(2)}=0$ and $n^{(2)}=n_D d_n$ compared to 1/4.3 in the former case. $\epsilon_2-\epsilon_1$, however, decreases now faster than $\epsilon_1-\epsilon_0$, namely by 1/4.2, whereas the corresponding decrease of $\epsilon_2-\epsilon_1$ by 1/3.5 was less pronounced for the first example. The two cases exemplify that it is possible to tailor details of the subband structure and of the relation between $\phi_n-\phi_p$ and $n^{(2)}$ simply by an appropriate choice of the design parameters n_D, n_A, d_n, d_p, and d_i, or by even going one step further and changing from zones of constant doping to continuous doping profiles $n_D(z)$ and $n_A(z)$.

The variation of the bandwidth near the classical free-particle threshold energy is less abrupt for the

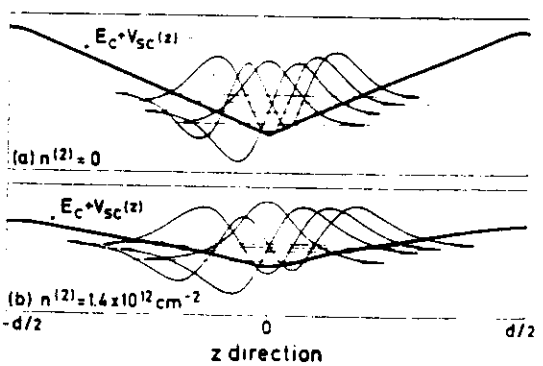

FIG. 6. Self-consistent potential $v_{sc}(z)$ (thick solid line), conduction-subband energies, and envelope wave functions for one period of a superlattice with the same design parameters as in Fig. 5. (a) Ground state ($n^{(2)}=0$) and (b) excited state ($n^{(2)}=1\times10^{12}$ cm^{-2}).

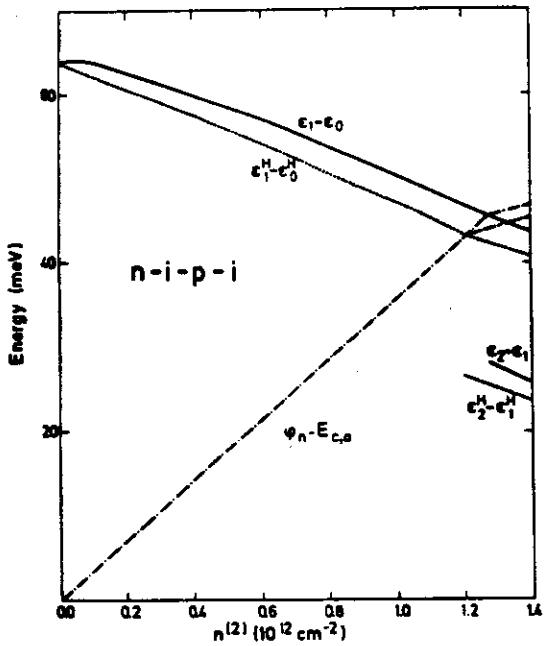

FIG. 7. Comparison of the subband splitting between occupied and nearest-neighbor subbands for low carrier concentrations calculated with (solid lines) and without (dotted lines) exchange and correlation corrections. The dashed-dotted and dashed-double-dotted lines represent the Fermi energy of the lowest subband $\phi_n - E_{c,0}$ for the case with and without exchange and correlation correction. The design parameters are those of Fig. 5.

n-i-p-i case with wide intrinsic layers than for the first example (compare the corresponding insets in Figs. 2 and 5), due to the smaller width of the zone with maximum barrier height (see Figs. 6 and 3 for a comparison).

Finally, a comparison of the exchange and correlation shift as depicted in Fig. 7 for the genuine *n-i-p-i* sample with the corresponding results for the sample without intrinsic layers shows that not only the absolute value of the $\epsilon_1 - \epsilon_0$ subband spacing is increased but even the relative importance of the exchange and correlation correction is larger. The result becomes plausible if we consider that in the present case the lowest subband wave function is less extended in the z direction for a given carrier concentration $n^{(2)}$. The resulting larger local density lowers the self-consistent potential in this region. Therefore the energy of the ϵ_0 band is lowered considerably, whereas the much more extended ϵ_1 band is much less affected by the exchange and correlation correction.

Our last example is a *n-i-p-i* heterojunction crystal consisting of *n*- and *p*-type doped layers of $Al_{0.2}Ga_{0.8}As$ with a layer thickness of $d_n = 20$ nm, $d_p = 40$ nm, and doping concentrations $n_D = 2 \times 10^{18}$ cm^{-3}, $n_A = 1 \times 10^{18}$ cm^{-3}. The *n*-type layers are separated into two layers (of thickness $d_n/2$) by an intrinsic GaAs layer of thickness $d_{GaAs} = 20$ nm.

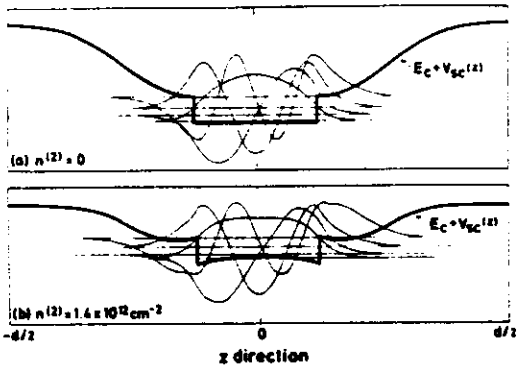

FIG. 8. Self-consistent potential $v_{sc}(z)$ (thick solid line), conduction-subband energies, and envelope wave functions for one period of an $Al_{0.2}Ga_{0.8}As/GaAs$ *n-p* heterojunction superlattice with the design parameters $n_D = 2 \times 10^{18}$ cm^{-3}, $n_A = 10^{6}$, cm^{-3}, $d_n = 20$ nm, $d_p = 40$ nm, $d_i = 0$, $d_{GaAs} = 20$ nm. (a) Ground state ($n^{(2)} = 0$) and (b) excited state ($n^{(2)} = 1.4 \times 10^{12}$ cm^{-2}). The discontinuity in the potential reflects the transition from *n*-type doped $Al_{0.2}Ga_{0.8}As$ to undoped GaAs. The *p*-type layers do not contain GaAs layers in this example.

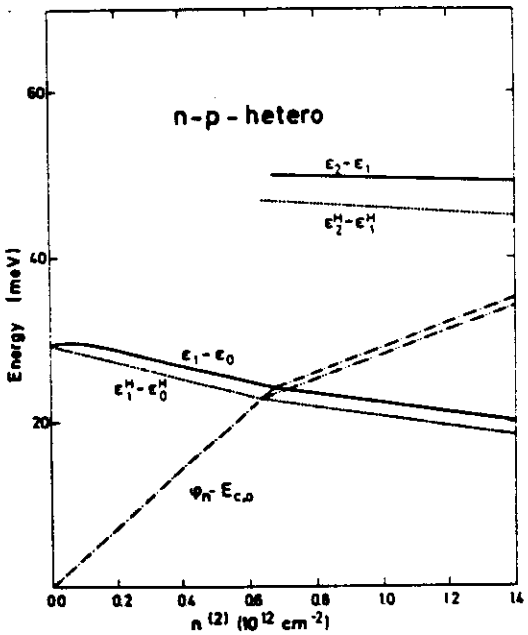

FIG. 9. Comparison of subband splitting between occupied and nearest-neighbor subbands for low carrier concentrations calculated with (solid lines) and without (dotted lines) exchange and correlation corrections. The dashed-dotted and dashed-double-dotted lines represent the Fermi energy of the lowest conduction subband $\phi_n - E_{c,0}$ for the case with and without the exchange and correlation correction. The design parameters are those of Fig. 8.

This system thus provides an example of a semiconductor superlattice whose subband structure in the ground state is determined by the doping parameters, the width of the GaAs layer, and the Al content of the $Al_xGa_{1-x}As$ alloy. Through its dependence on the variable carrier concentration $n^{(2)}$ the subband structure may be tuned over a wide range as in normal *n-i-p-i* crystals. This is not the case in the modulation doped heterojunction superlattices (the dependence of the subband structure on the electron concentration shown in Fig. 5 of Ref. 14 corresponds to a variation of the doping parameters and not to change in a tunable charge carrier concentration). The dependence of $E_{c,\mu}-\phi_p$ on $n^{(2)}$ is quite similar to the results of the first example and is, therefore, not shown here. It is interesting to consider the subband spacing as a function of $n^{(2)}$ because of the different nature of the quantum wells (Fig. 9). The spatial extent of the wave functions is now determined by the width of the GaAs layer (Fig. 8), whereas in the case of the space-charge–induced quantum wells it varied from one subband to another and changed appreciably as a function of $n^{(2)}$. Consequently, the subband energies are less dependent on the carrier concentration in a *n-i-p-i* heterojunction crystal. A remarkable result is the relatively large difference in the exchange and correlation corrections for the $\epsilon_1-\epsilon_0$ and the $\epsilon_2-\epsilon_0$ subband separations.

IV. CONCLUSIONS

We have shown that the subband structure and the effective band gap in *n-i-p-i* crystals can be tuned by variation of the nonequilibrium carrier concentration. Our discussion was exemplified by three systems with very different design parameters to show how the subband structure and its dependence on $n^{(2)}$ can be tailored within wide limits. The *n-i-p-i* heterojunction superlattice, in particular, may become of interest in the future because of the high electron mobility in the GaAs layers and the weak broadening of the subbands due to statistical potential fluctuations. These features will be more pronounced when the GaAs layers are separated from the doped $Al_xGa_{1-x}As$ layers by an intrinsic $Al_xGa_{1-x}As$ space layer as is the practice in normal modulation doped multiple–quantum-well structures.[16]

We have not discussed the hole subbands. Their calculation is quite straightforward as the self-consistency problem is a trivial one if the holes populate the acceptor impurity band. The only problem would be the coupling between light- and heavy-hole states due to the space-charge potential. The solution of this problem may, however, be of academic interest only, since the subband structure of the heavy holes may be broadened too much by random potential fluctuations in order to be detectable. In a planned subsequent paper we will, however, provide examples showing that the light-hole subbands will be relevant for the observation of a steplike structure in the optical-absorption coefficient.

We have restricted our discussion to semiconductors with a band structure of the GaAs type. Obviously, some of our results would change dramatically if, e.g., a many-valley band structure of the host material were considered.

[1]G. H. Döhler, H. Künzel, D. Olego, K. Ploog, P. Ruden, H. J. Stolz, and G. Abstreiter, Phys. Rev. Lett. 47, 864 (1981).
[2]G. H. Döhler, H. Künzel, and K. Ploog, Phys. Rev. B 25, 2616 (1982).
[3]H. Künzel, G. H. Döhler, A. Fischer, and K. Ploog, Appl. Phys. Lett. 38, 171 (1981).
[4]G. H. Döhler, Phys. Status Solidi B 52, 79 (1972).
[5]G. H. Döhler, J. Vac. Sci. Technol. 16, (3),851 (1979).
[6]G. H. Döhler and K. Ploog, Prog. Cryst. Growth Charact. 2, 145 (1979).
[7]L. Esaki and R. Tsu, IBM J. Res. Dev. 14, 61 (1970).
[8]G. A. Sai-Halasz, in *Proceedings of the 14th International Conference on the Physics of Semiconductors, Edinburgh, 1978*, edited by B. L. H. Wilson (IOP, Bristol, 1978).
[9]T. Ando, A. Fowler, and F. Stern, Rev. Mod. Phys. 54, 2 (1982), and references therein.
[10]P. Ruden and G. H. Döhler, Phys. Rev. B 27, 3547 (1983).
[11]Comments made by several colleagues in previous discussions with one of the authors (G.H.D.).
[12]P. Hohenberg and W. Kohn, Phys. Rev. 136, B864 (1964).
[13]W. Kohn and L. Sham, Phys. Rev. 140, A1133 (1965).
[14]Subband-structure calculations using this type of approach have, e.g., been carried out for $Al_xGa_{1-x}As$/GaAs superlattices by T. Ando and S. Mori, J. Phys. Soc. Jpn. 47, 1518 (1979).
[15]G. H. Döhler, Surf. Sci. 73, 97 (1978).
[16]H. L. Störmer, A. Pinczuk, A. C. Gossard, and W. Wiegmann, Appl. Phys. Lett. 38, 681 (1981).

PHYSICAL REVIEW B VOLUME 30, NUMBER 10 15 NOVEMBER 1984

Theory of absorption in doping superlattices

Gottfried H. Döhler* and Peter Paul Ruden†
Max-Planck Institut für Festkörperforschung, Heisenbergstrasse 1, D-7000 Stuttgart 80, Federal Republic of Germany
(Received 9 April 1984)

The absorption due to transitions between valence and conduction subbands in doping superlattices is calculated analytically and numerically. Results for various materials and design parameters of the superlattice configuration are presented for illustration. It is found that with an appropriate choice of design parameters the absorption coefficient exhibits a pronounced steplike structure for photon energies less than the band gap of the host material. The absorption of a given specimen is strongly tunable by external fields, by carrier injection, and by the generation of carriers due to the absorption process itself. At fixed photon energy, large-amplitude oscillations of the absorption coefficient as a function of both the external electric field and the induced carrier concentration are predicted. The limitations of our approach, and consequences of our results for interesting applications, are discussed briefly.

I. INTRODUCTION

Doping (n-i-p-i) superlattices are a periodic array of n- and p-type doped layers which may be separated by undoped (i-) layers of the same semiconductor material. They represent a new class of synthetic semiconductors.[1–4] The most striking features by which they differ from their compositional counterparts[5,6] (e.g., GaAs-$Al_xGa_{1-x}As$ or InAs-GaSb superlattices), and from any homogeneous bulk semiconductor, is the strong tunability of their electronic structure and, consequently, of the resulting electrical and optical properties.[7–13] This tunability originates from an efficient spatial separation of electrons and holes, which is induced by the space-charge potential of the impurities. In addition to the tunability, i.e., the possibility of modulating the properties of a given specimen by applying external potentials[8,12] or light radiation,[7,9,11,13] the n-i-p-i systems exhibit an extreme flexibility with respect to the tailoring of their electronic structure. Any semiconductor, which can be n and p doped, can be used as host material for the n-i-p-i structure, in contrast to the compositional superlattices, where the requirement of lattice matching severely restricts the choice of materials. Furthermore, any value of the effective band gap $E_g^{\text{eff},0}$ of the n-i-p-i crystal in the ground state that is smaller than the gap of the host material, E_g^0, can be generated by an appropriate choice of the design parameters, i.e., the doping concentration and the thickness of the layers. Similarly, the efficiency of the spatial separation of electrons and holes depends on the choice of the design parameters.[10] Finally, the two-dimensional subband structure can be tailored independently for electrons and holes, again due to their spatial separation.[14]

During the last few years intensive experimental studies on GaAs n-i-p-i crystals, grown by molecular-beam epitaxy (MBE),[15] have confirmed a large number of properties which were predicted in theoretical investigations, started by one of us (G.H.D.) more than a decade ago.[1,2] Simultaneously, the theory has been worked out in more detail.[14,16] The tunable optical absorption which will be the subject of the present paper has also been studied theoretically and experimentally in a previous investigation.[11] The superlattice period in that particular case was chosen to be rather large, such that a theoretical description in terms of a semiclassical treatment (spatially modulated internal Franz-Keldysh effect) was appropriate. Good agreement between measured and calculated absorption coefficients was found for the ground state as well as for their tunability by optical excitation.

The purpose of the present paper is a more rigorous theoretical treatment of the absorption processes, taking into account the real two-dimensional subband structure. We will see that this more sophisticated treatment yields interesting new results. The two-dimensional subband structure leads to pronounced steps in the absorption coefficient $\alpha^{n\text{-}i\text{-}p\text{-}i}(\omega)$ for photon energies $\hbar\omega$ corresponding to transitions between the edges of the electron and hole subbands. Similarly, the absorption coefficient for a fixed photon energy exhibits an oscillatory behavior as a function of excitation level or external field. The variation of the excitation level, which is tantamount to a variation of the effective band gap, can be accomplished by various means, among them population changes induced by the absorbed probe light itself, light of different photon energy, and/or different direction and/or polarization, and, in addition, by electrical bias applied via selective electrodes. These changes of the absorption coefficient also include the change of its sign, i.e., the transition from absorption to amplification for a fixed photon energy. The specific features of n-i-p-i crystals allow for such a transition at unusually low excitation intensities and within a very wide photon-energy range. Apart from the changes of the absorption coefficient which are of particular interest for the generation, modulation, and amplification of light signals, the above-mentioned self-induced changes yield intensity-dependent absorption coefficients and refractive indices. As a consequence, it turns out that n-i-p-i crystals represent a promising basic material for devices based on

 ©1984 The American Physical Society

optical nonlinearity, such as bistable or multistable optical switches.[17]

In Sec. II of this paper we calculate analytically the absorption coefficient in the ground state for *n-i-p-i* crystals with a set of design parameters which leads to a particularly simple electronic structure. The analytical approach has the advantage of making transparent the relationship between absorption coefficient and design and materials parameters of the *n-i-p-i* superlattice. It also allows us to discuss the effects of external fields.

In Sec. III the absorption coefficient under external electric fields and in the excited state will be considered. We will treat analytically the former case and present numerical results obtained from self-consistent calculations of the electronic structure[14] for the excited state. These examples will demonstrate the strong tunability of the absorption coefficient as a function of external fields and of the excitation level. In our concluding remarks we will summarize our present results and we will critically review the approximations made and consider their consequences.

II. ABSORPTION IN THE GROUND STATE

We consider a compensated *n-i-p-i* crystal with uniformly doped *n*- and *p*-type layers of thickness d_n and d_p, respectively, and doping concentrations n_D and n_A, respectively. The condition for compensation, i.e., the absence of free carriers in the ground state, reduces to

$$n_D d_n = n_A d_p \tag{1}$$

in this simple case.

The periodic space-charge potential of the ionized impurities is composed of parabolic segments and reads

$$v_0(z)=\begin{cases}(2\pi e^2 n_D/\kappa_0)z^2, & |z| \le d_n/2 \\ 2V_0-(2\pi e^2 n_A/\kappa_0)(|z|-d/2)^2, & \\ & (d-d_p)/2<|z|\le d/2\end{cases} \tag{2}$$

for the zeroth period. The static dielectric constant is κ_0 and e is the elementary change. The potential amplitude V_0 is given by

$$2V_0=(2\pi e^2/\kappa_0)[n_D(d_n/2)^2+n_A(d_p/2)^2]\,. \tag{3}$$

This superlattice potential is superposed on the crystal potential of the host semiconductor. In Fig. 1 the real-space band scheme with the lower conduction-band and upper valence-band edge modulated by the superlattice potential is shown. The motion of the charge carriers in the z direction is quantized by the steep space-charge potential $v_0(z)$. The electrons in the lowest discrete energy levels $E_{c,\mu}$ and holes in the uppermost valence-band states, $E_{v,\nu}$ are defined by the respective parabolic parts of the potential. The eigenvalues are therefore harmonic-oscillator energies

$$E_{c,\mu}^{(i)}=E_g^0-2V_0+\hbar\omega_c^{(i)}(\mu+\tfrac{1}{2}),\quad \mu=0,1,2,\ldots \tag{4}$$

and

$$E_{v,\nu}^{(j)}=-\hbar\omega_v^{(j)}(\nu+\tfrac{1}{2}),\quad \nu=0,1,2,\ldots \tag{5}$$

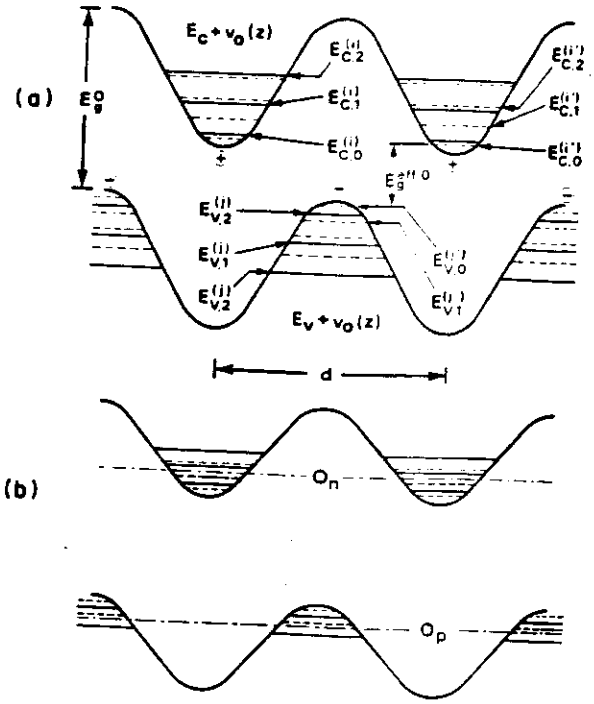

FIG. 1. Schematic real-space energy diagram of a compensated *n-i-p-i* crystal. The conduction- and valence-band edges are modulated by the space-charge potential of the ionized impurities (indicated by + and − signs for donors and acceptors, respectively). The dashed and solid horizontal lines close to the (real-space) conduction- and valence-band extrema correspond to the subband edges of different subband systems, $E_{c,\mu}^{(i)}$ and $E_{v,\nu}^{(j)}$ derived from different conduction and valence bands (i) and (j), respectively. (a) shows the ground state of an *n-i-p-i* crystal, and (b) shows an excited state with carriers in the subbands, reduced subband spacing, reduced band modulation, and different quasi Fermi levels for electrons and holes.

within the effective-mass approximation (EMA). The harmonic-oscillator approximation is quite accurate for

$$(\hbar\omega_c^{(i)}(\mu+\tfrac{1}{2}),\hbar\omega_v^{(j)}(\nu+\tfrac{1}{2}))\lesssim V_0\,, \tag{6}$$

to the extent that deviations of $v_0(z)$ from parabolas influence the energy eigenvalues. For the validity of the EMA, however, the more restrictive condition

$$(\hbar\omega_c^{(i)}(\mu+\tfrac{1}{2}),\hbar\omega_v^{(j)}(\nu+\tfrac{1}{2}))\ll E_g^0 \tag{7}$$

must be fulfilled. The error introduced by neglecting deviations from the EMA is not serious as long as the deviations between the exact and EMA values are substantially smaller than the oscillator level spacing, e.g.,

$$|(E_{c,\mu}^{(i)})^{\text{exact}}-(E_{c,\mu}^{(i)})^{\text{EMA}}|\lesssim 0.2\hbar\omega_c^{(i)}\,. \tag{8}$$

We have introduced the superscripts (i) and (j) in Eqs. (4) and (5) in order to take into account anisotropic and/or degenerate bands in realistic crystals. In the case of semiconductors with GaAs band structure, the conduction band is nearly isotropic and nondegenerate with an effective mass m_c. Therefore, we can omit the superscript; we obtain

$$\omega_c=[4\pi e^2 n_D/(\kappa_0 m_c)]^{1/2} \text{ for GaAs structures} . \quad (9)$$

For the two uppermost valence bands, the heavy-hole (HH) and the light-hole (LH) bands, we obtain, for tetrahedrally coordinated semiconductors,

$$\omega_v^{\mathrm{HH}}=[4\pi e^2 n_A/(\kappa_0 m_{\mathrm{HH}})]^{1/2} \quad (10)$$

and

$$\omega_v^{\mathrm{LH}}=[4\pi e^2 n_A/(\kappa_0 m_{\mathrm{LH}})]^{1/2} .$$

Strictly speaking, we must take into account the anisotropy of the valence bands (particularly for the HH band). Therefore, we must use the appropriate components of the effective-mass tensor, $m_{\mathrm{HH},z}$ and $m_{\mathrm{LH},z}$, in Eq. (10), which correspond to $m_{\mathrm{HH}}^{(100)}$ and $m_{\mathrm{LH}}^{(100)}$ if the z direction of the superstructure coincides with the (100) symmetry direction of the host-crystal lattice. We also note that the different bands of the host crystal interact because of the potential $v_0(z)$. The consequences of this interband coupling are probably always unimportant for our present problem and will be neglected in the following.

If the host crystal exhibits a many-valley band structure (Si, Ge, or GaP, but also IV-VI compounds such as PbTe, for example), we must take into account the anisotropy of the energy bands. The effective masses in Eqs. (9) and (10) must be replaced by the appropriate values m_z, depending on the orientation of the superlattice direction with respect to the crystal symmetry axes. The solution of the Schrödinger equation and the values of m_z in terms of the longitudinal and transverse masses m_l and m_t have been calculated by Stern and Howard[18] for the symmetry directions (100), (110), and (111). We give here only the results for a IV-VI compound with superlattice orientation along the (111) direction. These compounds have conduction- and valence-band edges at the L points.[19] Equations (9) and (10) now read, for (a)-type valleys,

$$\omega_c^{(1)}=[4\pi e^2 n_D/(\kappa_0 m_{cl})]^{1/2}, \quad \omega_v^{(a)}=[4\pi e^2 n_A/(\kappa_0 m_{vl})]^{1/2} \quad (11)$$

and, for (b)-type valleys,

$$\omega_c^{(b)}=\{4\pi e^2 n_D/[\kappa_0 9 m_{ct} m_{cl}/(m_{ct}+8m_{cl})]\}^{1/2}, \quad \omega_v^{(b)}=\{4\pi e^2 n_A/[\kappa_0 9 m_{vt} m_{vl}/(m_{vt}+8m_{cl})]\}^{1/2} , \quad (12)$$

where we have followed the convention that the valley whose symmetry axis coincides with the direction of symmetry breaking is designated as (a) type, and the other three degenerate valleys as (b) type.

The energies $E_{c,\mu}^{(i)}$ and $E_{v,\nu}^{(j)}$ form the edges of the subbands with energies $\epsilon_{c,\mu}^{(i)}(\vec{k}_{||})$ and $\epsilon_{v,\nu}^{(j)}(\vec{k}_{||})$ given by

$$\epsilon_{c,\mu}^{(i)}(\vec{k}_{||})=E_{c,\mu}^{(i)}+\hbar^2\sum_{l,m}(k_l-k_{0,l}^{(i)})(k_m-k_{0,m}^{(i)})[(m_c^{(i)})^{-1}]_{l,m} , \quad (13)$$

$$\epsilon_{v,\nu}^{(j)}(\vec{k}_{||})=E_{v,\nu}^{(j)}-\hbar^2\sum_{l,m}(k_l-k_{0,l}^{(j)})(k_m-k_{0,m}^{(j)})[(m_v^{(j)})^{-1}]_{l,m} , \quad (14)$$

where $[(m_c^{(i)})^{-1}]_{l,m}$ and $[(m_v^{(j)})^{-1}]_{l,m}$ are the (l,m) components of the reciprocal effective-mass tensor for the $\vec{k}_{||}=(k_x,k_y)$ direction. The $\vec{k}_0(j)$ are the wave vectors of the band extrema.[6] The two-dimensional densities of states per subband, $N_{c,\mu}^{(i)}(\epsilon)$ and $N_{v,\nu}^{(j)}(\epsilon)$, again in the EMA, are[20]

$$N_{c,\mu}(\epsilon)=(m_c/\pi\hbar^2)\Theta(\epsilon-E_{c,\mu}) , \quad (15)$$

for GaAs structure,

$$N_{v,\nu}^{\mathrm{HH}}(\epsilon)=(m_{\mathrm{HH}}/\pi\hbar^2)\Theta(E_{v,\nu}^{\mathrm{HH}}-\epsilon), \quad N_{v,\nu}^{\mathrm{LH}}(\epsilon)=(m_{\mathrm{LH}}/\pi\hbar^2)\Theta(E_{v,\nu}^{\mathrm{LH}}-\epsilon) , \quad (16)$$

for tetrahedrally coordinated semiconductors,

$$N_{c,\mu}^{(a)}(\epsilon)=(m_{ct}/\pi\hbar^2)\Theta(\epsilon-E_{c,\mu}^{(a)}), \quad N_{v,\nu}^{(a)}(\epsilon)=(m_{vl}/\pi\hbar^2)\Theta(E_{v,\nu}^{(a)}-\epsilon) , \quad (17)$$

for (a) valleys, and

$$N_{c,\mu}^{(b)}(\epsilon)=3(m_{c,\mathrm{DOS}}^{(b)}/\pi\hbar^2)\Theta(\epsilon-E_{c,\mu}^{(b)}), \quad N_{v,\nu}^{(b)}(\epsilon)=3(m_{v,\mathrm{DOS}}^{(b)}/\pi\hbar^2)\Theta(E_{v,\nu}^{(b)}-\epsilon) , \quad (18)$$

for (b) valleys, where the two-dimensional density-of-states (DOS) masses for motion of carriers parallel to the layers in the (b) valleys, $m_{c,\mathrm{DOS}}^{(b)}$ and $m_{v,\mathrm{DOS}}^{(b)}$, are given by

$$m_{c,\mathrm{DOS}}^{(b)}=[m_{ct}(m_{ct}+8m_{cl})/9]^{1/2}, \quad m_{v,\mathrm{DOS}}^{(b)}=[m_{vt}(m_{vt}+8m_{vl})/9]^{1/2} . \quad (19)$$

We have neglected the finite bandwidth of the subbands with respect to propagation in the z direction. This is justified by the fact that this bandwidth, in general, is negligibly small for all the subbands participating in optical transitions which will be of interest in this paper. Similarly, it is sufficient to use the wave functions of isolated potential wells for the calculation of the dipole matrix elements for the optical transitions.

The wave function for the μth (i)-type conduction subband becomes, in the layer of index m, in the EMA,

$$\langle \vec{r}\,|\,c,(i),\mu,\vec{k}_{||},m\rangle \simeq e^{i\vec{k}_{||}\cdot\vec{r}_{||}}\xi_{c,\mu}^{(i)}(z-md)u_{c,\vec{k}_0^{(i)}}^{(i)}(\vec{r})e^{ik_{0,z}^{(i)}z} , \quad (20)$$

and, for the νth (j)-type valence subband,

$$\langle \vec{r} \mid v,(j),\nu,\vec{k}_{||},m \rangle \simeq e^{i\vec{k}_{||}\cdot\vec{r}}\xi^{(j)}_{v,\nu}[z-(m+\tfrac{1}{2})d]u^{(j)}_{v,\vec{k}^{(j)}_0}(\vec{r})e^{ik^{(j)}_{0,z}z}\,, \tag{21}$$

where the u's are the (host-) lattice-periodic parts of the respective Bloch functions at the conduction-band minima $\vec{k}^{(i)}_0$ and valence-band maxima $\vec{k}^{(j)}_0$. The envelope wave functions $\xi^{(i)}_{c,\mu}(z)$ and $\xi^{(j)}_{v,\nu}(z)$ are harmonic-oscillator solutions within the approximations discussed at the beginning of this section. For $-d/2<z\le d/2$, we have

$$\xi^{(i)}_{c,\mu}(z)\simeq\pi^{-1/4}(\alpha^{(i)}_c)^{-1/2}\exp[-z^2/2(\alpha^{(i)}_c)^2](\mu!2^\mu)^{-1/2}H_\mu(z/\alpha^{(i)}_c) \tag{22}$$

and

$$\xi^{(j)}_{v,\nu}(z)\simeq\pi^{-1/4}(\alpha^{(j)}_v)^{-1/2}\exp[-(d/2-|z|)^2/2(\alpha^{(j)}_v)^2](\nu!2^\nu)^{-1/2}H_\nu[(d/2-|z|)/\alpha^{(j)}_v]\,, \tag{23}$$

where the $H_\lambda(\xi)$ are the Hermite polynomials,

$$H_0(\xi)=1,\quad H_1(\xi)=2\xi\,,$$
$$H_2(\xi)=4\xi^2-2,\quad H_3(\xi)=8\xi^3-12\xi\,, \tag{24}$$

and

$$\alpha^{(i)}_c=(\hbar/m^{(i)}_{c,z}\omega^{(i)}_c)^{1/2}\,, \tag{25}$$

$$\alpha^{(j)}_v=(\hbar/m^{(j)}_{v,z}\omega^{(j)}_v)^{1/2}\,. \tag{26}$$

We have treated in some detail the relationship between the two-dimensional subband structure of the *n-i-p-i* superlattice and the electronic structure of the host crystal because we will find that optical-interband-transition probabilities depend very sensitively on the specific subband system involved. We will exclude from our consideration the interesting case of absorption in *n-i-p-i* systems made from a host material with an indirect gap in momentum space, such as Si, Ge, or GaP. For valleys which are projected onto the Γ point of the (k_x,k_y) plane, the vertical valence-band-to—conduction-band transitions are no longer strictly forbidden, which means that the crystal becomes a direct-gap semiconductor. A reasonably realistic treatment of this situation, however, would lead beyond the scope of the present paper.

We now turn to the calculation of the absorption coefficient of an *n-i-p-i* crystal in its ground state $\alpha^{n\text{-}i\text{-}p\text{-}i}(\omega;E_g^{\text{eff},0})$. Here, $E_g^{\text{eff},0}$ stands for the effective band gap in the ground state, defined by (see Fig. 1)

$$E_g^{\text{eff},0}=E_g^0-2V_0+\min_{i,j}(\hbar\omega^{(i)}_c/2+\hbar\omega^{(j)}_v/2)\,. \tag{27}$$

This energy represents the threshold photon energy for absorption. Excitonic effects are normally negligible in *n-i-p-i* crystals because of the rather large average value of the electron-hole distance of $d/2$. The value of the absorption coefficient near $E_g^{\text{eff},0}$ is always considerably smaller than typical bulk values because the interband dipole matrix elements

$$\langle c,(i),0,\vec{k}_{||},m \mid \vec{p} \mid v,(j),0,\vec{k}_{||}m \rangle$$

are small due to the spatial separation of the initial and final states. With increasing photon energy, transitions between subbands with higher indices μ and ν becomes energetically possible. The imaginary part of the dielectric function $\epsilon_2^{n\text{-}i\text{-}p\text{-}i}(\omega_{\vec{\lambda}};E_g^{\text{eff},0})$, for photons $\hbar\omega_{\vec{\lambda}}$ with polarization vector $\vec{\lambda}$, becomes

$$\epsilon_2^{n\text{-}i\text{-}p\text{-}i}(\omega_{\vec{\lambda}};E_g^{\text{eff},0})=\frac{4\pi^2e^2}{A\alpha}\sum_{\mu,\nu,\vec{k}_{||},(i),(j)}\frac{2\hbar^2\mid\langle c,(i),\mu,\vec{k}_{||},m\mid\vec{p}\cdot\vec{\lambda}\mid v,(j),\nu,\vec{k}_{||},m\rangle\mid^2}{m_0^2[\epsilon^{(i)}_{c,\mu}(\vec{k}_{||})-\epsilon^{(j)}_{v,\nu}(\vec{k}_{||})]^2}\,\delta(\epsilon^{(i)}_{c,\mu}(\vec{k}_{||})-\epsilon^{(j)}_{v,\nu}(\vec{k}_{||})-\hbar\omega_{\vec{\lambda}})\,. \tag{28}$$

The absorption coefficient $\alpha^{n\text{-}i\text{-}p\text{-}i}(\omega_{\vec{\lambda}};E_g^{\text{eff},0})$ is related to $\epsilon_2^{n\text{-}i\text{-}p\text{-}i}(\omega_{\vec{\lambda}};E_g^{\text{eff},0})$ by

$$\alpha(\omega)=\epsilon_2(\omega)\omega/[n_{\text{opt}}(\omega)c]\,, \tag{29}$$

where $n_{\text{opt}}(\omega)$ is the refractive index and c is the velocity of light.

Equation (28) will be evaluated for two simple examples. We take advantage of the fact that the two-dimensional subband structure for electrons and holes can be tailored independently. We choose the design parameters d_n, d_p, n_D, and n_A such that $\omega^{(i)}_c=\omega^{(j)}_v$ for those subband systems which yield the major contributions to $\epsilon_2^{n\text{-}i\text{-}p\text{-}i}(\omega_{\vec{\lambda}};E_g^{\text{eff},0})$. This requirement is fulfilled if

$$\frac{n_D}{n_A}=\frac{d_p}{d_n}=\begin{cases}m_c/m_{\text{LH}}, & \text{for GaAs structure,}\quad (30)\\ m^{(b)}_{c,z}/m^{(b)}_{v,z} & \text{for IV-VI compounds,}\quad (31)\end{cases}$$

depending on the band structure of the host crystal.

This particular choice of design parameters has two advantages. The (i,j) contribution to the absorption increases at

equidistant photon energy intervals,

$$\hbar\omega_0=\hbar\omega_c^{(i)}=\hbar\omega_v^{(j)}\ , \tag{32}$$

and the analytical evaluation of (28) with the wave functions given by Eqs. (22)–(24) yields rather accurate results. We find

$$|\langle c,(i),\mu,\vec{k}_{||}|\vec{p}\cdot\vec{\lambda}|v,(j),\nu,\vec{k}_{||}\rangle|^2\simeq 2|\langle c,(i),\vec{k}_0^{(i)}|\vec{p}\cdot\vec{\lambda}|v,(j),\vec{k}_0^{(j)}\rangle|^2\left|\int dz\,\xi_{c,\mu}^{(i)}(z)\xi_{v,\nu}^{(j)}(d/2-|z|)\right|^2\ , \tag{33}$$

with

$$\left|\int \xi_{c,\mu}^{(i)}(z)\xi_{v,\nu}^{(j)}(d/2-|z|)dz\right|^2=\exp\{-(d/2)^2/[(\alpha_c^{(i)})^2+(\alpha_v^{(j)})^2]\}I_{\mu,\nu}^{(i)(j)}\ . \tag{34}$$

Equation (33) contains only a contribution of $\vec{p}$ operating on the Bloch states, but no contribution of $\vec{p}$ acting on the envelope functions because of the orthogonality of Bloch states belonging to different bands. The exponent in Eq. (34) can be rewritten as

$$\frac{(d/2)^2}{(\alpha_c^{(i)})^2+(\alpha_v^{(j)})^2}=2\frac{2V_0(d_n+d_p)}{\hbar\omega_c^{(i)}d_n+\hbar\omega_v^{(j)}d_p}\ , \tag{35}$$

and reduces to

$$\frac{(d/2)^2}{(\alpha_c^{(i)})^2+(\alpha_v^{(j)})^2}=2\frac{2V_0}{\hbar\omega_c^{(j)}} \tag{36}$$

for transitions between those bands for which $\omega_c^{(i)}=\omega_v^{(j)}$. The integrand in the expression

$$I_{\mu,\nu}^{(i)(j)}=\exp[(d/2)^2/[(\alpha_c^{(i)})^2+(\alpha_v^{(j)})^2]]\left|\int dz\,\xi_{c,\mu}^{(i)}(z)\xi_{v,\nu}^{(i)}(d/2-|z|)\right|^2 \tag{37}$$

has its maximum near the boundary between the n- and p-doped regions for the subband wave functions under consideration. This is not the case for transitions between the electron and heavy-hole subbands. Therefore the analytical results are less accurate for the latter case because the wave functions differ significantly from harmonic-oscillator solutions in the region where the integrand is large.

For the lowest subbands, one finds

$$\begin{aligned}
I_{0,0}^{(i)(j)}&=2\alpha_c^{(i)}\alpha_v^{(j)}/[(\alpha_c^{(i)})^2+(\alpha_v^{(j)})^2]\ ,\\
I_{1,0}^{(i)(j)}&=I_{0,0}^{(i)(j)}(\alpha_c^{(i)}d)^2/\{2[(\alpha_c^{(i)})^2+(\alpha_v^{(j)})^2]^2\}\ ,\\
I_{2,0}^{(i)(j)}&=I_{0,0}^{(i)(j)}(\alpha_c^{(i)})^4/\{8[(\alpha_c^{(i)})^2+(\alpha_v^{(j)})^2]^2\}\{d^2/[(\alpha_c^{(i)})^2+(\alpha_v^{(j)})^2]+2(\alpha_v^{(j)})^2/(\alpha_c^{(i)})^2-2\}^2\ ,\\
I_{1,1}^{(i)(j)}&=I_{0,0}^{(i)(j)}(\alpha_c^{(i)}\alpha_v^{(j)})^2/\{4[(\alpha_c^{(i)})^2+(\alpha_v^{(j)})^2]^2\}\{d^2/[(\alpha_c^{(i)})^2+(\alpha_v^{(j)})^2]-4\}^2\ ,\\
I_{3,0}^{(i)(j)}&=I_{0,0}^{(i)(j)}(\alpha_c^{(i)}d)^2/\{48[(\alpha_c^{(i)})^2+(\alpha_v^{(j)})^2]^2\}\{(\alpha_c^{(i)}d)^2/[(\alpha_c^{(i)})^2+(\alpha_v^{(j)})^2]^2+6[(\alpha_v^{(i)})^2-(\alpha_c^{(j)})^2]/[(\alpha_c^{(i)})^2+(\alpha_v^{(j)})^2]\}^2\ ,\\
I_{2,1}^{(i)(j)}&=I_{0,0}^{(i)(j)}d\alpha_v^{(j)}/[(\alpha_c^{(i)})^2+(\alpha_v^{(j)})^2]^2((\alpha_c^{(i)})^2d^2/\{4[(\alpha_c^{(i)})^2+(\alpha_v^{(j)})^2]^2\}+[-2(\alpha_c^{(i)})^2+(\alpha_v^{(j)})^2]/[(\alpha_c^{(i)})^2+(\alpha_v^{(j)})^2]-\tfrac{1}{2})^2\ .
\end{aligned} \tag{38}$$

(The integrals $I_{0,1}^{(i)(j)}$, $I_{0,2}^{(i)(j)}$, and $I_{0,3}^{(i)(j)}$ follow from the corresponding terms by interchanging $\alpha_c^{(i)}\leftrightarrow\alpha_v^{(j)}$.)

We note the following observations.

(1) The interband dipole matrix elements in n-i-p-i crystals are reduced by an exponential factor

$$\exp\left[-\frac{4V_0(d_n+d_p)}{\hbar\omega_c^{(i)}d_n+\hbar\omega_v^{(j)}d_p}\right]$$

with respect to bulk transitions or those in heterostructure superlattices.

(2) The matrix elements depend strongly on the effective masses of the bands, as $\omega_{c,v}\propto m_{c,v}^{-1/2}$. Thus, for $V_0>(\hbar\omega_c^{(i)},\hbar\omega_v^{(j)})$, the heavy-hole-subband—to—conduction-subband transitions are negligible compared to the light-hole-subband—to—conduction-subband transitions in typical n-i-p-i structures if the host crystal has GaAs-type band structure. For $n_A=4\times10^{18}$ cm^{-3}, $n_D=(m_c/m_{\rm LH})n_A$, and $d=40$ nm, we find

$$|\langle c,\mu=0,\vec{k}_{||},m|\vec{p}\cdot\vec{\lambda}|v,\mathrm{LH},\nu=0,\vec{k}_{||},m\rangle|^2\simeq 2|\langle c,\vec{k}|\vec{p}\cdot\vec{\lambda}|v,\mathrm{LH},\vec{k}\rangle|^2e^{-14} \tag{39}$$

and

$$|\langle c,\mu=0,\vec{k}_{||},m|\vec{p}\cdot\vec{\lambda}|v,\mathrm{HH},\nu=0,\vec{k}_{||},m\rangle|^2\simeq 2|\langle c,\vec{k}|\vec{p}\cdot\vec{\lambda}|v,\mathrm{HH},\vec{k}\rangle|^2e^{-20}\ . \tag{40}$$

Similarly, we find, for PbTe, n-i-p-i structure with $n_D=n_A=2\times10^{18}$ cm^{-3} and $d_n=d_p=90$ nm,

$$|\langle c,(b),\mu=0,\vec{k}_{||},m|\vec{p}\cdot\vec{\lambda}|v,(b),\nu=0,\vec{k}_{||},m\rangle|^2=2|\langle c,(b),\vec{k}|\vec{p}\cdot\vec{\lambda}|v,(b),\vec{k}\rangle|^2e^{-10}\ , \tag{41}$$

whereas the corresponding matrix elements for transitions

between the (large-effective-mass) (a) valleys are much smaller

$$|\langle c,(a),\mu=0,\vec{k}_{||},m\,|\,\vec{p}\cdot\vec{\lambda}\,|\,v,(a),\nu=0,\vec{k}_{||},m\rangle|^2 = 2|\langle c,(a),\vec{k}\,|\,\vec{p}\cdot\vec{\lambda}\,|\,v,(a),\vec{k}\rangle|^2 e^{-35}. \quad (42)$$

Note, that (a)-to-(b) transitions are forbidden by the $\vec{k}_{||}$-selection rule.

(3) There is no (μ,ν) selection or quasi selection rule because of the spatial shift between the initial- and the final-state harmonic-oscillator wave functions ("indirect gap in real space"[3,4]). This is in contrast to heterojunction superlattices with a direct gap in real space.

(4) The matrix elements increase rapidly with increasing subband indices, i.e., for transitions which become energetically allowed for higher photon energies the absorption is much larger.

(5) For a GaAs-type band structure we can use the Kane model to describe the cell periodic part of the Bloch functions.[21] For the light-hole band with an effective spin of $+\frac{1}{2}$, for instance, one has

$$u_{vk}^{(\mathrm{LH})+} = a^{(\mathrm{LH})}(k)\,|\,iS\beta\rangle + b^{(\mathrm{LH})}(k)\,|\,(X-iY)\alpha\rangle 2^{-1/2} + c^{(\mathrm{LH})}(k)\,|\,Z\beta\rangle, \quad (43)$$

where $|\,S\rangle$, $|\,X\rangle$, $|\,Y\rangle$, and $|\,Z\rangle$ stand for wave functions of s and p symmetry, and α and β are spinors. The k-dependent coefficients $a^{(\mathrm{LH})}(k)$, $b^{(\mathrm{LH})}(k)$, and $c^{(\mathrm{LH})}(k)$ reduce, in the limit $k\to 0$, to

$$a^{(\mathrm{LH})}(0)=0,\quad b^{(\mathrm{LH})}(0)=3^{-1/2},\quad c^{(\mathrm{LH})}(0)=(\tfrac{2}{3})^{1/2}. \quad (44)$$

The conduction-band wave function is given by a similar linear combination. Its coefficients for $k\to 0$ reduce to

$$a^{(c)}(0)=1,\quad b^{(c)}(0)=0,\quad c^{(c)}(0)=0. \quad (45)$$

This form of the wave functions has the following two interesting consequences for optical absorption in doping superlattices.

(a) The absorption coefficient will be polarization dependent since the momentum matrix elements p_x,p_y will, in general, not be equal to that of p_z. However, a factor-of-4 difference between polarization $\vec{\lambda}$ in the plane of the layers and perpendicular to it, which is expected from Eq. (44), i.e., from using the effective-mass approximation, will not be observed. Even for the lowest subband the superlattice potential will mix Bloch functions of appreciable k_z ($\vec{k}$ vector along the superlattice axis). This mixing is not described by the (lowest-order) wave function of Eqs. (20) and (21). The superposition of Bloch states of different k_z causes the differences in the matrix elements to diminish even for states near the subband edges, i.e., states with zero transverse momentum $\vec{k}_{||}$.

(b) The form of the wave functions (43) implies the possibility of exciting electrons of only one spin direction from the light-mass valence into the conduction band by applying circularly polarized light which propagates along the superlattice axis. Large degrees of conduction-electron spin polarization should be obtainable by absorption near the subband edges in n-i-p-i crystals due to the separation of light- and heavy-mass valence-bands (dispar-

TABLE I. Material parameters for GaAs, InAs, and PbTe, and one example of a set of doping superlattice parameters for each material.

	Material parameters ($T=4$ K)						Example superlattice parameters						
	E_g^0 (eV)	κ_0	$P^2_{(\mathrm{mm})}$ (eV)		n_D (cm^{-3})	n_A (cm^{-3})	d_n (nm)	d_p (nm)	$E_g^{\mathrm{eff},0}$ (eV)	$\left\lvert\frac{m_{c,\nu}}{m_0}\right\rvert_z$	$\left\lvert\frac{m_{c,\nu}}{m_0}\right\rvert_{\mathrm{DOS}}$		$\hbar\omega_{c,\nu}^{(1)}$ (meV)
GaAs	1.52	12.5	28.9	c 0.067						0.067	0.067		76.9
				LH 0.074	3.62×10^{18}	4.00×10^{18}	21	19	1.02	0.074	0.074		76.9
				0.4									
				HH 0.8						0.4	0.47		33.1
InAs	0.42	15.2	22.2	c 0.023						0.023	0.023		44.2
				LH 0.025	5.00×10^{17}	5.43×10^{17}	50	46	0.090	0.025	0.025		44.2
				HH 0.4						0.4	0.4		11.1
PbTe	0.19	1500	(111) 0.6	c (111) 0.24						a 0.24	0.02		2.8
				($1\bar{1}0$) 0.02	2.00×10^{18}	2.00×10^{18}	90	90	0.144	b 0.02	0.06		9.5
			($1\bar{1}0$) 5.9	v (111) 0.31						a 0.31	0.02		2.4
				($1\bar{1}0$) 0.02						b 0.02	0.07		9.5

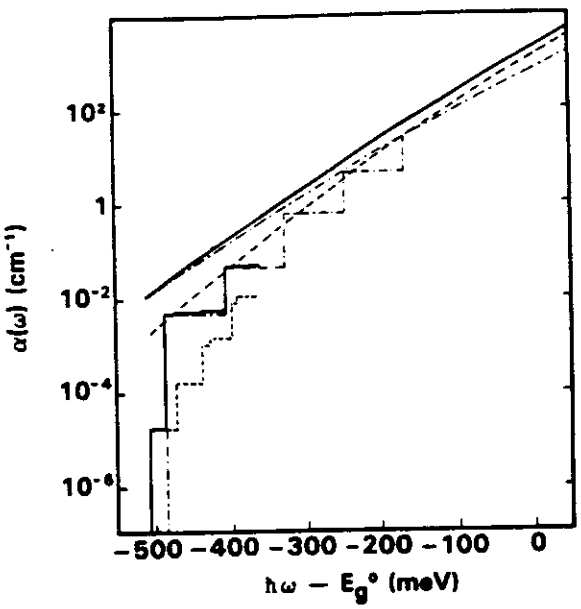

FIG. 2. Calculated absorption coefficient $\alpha(\omega)$ for a GaAs n-i-p-i crystal with $n_A = 4\times10^{18}$, $n_A = (m_{LH}m_c)n_D$, and $d = 40$ nm. Dashed lines depict the heavy-hole and the dashed-dotted lines the light-hole contributions, whereas the solid lines correspond to the sum of these contributions. The analytic calculation has only been performed for transitions with $\mu,\nu \le 3$. The continuous curves show corresponding results of semiclassical calculations similar to those presented in Ref. 11.

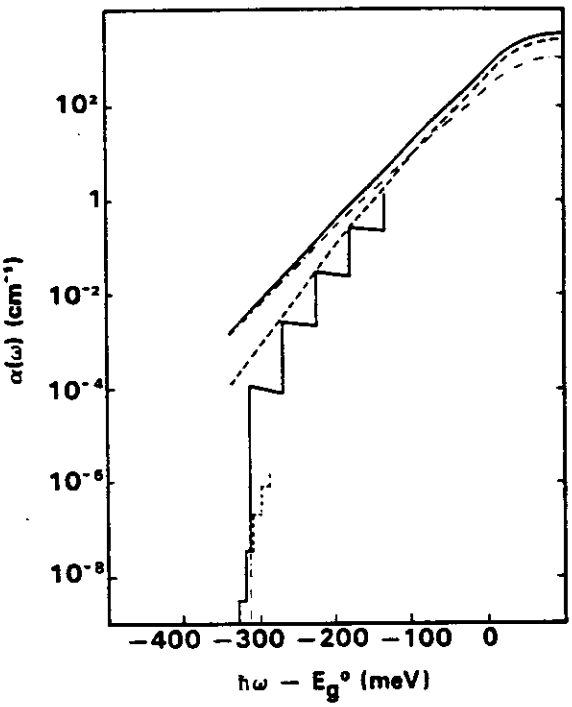

FIG. 3. Same as Fig. 2, but for an InAs n-i-p-i crystal with $n_D = 5\times10^{17}$ cm^{-3} and $d = 96$ nm. The difference between the heavy- and light-hole contributions is more pronounced than in the former case. In addition, the semiclassical description is found to overestimate considerably the absorption coefficient in this low-effective-band-gap example.

ity in the momentum matrix elements) and the imposition of a symmetry axis given by the direction of the built-in electric fields. This is particularly significant since the electron-hole scattering, which is thought to be the dominant spin-relaxation mechanism in GaAs at low carrier energies,[22] is much less effective in n-i-p-i crystals than in bulk GaAs due to the large spatial separation of electrons and holes. Appropriate treatment of a surface perpendicular to the layers with cesium oxide, yielding a negative electron affinity,[23] may turn GaAs-doping superlattices into a very efficient source of spin-polarized electrons.

The $\vec{k}_{\parallel}$ summation in Eq. (28) yields two-dimensional interband densities of states,

$$N_{\mu\nu}^{(i)(j)}(\epsilon) = \{[(m_{c,\mathrm{DOS}}^{(i)})^{-1} + (m_{v,\mathrm{DOS}}^{(j)})^{-1}]^{-1}/\pi\hbar^2\} \times \Theta(\epsilon - E_{c,\mu}^{(i)} + E_{v,\nu}^{(j)}) . \tag{46}$$

For our two cases under consideration the interband density-of-states masses in (46) are given by

$$(m_{c,\mathrm{DOS}}^{(i)})^{-1} + (m_{v,\mathrm{DOS}}^{(j)})^{-1} = \begin{cases} m_c^{-1} + m_{\mathrm{HH}}^{-1} \quad m_c^{-1} + m_{\mathrm{LH}}^{-1} & \text{for GaAs band structures,} \\ m_{ct}^{-1} + m_{vt}^{-1} & \text{for } (a) \text{ valleys,} \\ 3[m_{ct}(m_{ct}+8m_{cl})]^{-1/2} + 3[m_{vt}(m_{vt}+8m_{vl})]^{-1/2} & \text{for } (b) \text{ valleys.} \end{cases} \tag{47}$$

In both cases the absorption near the threshold photon energy

$$\hbar\omega^{\mathrm{th}} = E_g^{\mathrm{eff},0} \tag{48}$$

is due to the $\nu=0$-to-$\mu=0$ transition with the smallest matrix elements. Above the threshold for light-hole-band—to—conduction-band, or (b)-valley, transitions,

$$\hbar\tilde{\omega}^{\mathrm{th}} = \tilde{E}_g^{\mathrm{eff},0} = \begin{cases} E_{c,0} - E_{v,0}^{\mathrm{LH}} & \text{for GaAs structures,} \\ E_{c,0}^{(b)} - E_{v,0}^{(b)} & \text{for IV-VI compounds,} \end{cases} \tag{49}$$

the latter contributions dominate the absorption coefficient. This is true, in particular, for the IV-VI compounds as the density-of-states factor is much larger for the (b) valleys, in addition to the larger matrix elements.

In Figs. 2 and 3 analytically calculated absorption coefficients for the ground state $\alpha^{n\text{-}i\text{-}p\text{-}i}(\omega; E_g^{\mathrm{eff},0})$ for GaAs and InAs n-i-p-i crystals, respectively, are shown. The materials and design parameters are given in Table I. Also shown are the absorption curves which would be obtained from a semiclassical calculation as it was used in Ref. 11. Note that the in-

terband effective mass μ_l, defined by Eq. (36) in Ref. 11, must be replaced by the appropriate quantities $\mu_{i,z}$ in Eq. (34) and by $\mu_{i,\mathrm{DOS}}^{2/3}\mu_{i,z}^{1/3}$ in Eq. (33) if the bands are anisotropic. Here, $\mu_{i,\mathrm{DOS}}$ is identical with the expressions given in Eq. (47), and $\mu_{i,z}$ is defined by

$$\mu_{i,z}^{-1}=\begin{cases} m_{c,l}^{-1}+m_{v,l}^{-1} & \text{for } (a) \text{ valleys,} \\ (9m_{cl})^{-1}+(9m_{ct}/8)^{-1}+(9m_{vl})^{-1}+(9m_{vt}/8)^{-1} & \text{for } (b) \text{ valleys.} \end{cases} \tag{50}$$

It is now quite obvious how we can tailor the absorption coefficient of an n-i-p-i crystal by an appropriate choice of host material and design parameters n_D, n_A, and d.

The absorption edge $\hbar\omega^{\mathrm{th}}$ shifts to lower values with increasing V_0, which, according to Eq. (3), is proportional to the doping concentration, the square of the superlattice period, and the inverse of the static dielectric constant. The width between the steps, with our particular choice of the subband distances $\hbar\omega_c=\hbar\omega_{\mathrm{LH}}$ or $\hbar\omega_c^{(b)}=\hbar\omega_v^{(b)}$, is proportional to the square root of the doping concentration, over the relevant effective mass and the inverse static dielectric constant, according to Eqs. (9)–(12). The average slope in the region $\hbar\omega^{\mathrm{th}}<\hbar\omega<E_g^0$, where $\ln\alpha^{n\text{-}i\text{-}p\text{-}i}(\omega)$ is staircase shaped, can easily be estimated from the semiclassical calculation. We find that the average slope is approximately proportional to the inverse maximum space-charge field $F_{\max}$,

$$F_{\max}=2\pi e n_D d_n/\kappa_0 , \tag{51}$$

and to the square root of the smallest reduced mass $\mu_{i,z}$. Thus, $\ln\alpha^{n\text{-}i\text{-}p\text{-}i}(\omega)$ versus ω becomes particularly flat in materials with small effective masses if the product $n_D d_n=n_A d_p$ is made large. Figure 4 shows the absorption coefficient of a PbTe n-i-p-i crystal.

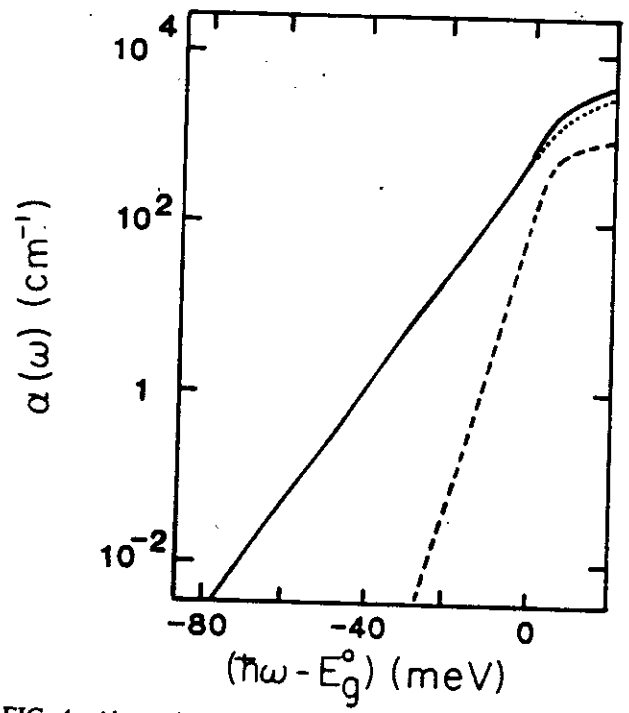

FIG. 4. Absorption coefficient of a PbTe doping superlattice with $n_D=n_A=10^{18}$ cm^{-3} and $d=500$ nm. The dashed line represents the contribution of the (a) transitions. The contribution of the (b) transitions (dotted line) practically coincides with the total absorption coefficient (solid line) for photon energies smaller than E_g^0. The steplike structure is not shown due to the smallness of the subband spacing in this particular example.

III. TUNABLE ABSORPTION COEFFICIENT

The absorption coefficient of an n-i-p-i crystal can be changed drastically by the application of external electric or magnetic fields or by varying the effective band gap E_g^{eff} through the injection or optical generation of electrons and holes. We defer the magnetoabsorption to a planned later publication and restrict ourselves to the modifications induced by an external electric field F_z, applied in the direction of periodicity (Sec. III A), and the variation of $\alpha^{n\text{-}i\text{-}p\text{-}i}(\omega;E_g^{\mathrm{eff},n})$ induced by variation of the effective band gap in the excited state (Sec. III B).

A. Absorption with external electric field

In Fig. 5 the band profiles $\epsilon_c(z)$ and $\epsilon_v(z)$ of an n-i-p-i crystal with an external field F_z applied in the direction of periodicity are shown. Such a field can be induced by an external bias U_z applied between sandwich electrodes on the top and the bottom of the n-i-p-i structure,

$$F_z=U_z/(N_{\mathrm{sl}}d) , \tag{52}$$

if the n-i-p-i structure consists of N_{sl} periods.

The uniform field F_z does not affect the parabolic shape of the superlattice potential

$$v_F(z)=v_0(z)-eF_z z . \tag{53}$$

Therefore, the energetic separation between subbands of the *same* subband system, $\hbar\omega^{(i)}$, does not change either. The energetic and spatial distance between subband states

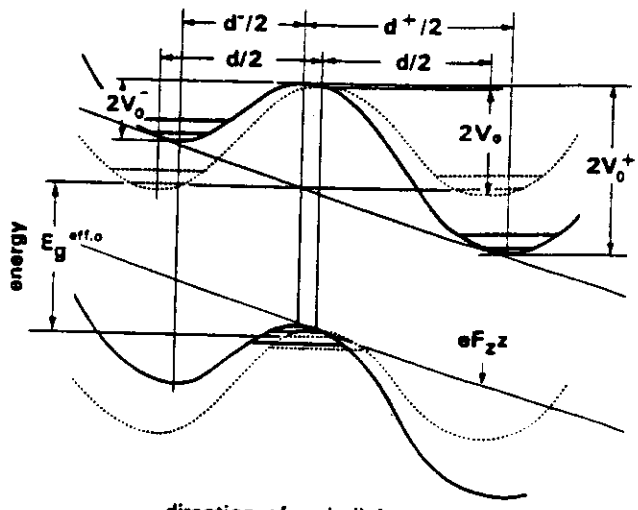

FIG. 5. n-i-p-i crystal with an electric field F_z applied normal to the layers. The effective band gap and, therefore, the threshold energy for absorption is lowered. The subband spacings remain unaffected.

in adjacent layers, however, changes drastically. Therefore, the field F_z strongly influences the absorption coefficient $\alpha^{n\text{-}i\text{-}p\text{-}i}(\omega;E_g^{\text{eff},0};F_z)$. Inspection of Fig. 5 and some elementary algebra tell us that the absorption coefficient can be calculated in the same manner as before. Evaluating expression (28) for $\epsilon_2^{n\text{-}i\text{-}p\text{-}i}(\omega_\chi;E_g^{\text{eff},0})$, one has only to replace it by one-half of the sum of two analogous contributions, obtained by substituting for $2V_0$ and d by

$$2V_0 \rightarrow \begin{cases} 2V_0^+ = 2V_0(d^+) \\ 2V_0^- = 2V_0(d^-) \end{cases} \tag{54}$$

and

$$d \rightarrow \begin{cases} d^+ = d(1+|F_z|/F_{\max}) \\ d^- = d(1-|F_z|/F_{\max}). \end{cases} \tag{55}$$

The potential amplitudes $V_0(d^+)$ and $V_0(d^-)$ are calculated according to Eq. (3) with the new effective superlattice periods d^+ and d^-, respectively. $F_{\max}$ is the ground-state maximum space-charge field at the interface between n and p layers, given by Eq. (51). From Eqs. (54) and (55) we see that the effect of F_z on the absorption will be twofold.

The field dependence of d^+ and d^- results in strong superlinear changes of the transition probabilities. From Eqs. (33) and (37) we find, for $\alpha_c=\alpha_v=\alpha$,

$$|\langle c,\mu|v,\nu\rangle^+|^2 \simeq |\langle c,\mu|v,\nu\rangle|^2(1+|F_z|/F_{\max})^{2(\mu+\nu)}\exp[(-1/8)(d/\alpha)^2(|F_z|/F_{\max})(|F_z|/F_{\max}+2)] \tag{56}$$

and

$$|\langle c,\nu|v,\nu\rangle^-|^2 \simeq |\langle c,\mu|v,\nu\rangle|^2(1-|F_z|/F_{\max})^{2(\mu+\nu)}\exp[(-1/8)(d/\alpha)^2(|F_z|/F_{\max})(|F_z|/F_{\max}-2)]\,. \tag{57}$$

Consequently, the increase of the transition probabilities according to (57) (or to the adjacent n-type layer on the left-hand side in Fig. 5) overcompensates for the decrease following from Eq. (56) (for transitions to the neighboring n-type layer on the right-hand side in Fig. 5). Thus, an overall increase of $\alpha^{n\text{-}i\text{-}p\text{-}i}(\omega;E_g^{\text{eff},0};F_z)$ according to

$$\alpha^{n\text{-}i\text{-}p\text{-}i}(\omega;E_g^{\text{eff},0};F_z) \tilde{\propto} \cosh[(d^2/8\alpha^2)(2|F_z|/F_{\max})]\exp(-d^2F_z^2/8\alpha^2F_{\max}^2) \tag{58}$$

results from the field-induced changes of the effective layer thicknesses.

The second effect of F_z concerns the splitting of the energy separation between conduction and valence subbands,

$$E_{\mu\nu}^0 = E_{c\mu} - E_{v\nu} = E_g^0 - 2V_0 + \hbar\omega_0(\mu+\nu+1)\,, \tag{59}$$

into two sets, $E_{\mu\nu}^+$ and $E_{\mu\nu}^-$,

$$E_{\mu\nu}^+ = E_{\mu\nu}^0 - 2V_0(2|F_z|/F_{\max} + F_z^2/F_{\max}^2) \tag{60}$$

and

$$E_{\mu\nu}^- = E_{\mu\nu}^0 + 2V_0(2|F_z|/F_{\max} - F_z^2/F_{\max}^2)\,. \tag{61}$$

This splitting lowers the threshold for $(\mu\nu)^+$ transitions at a given photon energy if F_z increases, which results in (strong) steplike *increases* of $\alpha^{n\text{-}i\text{-}p\text{-}i}(\omega;E_g^{\text{eff},0};F_z)$ each time the condition

$$E_{\mu\nu}^+(F_z) = \hbar\omega \tag{62}$$

is fulfilled. Similarly, a steplike *decrease* of $\alpha^{n\text{-}i\text{-}p\text{-}i}(\omega;E_g^{\text{eff},0};F_z)$ is expected if, with increasing F_z, the condition

$$E_{\mu\nu}^-(F_z) = \hbar\omega \tag{63}$$

is met.

In order to illustrate this rather complicated field dependence of the absorption coefficient, the situation is depicted in Figs. 6 and 7 for a simple situation where $\hbar\omega$ is chosen such that only the lowest two conduction and valence subbands are participating in absorption processes at $F_z=0$. The design parameters ($d=50$ nm, $n_D=1.5\times10^{18}$ cm^{-3}, and $n_D/n_A=d_p/d_n=m_c/m_{\text{LH}}$) were determined such that $\hbar\omega_c=\hbar\omega_{\text{LH}}\simeq50$ meV and $2V_0\simeq400$ meV. In Fig. 6 the valence-subband–conduction-subband separations $E_{\mu\nu}^+$ and $E_{\mu\nu}^-$ as a function of F_z are indicated by solid lines for $E_{\mu\nu}^+(F_z)$ and $E_{\mu\nu}^-(F_z)<\hbar\omega$, i.e., for the region where transitions occur,

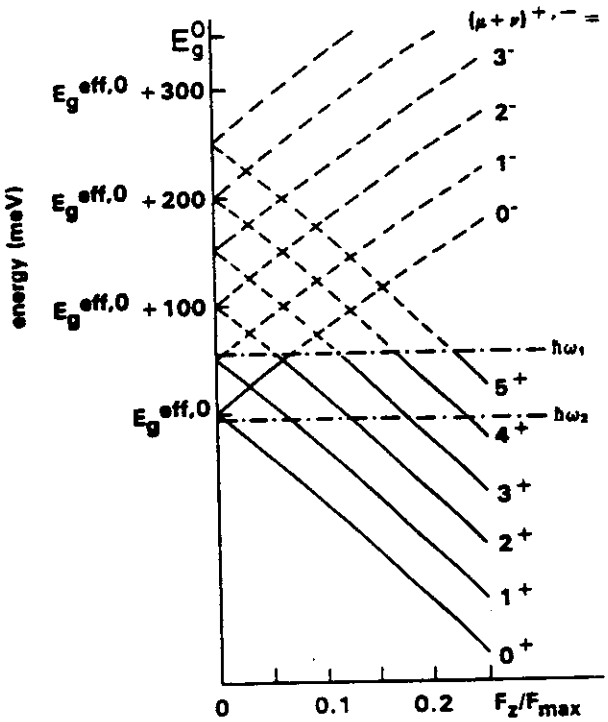

FIG. 6. Effective band gaps $E_{\mu\nu}^+$ and $E_{\mu\nu}^-$ as defined in Eqs. (61) and (62) for transitions between the νth valence and the μth conduction subbands to the left and the right neighboring layers as a function of the field F_z. Absorption is possible only for intersubband gaps $E_{\mu\nu}$ smaller than the photon energy (see dashed-dotted lines labeled $\hbar\omega_1$ and $\hbar\omega_2$).

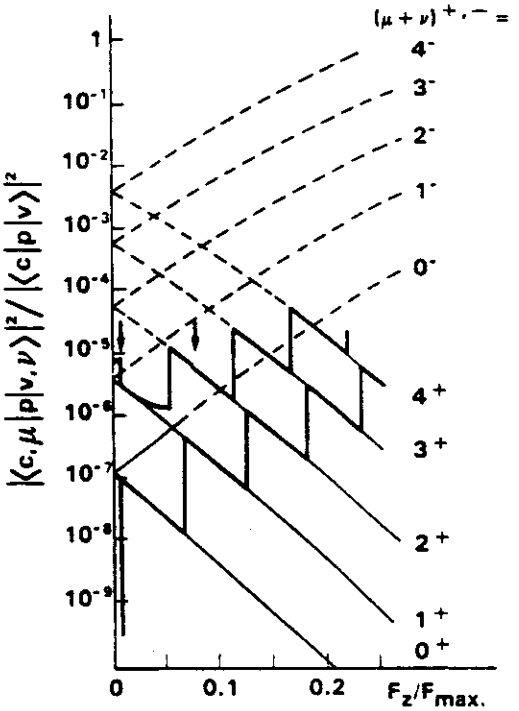

FIG. 7. Transition probabilities between different valence and conduction subbands ν and μ as a function of field F_z. The bold lines represent the sum of all allowed transitions at the photon energies indicated in Fig. 5. They reflect directly the field dependence of the absorption coefficient.

and by dashed lines above the photon energy. In Fig. 7 the squared interband matrix elements $\langle c,\mu|\vec{p}|v,\nu\rangle^+$ and $\langle c,\mu|\vec{p}|v,\nu\rangle^-$ are shown as a function of F_z. Again, the solid lines indicate the range where these matrix elements contribute to the absorption coefficient at the given photon energy. The bold line displays the sum of all contributions, i.e., the total absorption coefficient (see scale on the right-hand side of the figure). At low values of F_z we observe two steplike *decreases*, marked by arrows, associated with the cutoff for the $\mu+\nu=1$ and $\mu+\nu=0$ transitions to the left. The steplike *increases* result from transitions with $\mu+\nu=2$, 3, 4, and 5, respectively, coming in with increasing field F_z. We also note a considerable increase of the absorption coefficient which is superimposed on the sawtooth-shaped oscillations of $\alpha^{n\text{-}i\text{-}p\text{-}i}(\omega;E_g^{\text{eff},0};F_z)$. It is also worthwhile to mention that these oscillations occur at rather low values of F_z (F_{max} is *only about* 3×10^5 *V cm*$^{-1}$ for our present example). Such fields can be created by the built-in voltage in an *n-i-p-i* structure of about 10 periods, sandwiched between an *n*-bottom and *p*-top layer, or vice versa. This means that very small *external* voltages are required in order to induce large relative changes of the absorption coefficient.

B. Absorption in the excited state

The low recombination probability of photoexcited carriers in doping superlattices implies that the system will usually be in a metastable excited state even at low light intensities and/or low values of the absorption coefficient. The crystal then contains a finite number of electrons in the n layers and holes in the p layers whose distribution can be characterized by (different) quasi Fermi levels ϕ_n and ϕ_p. The presence of charge carriers has two striking consequences for optical absorption.

(1) The superlattice potential, and therefore the effective band gap and the subband structure, will be different from the one in the ground state due to the partial compensation of the built-in impurity space charge by the electrons and holes. This has been discussed in great detail in the context of self-consistent subband-structure calculations for GaAs-doping superlattices in Ref. 14. For *n-i-p-i* structures in IV-VI materials it should be remarked that a much larger number of charge carriers than in GaAs is required to induce a significant change in the superlattice potential because of the large static dielectric constant of the host lattice.

(2) The partial occupation of subbands causes a Burstein shift in the absorption edge. The absorption threshold will no longer be given by Eq. (27), but by

$$\hbar\omega^{\text{th}}=\min_{i,j}\{E_{c,\mu}^{(i)}-E_{v,\nu}^{(j)}+(\hbar^2/2)\max_{i,j}((k_{f,\mu}^{(i)})^2,(k_{f,\nu}^{(j)})^2)[(m_c^{(i)})_{xy}^{-1}+(m_v^{(j)})_{xy}^{-1}]\}\ , \tag{64}$$

provided the transition $|v,(j),\nu\rangle\rightarrow|c,(i),\mu\rangle$ is allowed and the k-selection rule applies strictly for the momentum $\hbar\vec{k}_{||}$ of carriers in these subbands. Here, $k_{f,\mu}^{(i)}$ and $k_{f,\nu}^{(j)}$ are the quasi Fermi wave vectors for electrons and holes, respectively. The Burstein shift in GaAs-doping superlattices is more important than in bulk material because even a relatively low excitation intensity can induce a large concentration of photoexcited carriers and, therefore, large quasi Fermi wave vectors. Furthermore, the fact that transitions from the light-mass valence bands dominate the absorption enhances the Burstein shift over that observed in the bulk, where the transitions from the heavy-mass valence band dominate. The Burstein shift also implies that the lowest transition is not necessarily the one between the lowest conduction and valence subbands.

We have used the results of self-consistent subband-structure calculations for GaAs-doping superlattices[14] to calculate the absorption coefficient for various excitation levels. As design parameters we selected $n_D=4\times10^{18}$ cm^{-3}, $n_A=(m_{LH}/m_e)n_D$, and $d=40$ nm. The results are shown in Figs. 8–12. Obviously, the absorption coefficient changes in magnitude and, in particular, in its frequency dependence as a function of carrier concentration.

In Fig. 13 we have plotted the absorption coefficient for a fixed photon energy as a function of the excitation level for the same GaAs *n-i-p-i* crystal. It should be noted that some of the steps in the absorption coefficient correspond to changes by almost an order of magnitude. Since the charge carriers may simply be produced by photoexcitation their concentration will be related to the intensity of the absorbed light. Therefore, the absorption in doping

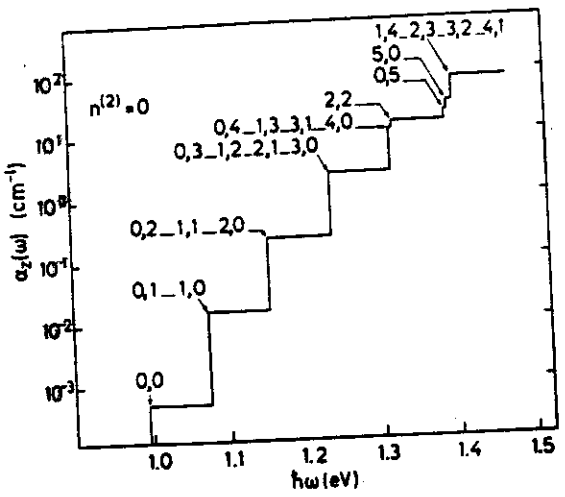

FIG. 8. Absorption coefficient of a compensated GaAs *n-i-p-i* crystal with $n_D=4\times10^{18}$ cm^{-3}, $n_A=(m_{LH}/m_c)n_D$, and $d=40$ nm at different nonequilibrium carrier concentrations, calculated numerically. The numbers indicate the valence- and conduction-band indices of transitions becoming allowed at a given photon energy. The absorption coefficient for $\mu+\nu\leq3$ has also been calculated analytically for the carrier-free ground state. The deviations from the numerical results are too small to be shown in the plot. At higher subband indices deviations from the harmonic-oscillator energies become apparent. The heavy-hole contributions are neglected in this example. $n^{(2)}=0$.

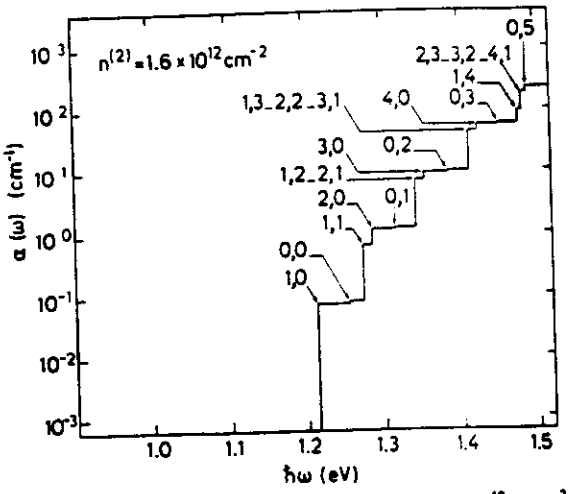

FIG. 10. Same as Fig. 8, except $n^{(2)}=1.6\times10^{12}$ cm^{-2}.

superlattices is strongly intensity dependent, i.e., nonlinear. The discussion of the excitation kinetics and their consequences for low-intensity nonlinear phenomena is deferred to a planned subsequent publication.

IV. CONCLUSIONS

In this paper we have presented the theory of optical absorption in *n-i-p-i* doping superlattices together with the results of analytical and numerical calculations of the absorption coefficient $\alpha(\omega)$. We have found a pronounced steplike structure of the absorption coefficient as a function of photon energy which can extend far below the band gap of the host material of the *n-i-p-i* structure. The strength of absorption for a given photon energy, and the threshold energy at which the absorption becomes zero, can be modulated for a given specimen within wide limits by the application of external fields normal to the layers of the superlattice or by changing the nonequilibrium carrier concentration.

We have tried to demonstrate the wide range of situations which can be encountered, depending on the choice of host material and design parameters. We have neglected a number of physical mechanisms which may affect the observed behavior in real *n-i-p-i* crystals, depending on the host material, the design parameters, and the photon energy. None of them, however, is expected to make the observation of any of the phenomena discussed in the present paper impossible.

The potential fluctuations, for instance, which result from the random spatial distribution of the impurity atoms,[14] may broaden the expected steps of the absorption coefficient. This will be important if the fluctuations are not screened by (a relatively small number of) charge carriers in the layers. The conditions for the observation of

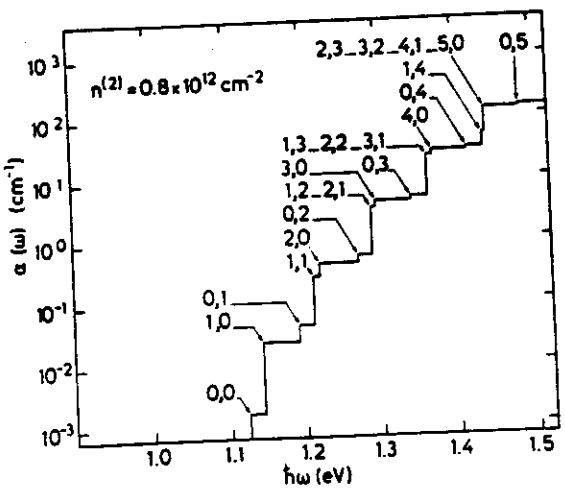

FIG. 9. Same as Fig. 8, except $n^{(2)}=0.8\times10^{12}$ cm^{-2}.

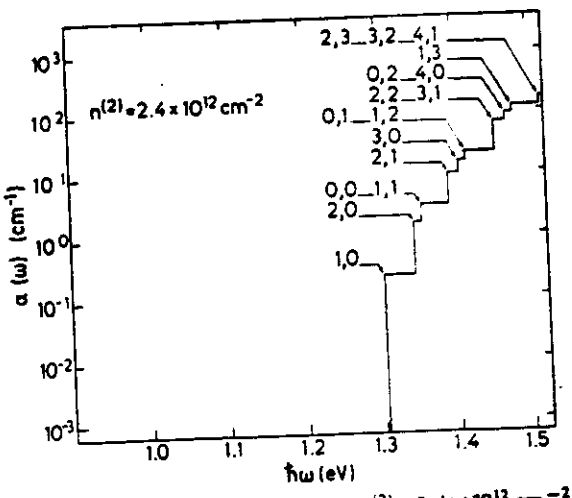

FIG. 11. Same as Fig. 8, except $n^{(2)}=2.4\times10^{12}$ cm^{-2}.

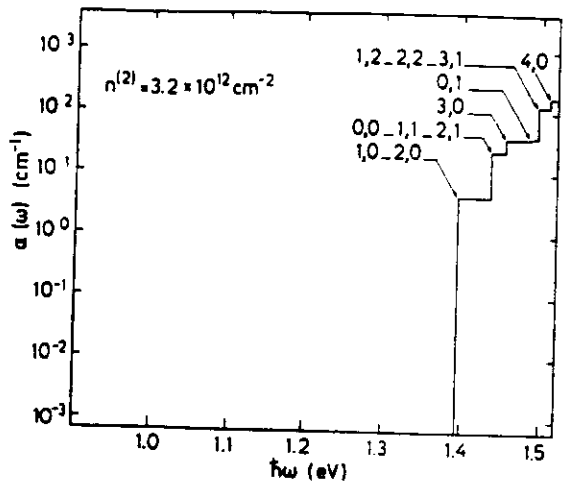

FIG. 12. Same as Fig. 8, except $n^{(2)}=3.2\times10^{12}$ cm^{-2}.

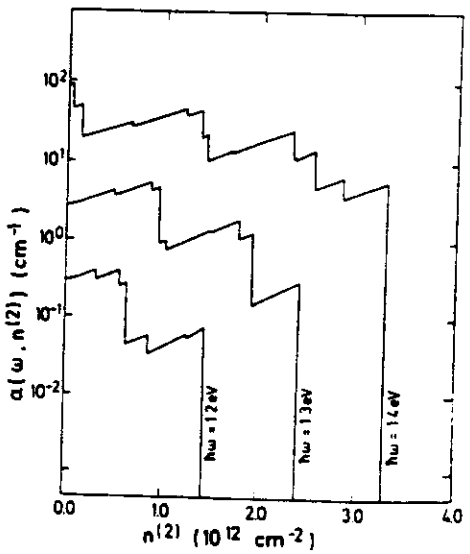

FIG. 13. Absorption coefficient as a function of carrier concentration for the photon energies indicated for the same example as in Fig. 8.

the quantum structure in the absorption coefficient generally will be more favorable at high doping levels since the subband spacing increases faster than the potential fluctuations with increasing doping concentration. Moreover, a lower-band-gap material, such as InAs, will be more suitable than GaAs because of the larger subband spacing resulting from smaller electron and light-hole masses. *n-i-p-i* structures grown in IV-VI compounds, finally, seem ideal from the point of view of neglecting potential fluctuations and problems associated with impurity-band formation (see Refs. 14 and 20) because of their large static dielectric constant which makes the potential fluctuations small and prevents the formation of impurity bands.

The effective-mass approximation, which has been used throughout this paper, on the other hand, will become unsatisfactory more often in the lower-band-gap materials. The subband spacing will be overestimated because of the neglected nonparabolicity at higher subband indices. The matrix elements, on the other hand, will be underestimated because of the errors introduced by the EMA calculation for the overlap between conduction- and valence-subband envelope wave functions.

We have not considered in detail the consequences of our results for the observation of pecularities in the photoconductive response, of nonlinearities in the absorption coefficient, for optical gain, or for the generation of spin-polarized electrons, nor have we discussed device applications of these unusual properties.

We should also point out that the choice of design parameters for the examples presented in this study was not made aiming for favorable conditions for device applications. The appropriate design for devices depends on their purpose. For ultrafast modulation of the absorption coefficient at given photon energy by a field F_z in an electro-optical modulator, e.g., see Sec. III A, the optimized design is achieved by high doping levels and small superlattice period. Such a configuration will combine a sharp increase of α values from close to 0 up to 10^1–10^3 cm^{-1} at the given photon energy $\hbar\omega \lesssim E_g^{\text{eff},0}$ under low values of F_z and with recombination lifetimes which are sufficiently short to prevent a signal-dependent "floating" of the absorption edge. If, on the other hand, a sensitive photoconductive detector working quite far below the gap of the host material is to be designed, a device with $E_g^{\text{eff},0} \ll E_g^0$ provides a wide absorption tail. Long carrier-recombination lifetimes are obtained by moderate doping and a large superlattice period. While an adequate description for the former case is only provided by our present theory, the latter case can be treated with our semiclassical theory.[11] In fact, the latter case is more appropriate, not only from the point of view of requiring much less computational effort, but also on theoretical grounds. In cases where $E_g^{\text{eff},0} \simeq 0$, the absorption for photon energies not far below the gap of the host material, E_g^0, involves transitions between high-index subbands, to which the EMA can no longer be applied.

---

*On leave of absence at Hewlett-Packard Laboratories, 1501 Page Mill Road, Palo Alto, CA 94603.

†Present address: Code 6877, Naval Research Laboratory, Department of the Navy, Washington, D.C. 20375.

[1]G. H. Döhler, Phys. Status Solidi B 52, 79 (1972); 52, 533 (1972).

[2]G. H. Döhler, J. Vac. Sci. Technol. 16, 851 (1979).

[3]G. H. Döhler, in *Festköperprobleme: Advances in Solid State Physics*, edited by P. Grosse (Vieweg, Braunschweig, 1983), Vol. XXIII, p. 207.

[4]G. H. Döhler, Jpn. J. Appl. Phys. Suppl. 22, 29 (1983).

[5]R. Dingle, in *Festköperprobleme: Advances in Solid State Physics*, edited by H. J. Queisser (Vieweg, Braunschweig, 1975), Vol. XV, p. 21.

[6]L. Esaki, J. Cryst. Growth, 52, 227 (1981).

[7]G. H. Döhler, H. Künzel, D. Olego, K. Ploog, P. Ruden, H. J. Stolz, and G. Abstreiter, Phys. Rev. Lett. 47, 864 (1981).

[8]K. Ploog, H. Künzel, J. Knecht, A. Fischer, and G. H. Döhler, Appl. Phys. Lett. 38, 870 (1981).

[9]K. Ploog, H. Jung, H. Künzel, and P. Ruden, Jpn. J. Appl.

Phys. Suppl. 22, 287 (1983).
[10]H. Jung, G. H. Döhler, H. Künzel, K. Ploog, P. Ruden, and H. J. Stolz, Solid State Commun. 43, 291 (1982).
[11]G. H. Döhler, H. Künzel, and K. Ploog, Phys. Rev. B 25, 2616 (1982).
[12]H. Künzel, G. H. Döhler, P. Ruden, and K. Ploog, Appl. Phys. Lett. 41, 852 (1982).
[13]H. Jung, G. H. Döhler, E. O. Göbel, and K. Ploog, Appl. Phys. Lett. 43, 40 (1983).
[14]P. Ruden and G. H. Döhler, Phys. Rev. B 27, 3538 (1983).
[15]K. Ploog, A. Fischer, and H. Künzel, J. Electrochem. Soc. 128, 400 (1981).
[16]P. Ruden and G. H. Döhler, Phys. Rev. B 27, 3547 (1983).
[17]H. M. Gibbs, S. S. Tarng, J. L. Jewell, D. A. Weinberger, K. Tai, A. C. Gossard, S. L. McCall, A. Passner, and W. Wiegmann, Appl. Phys. Lett. 41, 221 (1982).
[18]F. Stern and W. E. Howard, Phys. Rev. 163, 816 (1967).
[19]D. L. Mitchell and R. F. Wallis, Phys. Rev. 151, 581 (1966).
[20]D. H. Döhler and P. Ruden, Surf. Sci. (to be published).
[21]E. O. Kane, in *Semiconductors and Semimetals*, edited by R. K. Willardson and A. C. Beer (Academic, New York, 1972), Vol. 1, p. 75.
[22]G. Fishman and G. Lampel, Phys. Rev. B 16, 820 (1977).
[23]D. T. Pierce and F. Meier, Phys. Rev. B 13, 5484 (1976).

n-i-p-i Doping Superlattices Under High Magnetic Fields

G.H. Döhler

Institut für Technische Physik, Erwin-Rommel-Str. 1
D-8520 Erlangen, Fed. Rep. of Germany

1. Introduction

It is well known, that the spatial separation between electrons and holes in doping superlattices results in quite remarkable pecularities of the electronic structure and the electrical and optical properties of semiconductors belonging to this class of materials /1,2/. Due to a strongly reduced overlap between electron and hole wave functions the recombination lifetimes may be enhanced by orders of magnitude compared with the uniform bulk material. Large deviations of the electron and hole concentrations in the n- and p-layers are metastable. The effective bandgap and also the energetic separation between the electric subbands become dynamically tunable. This tuning can be achieved by changing the carrier densities either by optical excitation or by carrier injection or extraction by means of selective n- and p-contacts /3,4/. Another important aspect when dealing with n-i-p-i doping superlattices is the role of impurities causing bound electronic states and, because of their random distribution, spatial potential fluctuations /1/. Although, in many cases, the impurities lead to undesired broadening of the energy levels, they can also lead to interesting properties, including metal-insulator transitions, in systems of appropriate design as pointed out in a recent paper /4/.

In spite of the fact that the properties of n-i-p-i doping superlattices can be modulated optically or electrically within a wide range it turns out, that high magnetic fields add an exciting new dimension for tuning the electronic properties of these materials. The effect of a magnetic field on the electronic structure does not only show up as a change of subband energies. Because of the conduction-valence band transitions, which depend sensitively on the overlap between electron and hole wave functions within the energy gap, we have a very delicate tool to monitor magnetic field induced changes of the wave functions even in the region far away from their origin. Such studies imply the possibility to obtain a lot of information which is not obtained in the simple variational calculations which are frequently used to solve similar problems. A variational approach may provide reasonably good results for the energy levels but will yield completely unsatisfactory approximations for the wave functions. These aspects and their implications will be discussed in section 2 of this paper.

In section 3 we will investigate some of the impurity related aspects of high magnetic fields applied to n-i-p-i doping superlattices, or to "hetero n-i-p-i's", an extension of the original concept in which compositional modulation is combined with modulation by periodic n- and p-doping. We will see, that variation of the

Springer Series in Solid-State Sciences, Vol. 87
High Magnetic Fields in Semiconductor Physics II Editor: G. Landwehr
© Springer-Verlag Berlin, Heidelberg 1989

magnetic field allows for a geometrical scaling of the structure, while electrical and/or optical tuning allows for depleting or filling up the densitiy of state distribution. Within this 2-dimensional parameter space we expect unique possibilities to study metal insulator transition of the Mott-Anderson and of the Mott-Hubbard type by optical and by transport measurements.

2. Effect of High Magnetic Fields on Energies and Transition Probabilities

In this section we will investigate the effect of a magnetic field which is oriented parallel to the layers or normal to them on the dynamically 2-dimensional states of an idealized n-i-p-i crystal (potential fluctuations due to random impurity distribution neglected).

2. 1. Magnetic Field Parallel to the Layers

We assume a n-i-p-i crystal consisting of a uniform semiconductor host material with band gap E_g^o, dielectric constant $\varkappa_o$ and effective masses m_e, m_{hh} and m_{lh} for electron, heavy and light holes near the band edges. Due to the periodic n- and p-doping in the superlattice direction, z, there is a periodic space charge

$$\rho(z) = e(n_D(z) - n_A(z) - n(z) + p(z)) \qquad (1)$$

due to ionized donors and acceptors as well as due to free electrons and holes, respectively. The space charge potential

$$v(z) = (4\pi e/\varkappa) \int^{z} dz' \int^{z'} \rho(z'')dz'' \qquad (2)$$

with the superlattice period d superposed to the lattice-periodic potential $H_o = p^2/2m + V_o(r)$ of the host material. In the following we are using the effective mass approximation

$$H_o \approx p^2/2m_i \; ; \text{ with } i = e, hh, lh \qquad (3)$$

for electrons, heavy and light holes, respectively. Thus, the energies and Bloch functions for the bulk material become

$$\varepsilon_i(k) \approx \begin{cases} E_c + (\hbar^2/2m_e)k^2; & i = e \\ (-\hbar^2/2m_i)k^2; & i = lh, hh \end{cases} \qquad (4)$$

and

$$\varphi_{i,k}(r) \approx e^{ikr} u_{i,k_o}(r); \qquad i = e, lh, hh \; . \qquad (5)$$

We introduce the magnetic field B in the xy-plane by the vector potential

$$\mathbf{A} = (0,-Bz,0) \qquad (6)$$

whence

$$\mathbf{B} = \mathrm{rot}\ \mathbf{A} = (B, 0, 0) \quad . \tag{7}$$

Thus, the effective mass Schrödinger equation to be solved reads

$$\{(1/2m_l)[p_x^2 + (p_y+eBz/c)^2 + p_z^2] + v(z) - \varepsilon^B_{i,\mu,k_\perp}\}\ \psi^B_{i,\mu,k_\perp}(\mathbf{r}) = 0 \quad . \tag{8}$$

In equ. (8) we have already taken into account that the carriers remain free with respect to their motion in the (x,y)-plane and therefore will be described by their momentum $\mathbf{k}_\perp$ and the subband quantum number μ (we will neglect miniband dispersion $\varepsilon(k_z)$ due to interaction between neighbouring potential wells, assuming a sufficiently high and long-period space charge potential). Using the ansatz

$$\psi^B_{i,\mu,k_\perp}(\mathbf{r}) = e^{i(k_x x+k_y y)}\ u_{i,k_0}(\mathbf{r})\ \zeta^B_{i,\mu}(z) \tag{9}$$

in equ. (8) allows one to separate the z-dependent part

$$\{-(\hbar^2/2m_l)\partial^2/\partial z^2 + v(z) + (e^2B^2/2m_lc^2)(z-z_{k_y})^2 - \varepsilon_{i,\mu}(\mathbf{k}_\perp) + \hbar^2k_x^2/2m_l\}\ \zeta^B_{i,\mu}(z) = 0\ ; \qquad i = e,\ hh,\ lh \tag{10}$$

where

$$z_{k_y} = \hbar k_y c/eB \quad . \tag{11}$$

A good approximate solution of equ. (10) can be obtained easily if the n- and p-layer are zones of uniform n- and p-doping, respectively, with thicknesses fulfilling the condition $n_D d_n = n_A d_p$. In this case equ. (10) becomes the Schrödinger equation for harmonic oscillators with energy levels given by

$$\varepsilon_{i,\mu,k_\perp} = \begin{cases} E_g^o - 2V_o + (\hbar^2/2m_e)\{k_x^2 + (\omega_{p,e}/\omega_e^B)^2 k_y^2\} + \hbar\omega_e^B(\mu+1/2); & i = e \\ -(\hbar^2/2m_l)\{k_x^2 + (\omega_{p,l}/\omega_l^B)^2 k_y^2\} + \hbar\omega_l^B(\mu+1/2); & i = hh,\ lh, \end{cases} \tag{12}$$

with

$$2V_o = (\pi e^2/2\varepsilon_o)\ (n_D d_n^2 + n_A d_p^2) \tag{13}$$

and

$$\omega_l^B = (\omega_{p,l}^2 + \omega_{c,l}^2)^{1/2} \quad . \tag{14}$$

Compared with the B = 0 case where the subband spacing is given by the (formal) plasmon energies

$$\hbar\omega_{p,l} = (4\pi e^2\hbar^2/\varepsilon_o)^{1/2} \begin{cases} (n_D/m_e)^{1/2}\ ; & i = e \\ (n_A/m_l)^{1/2}\ ; & i = hh,\ lh \end{cases} \tag{15}$$

the subband spacing is now renormalized by the Landau energies

$$\hbar\omega_{c,i} = \hbar eB/m_i c \quad . \tag{16}$$

Also, the energies are shifted by the (diamagnetic) term $\hbar(\omega_i^B - \omega_{i,p})/2$. In GaAs with $n_D = 4 \times 10^{17} cm^{-3}$ and B = 15T we find, for instance,

$\hbar(4\pi e^2 n_D/\chi_o m_e)^{1/2} \approx 25$ meV $\approx \hbar eB/m_e c$, or $\hbar\omega_e^B \approx 35$ meV.

The wave functions are also renormalized and shifted into the z-direction.

$$\zeta_{i\mu}^B(z) = (m_i\omega_i^B/\pi\hbar)^{1/4}(2^n n!)^{-1/2} H_\mu\left((m_i\omega_i^B/\hbar)^{1/2}(z-\Delta_{i,k_y}-z_{in})\right) \cdot \exp[-(m_i\omega_i^B/2\hbar)(z-\Delta_{i,k}-z_{in})^2] \quad , \tag{17}$$

where

$$z_{in} = nd \; ; \quad i = e \quad \text{and} \quad (n-\tfrac{1}{2})d < z < (n+_2)d \tag{18}$$

and

$$z_{in} = (n+\tfrac{1}{2})d \; ; \quad i = hh, lh \quad \text{and} \quad nd < z < (n+1)d \quad . \tag{19}$$

The shift of the wave functions in z-direction

$$\Delta_{i,k_y} = z_{k_y}(\omega_{c,i}/\omega_i^B)^2 = (\hbar k_y/m_i)\omega_{c,i}/(\omega_i^B)^2 \tag{20}$$

is a consequence of the Lorentz force experienced by particles with a momentum $\hbar k_y$ perpendicular to the B-field. The Lorentz force is also the reason for the increase of the effective mass with respect to the in-plane motion perpendicular to the B-field (see kin energy term in Eq. (12)).

The renormalization of the subband energies has been investigated by Maan et al. /5/ in magnetoresistance experiments. These authors were able to demonstrate that the conductance showed quantum oscillation as a function of magnetic field in quantitative agreement with the expected behavior.

From equs. (17) to (19) we can calculate the changes of overlap and the resulting changes of the conduction to valence subband transition probabilities. A comparison between experiment and theory is particularly interesting as we are investigating with high sensitivity the changes of the *wave function* induced by the B-field. Usually, only the changes of the *energies* induced by a perturbation are observed. For the $\mu = 0$ electron light-hole transition we find for the change of transition probability reduction factors with and without B-field (assuming $n_D = n_A$, $d_n = d_p$, $m_{lh} \approx m_e$)

$$w_{oo}^B = w_{cv}^{bulk} \exp[-m_e\omega_e^B d^2/8\hbar] \tag{21}$$

and

$$w_{oo} = w_{cv}^{bulk} \exp[-m_e \omega_{p,e} d^2/8\hbar] \qquad (22)$$

respectively. We have used Equ. (35) from Ref. 6 in order ot obtain Eqs. (21) and (22).

For our previous example ($\hbar\omega_{p,e}$ = 25 meV, B = 15 T) we find for d ≈ 50 nm a red shift of the luminescence of about 85 meV. The transition probability reduction factor which is ≈ 10^{-16} at B = 0 becomes ≈ $4 \cdot 10^{-9}$ at B = 15 T, i.e., the transition probabilities for luminescent or absorptive transitions change by a factor ≈ 250 by the applications of the B-field.

So far we have neglected the shift Δ_{1,k_y} of the wave functions which occurs for carriers with a finite momentum $\hbar k_y$ perpendicular to the B-field. From (11) and (20) we see, that the sign of this shift depends on the direction of the y-component of the motion of the carriers. Also it has opposite sign for electrons and holes. We can easily calculate the effect on the transition probabilities for the symmetric case discussed before. Equation (21) has to be modified by replacing d/2 by $d/2 - \Delta_{e,k_y} + \Delta_{lh,k_y} \approx d/2 - 2\Delta_{e,k_y}$. We find

$$w_{oo}^{B}(k_y) = w_{cv}^{bulk} \exp[-m_e \omega_e^B (d/2 - 2\Delta_{k_y})^2/2\hbar] \ , \qquad (23)$$

whereas (21) remains unchanged.

For our previous values and assuming a reasonable electron concentration of $n^{(2)} = 5 \cdot 10^{11} cm^{-2}$ we find for the recombination probability of electrons and light holes with the Fermi momentum $k_{F,y} = 2^{1/4}(2\pi n)^{1/2}$ (the factor $2^{1/4}$ is a consequence of the change of effective mass, m_y)

$$w_{oo}^{1ST}(k_{F,y} = 2 \cdot 10^6\ cm^{-1}) \approx 120\ w_{oo}^{B=0} \approx 3 \cdot 10^4\ w_{oo}^{1ST}(k_y = 0) \ .$$

Thus, we find, that the *strong reduction* of transition probability for carriers of zero momentum perpendicular to the B-field, which is due to the potential becoming steeper, can be *largely overcome* by the Lorentz force driving electrons and holes towards each other for carriers with momentum close to the Fermi momentum. For our specific example the overall transition probability remains unchanged if $n^{(2)} \approx 10^{11} cm^{-2}$, but changes by about +2 (-2) orders of magnitude for $n^{(2)} \approx 5 \cdot 10^{11} cm^{-2}$ ($2 \cdot 10^{10} cm^{-2}$), if a B-field of 15 T is switched on.

We have discussed here only the simplest case in order to illustrate the expected phenomena. An ideal system for the observation of the carrier density dependent effect of a parallel magnetic field on the interband transition probabilities is the PbTe n-i-p-i /7/. The high field case, $\hbar\omega_{c,l} \geq \hbar\omega_{p,l}$, is not only realized at relatively low B-fields, but also the assumption of free electrons and holes is justified for electrons and holes as well. The present results have only to be extended to the (nearly symmetric with respect to electrons and holes) multi-valley band structure of PbTe /8/. It is clear, that the results will change qualitatively for other doping profiles, such as δ-doping /1,8/ or in hetero - n-i-p-i's /2/. Of particular interest is the situation, if the carriers are no longer moving perpendicular to the B-field. This can be due to the formation of Landau orbitals under a B-field having also

a z-component or due to localization by impurity potentials or spatially random potential fluctuations. These cases, for which we expect qualitative changes will be discussed in sections 2.2 and 3.

2.2. Magnetic Field Normal to the Layers

We chose the gauge

$$\mathbf{A} = (By/2, -Bx/2, 0) \quad . \tag{24}$$

This is also the appropriate gauge for a system with additional potentials v(x,y) which we will treat in section 3. Replacing p by (p-eA/c) in the effective mass Schrödinger equation now yields, instead of our previous eq. (8)

$$\{(1/2m_i)(p_x^2+p_y^2+p_z^2) + \frac{m_i\omega_c^2}{8}(x^2+y^2) + \hbar\omega_c L_z + v_o(z) - \varepsilon_{i,\mu,n,L_z}\}\,\psi^B_{i,\mu,n,L_z}(r) = 0 \quad . \tag{25}$$

Eq. (25) reflects the full quantization of the system by the formation of Landau orbits in the (x,y)-plane with quantum numbers n and L_z and the confining superlattice potential $v_o(z)$ in the z-direction. Eq. (25) can be separated into a z-dependent and a (x,y)-dependent part. For the ground state we find (assuming again uniform doping in the n- and p-layers)

$$\psi^B_{i,o,o,o} = N^{-1/2}\exp\{-\frac{m_i\omega_{c,i}}{2\hbar}(x^2+y^2)\}\exp\{-\frac{m_i\omega_{p,i}}{2\hbar}(z-z_{in})^2\};\quad i = e,\ lh,\ hh \tag{26}$$

and

$$\varepsilon_{i,o,o,o} = \begin{cases} E_c - 2V_o + \hbar\omega_{c,e}/2 + \hbar\omega_{p,e}/2; & i = e \\ -\hbar\omega_{c,i}/2 - \hbar\omega_{p,e}/2 \quad ; & i = hh,\ lh \quad . \end{cases} \tag{27}$$

where the degeneracy of the Landau levels per layer is $(eB/\pi\hbar c)$-fold, as known from any 2-D system. From (2b) we see, that the interband transition probabilities should not be affected by the normal B-field, as the z-dependence of the wave function isn't.

2.3. Arbitrary Orientation of the Magnetic Field

Without loss of generality (except for the case of an anisotropic band structure of the host material) we can choose a magnetic field

$$\mathbf{B} = (B_x,\ 0,\ B_z) \quad . \tag{28}$$

Having the results of 2.1 and 2.2 in mind, one might first expect that the system is now fully quantized due to the B_z-induced Landau level formation, but with the space charge induced subband energies renormalized by the field component B_x

parallel to the layers. Actually, however, the system is now 1-dimensional, as the carriers are still free to move in the x-direction, although experiencing a Lorentz force due to the z-component of the B-field.

The B-field (28) can be derived from the vector potential

$$\mathbf{A} = (-B_z y,\ -B_{x1} z,\ B_{x2} y) \tag{29}$$

with

$$B_{x1} + B_{x2} = B_x \quad . \tag{30}$$

Inserting the ansatz

$$\psi_{i,\mu,n}(r) = N^{-1/2} e^{ik_x x} \Phi_n(y) \zeta_\mu(z) \tag{31}$$

into the effective mass Schrödinger equation yields

$$\{\hbar^2 k_x^2/2m_i - (\hbar^2/2m_i)(\partial^2/\partial y^2 + \partial^2/\partial z^2) + (m\omega_y^2/2)(y + \Delta_{k_y}^2) + (m\omega_z/2)z - i\hbar\omega_{x1} z(\partial/\partial y) + i\hbar\omega_{x2} y(\partial/\partial z) - \varepsilon_{i,\mu,n}(k_x)\}\varphi_n(y)\zeta_\mu(z) = 0 \tag{32}$$

with

$$\Delta_{i,k_x} = (\hbar k_x/m_i)(\omega_{c,i}/\omega_{y,i}^2) \quad , \tag{33}$$

$$\omega_{c,i} = eB_z/m_i c \ ; \quad \omega_{x1,i} = eB_{x1}/m_i c \ ; \quad \omega_{x2,i} = eB_{x2}/m_i c \ , \tag{34}$$

$$\omega_{y,i}^2 = \omega_{c,i}^2 + \omega_{x2,i}^2 \ , \tag{35}$$

$$\omega_{z,i}^2 = \omega_{p,i}^2 + \omega_{x1,i}^2 \quad . \tag{36}$$

The ansatz

$$\Phi_o(z)\ \zeta_o(z) = \exp\{-(m_i\omega_{yi}/2\hbar)(y+\Delta_{i,k_x})^2\}\ \exp\{-(m\omega_{z,i}/2\hbar)(z-z_{1n})^2\}; \quad i = e,\ hh,\ lh \tag{37}$$

turns out to be the solution for the lowest index subbands, if the gauge of B_x is chosen such that

$$\omega_{x1}\omega_z = \omega_{x2}\omega_y \quad . \tag{38}$$

From the definitions for the frequencies (38) it follows, that this is equivalent to

$$B_{x2}/B_{x1} = \omega_c/\omega_p \quad . \tag{39}$$

The energies become

$$\varepsilon_{i,o,o}(k_x) = \begin{cases} E_g^o - 2V_o + (\hbar\omega_{y,i} + \hbar\omega_{z,i})/2 + (\hbar^2/2m_i)(\omega_{x1,i}/\omega_{y,i})^2 k_x^2 ; & i = e \\ -(\hbar\omega_{y,i} + \hbar\omega_{z,i})/2 - (\hbar^2/2m_i)(\omega_{x1,i}/\omega_{y,i})^2 k_x^2 ; & i = hh,lh \end{cases} . \quad (40)$$

The expression for the 1-dimensional subband reduces to the 0-dimensional Landau system (27) in the limiting case of $B_x \to 0$. Note, that in this case the renormalized effective mass for the motion in x-direction in (40) diverges, i.e., $m_i^{eff} = m_i(\omega_{y,i}/\omega_{x1,i})^2 \to \infty$. This implies the transition from the 1-dimensional density of states, which exhibits logarithmic singularities at the discrete energy levels $(n+1/2)\hbar\omega_c + (\mu+1/2)\hbar\omega_z$ to the δ-function-density of states of the Landau level system discussed in 2.2.

From (37) and (33) we see that a finite momentum in x-direction shifts the wave function in y-direction. The z-dependent part of the wave function, however, remains centered at the middle of the n- and the p-layers. Thus, the k_y-dependent *increase* of the transition probabilities, discussed in section 2.1 will not occur, if, in addition to the magnetic field parallel to the layer, B_x, there is also a magnetic field, B_z, normal to them (at least, if it is strong enough to achieve the magnetic quantum limit).

For our previous example this means, that the transition probabilities, which are enhanced for carriers the Fermi level by the field $B_x = 15$ T by a factor ≈ 120, compared with the field-free case will drop to a value which is even by a factor of ≈ 20 lower than the field-free case value if a B_z-field of 9 T is added.

3. Effects of High Magnetic Fields in the Case of Localized States

So far we have assumed that the carriers are moving free in the (xy)-plane as long as no magnetic fields are applied. In particular, we found for a Fermi system that the transition probabilities may increase upon the application of a field parallel to the layers, instead of the expected reduction if the density is high enough. An additional field normal to the layers, however, may turn the increase back into a strong reduction, due to the formation of Landau levels. In this section we will investigate the consequences of disorder which causes localization of the states in the (xy)-plane.

3.1 Magnetic Fields Parallel to the Layers

We expect that the effect of localization on the magnetic field dependence will be weak, if the random potential, which results from the disorder, is small. If, however, the spatial potential fluctuations are so strong that the classical motion in the ground state of a localized state corresponds to kinetic energies at which the k_y-dependence from eq. (23) leads to strong *increase* of the interband transition probabilities, it is of interest to know whether this *increase* also applies to bound states. In the following we will treat a simple model which can be solved analytically. We assume, that, in addition to the parabolic space charge potential $v_o(z) = (m_i\omega_{i,p}^2/2)\, z^2$ there is also a parabolic potential

$$V_o(x,y) = (m_i\omega_{xo}^2/2)x^2 + (m_i\omega_{yo}^2/2)y^2 \quad . \tag{41}$$

The ground state of this system will be renormalized by a magnetic field parallel to the plane, B_x. Using the gauge

$$\mathbf{A} = (0, -B_{x1}z, B_{x2}y) \; ; \quad B_{x1} + B_{x2} = B \tag{42}$$

and the ansatz

$$\psi_o(\mathbf{r}) = N^{-1/2}\, e^{-(m_i\omega_{xi}^2/2\hbar)x^2}\, e^{-(m_i\omega_{yi}^2/2\hbar)y^2}\, e^{-(m_i\omega_{zi}^2/2\hbar)z^2} \tag{43}$$

we find that (43) is the ground state solution of the effective mass Schrödinger equation with

$$\varepsilon_o = \begin{cases} E_g^o - 2V_o + (\hbar\omega_{x1} + \hbar\omega_{y1} + \hbar\omega_{z1})/2 \; ; & i = e \\ -(\hbar\omega_{x,i} + \hbar\omega_{y,i} + \hbar\omega_{z,i})/2 \; ; & i = hh,\ lh \end{cases} \tag{44}$$

given by

$$\begin{aligned} \omega_{x,i}^2 &= \omega_{xo,i}^2 \\ \omega_{y,i}^2 &= \omega_{yo,i}^2 \{1 + [(eB/m_ic)/(\omega_{p,i} + \omega_{yo,i})]^2\} \\ \omega_{z,i}^2 &= \omega_{p,i}^2 \{1 + [(eB/m_ic)/(\omega_{p,i} + \omega_{yo,i})]^2\} \quad . \end{aligned} \tag{45}$$

This result shows that the localization increases in the two directions perpendicular to the B-field, whereas the wave function is unaffected in the direction of the B-field. By comparison of (45) and (43) with (17) (for μ=0) and (21) we see that the transition probabilities *decrease* with increasing B_x-field, though less strongly as in the case of $k_y = 0$. Specifically we find for $\hbar\omega_{yo}/2 = \varepsilon_F(5\cdot10^{11}\ cm^{-2}) = 15$ meV in our previous example

$$\omega_{z,i} = 1.1\ \omega_{p,i} \tag{46}$$

and

$$w_{oo,loc}^{15T} \approx 0.25\, w_{oo}^{B=o} \approx 2\cdot10^{-3}\, w_{oo}^{15T}(k_y = k_{F,y}(5\cdot10^{11}\ cm^{-2}) \tag{47}$$

if conduction and valence band states are localized. The last number in (47) demonstrates the dramatic difference betweeen extended and localized states with respect to interband transition probabilities, quite analoguous to the results obtained by the reduction of dimensionality introduced by an additional B-field component normal to the layer. This difference in transition probabilities may be a useful tool to distinguish experimentally between extended and localized states.

In this section we have only treated the ground state for a simple model. We expect, however, that the results will not change qualitatively if more realistic situations are assumed.

3.2 Magnetic Field Perpendicular to the Layer

If we assume the same potential $v_o(z)$ due to the space charge potential and $v_o(x,y)$ due to disorder as in section 3.1, with the magnetic field, however, oriented in z-direction, we obtain, with the gauge for the vector potential given in (24), the same results (43) and (44) for the ground state solution of the effective mass Schrödinger equation. The values of ω_x, ω_y, and ω_z, however, are now given by

$$\omega_{x,l} = \omega_{y,l} = [\omega_{0,l}^2 + (eB/m_l c)^2]^{1/2}$$
$$\omega_{z,l} = \omega_{p,l} \quad . \tag{48}$$

These results confirm the expectation that a magnetic field normal to the layers will not influence the z-dependent part of the ground state wave function, also in the case that one is dealing with states localized in the (xy)-plane. The results will not change drastically if $v_o(x,y)$ is no longer a harmonic potential, as long as it is weak compared with $v_o(z)$. A case of particular interest is, of course, the Coulomb potential of an impurity atom /10/. One has to be aware that a solution obtained, say for an impurity at the center of a uniformly doped n- or p-layer, is of limited relevance for a realistic system. For the realistic system we have to take into account that the potential v(r) is not simply the superposititon of the average potential of the uniform space charge back-ground, $v_o(z)$, and the potential of a specific impurity at $\mathbf{R}_i$.

$$v_i(r) = e^2/(\kappa_o |r - R_i|) \quad . \tag{49}$$

In addition, there are strong spatial fluctuations, due to the random distribution of the impurities in the doping layers. There are, however, a number of possibilities to create systems in which the potential can be treated as a superposition of a one-dimensional and a point charge potential, if the requirement of a parabolic shape of $v_o(z)$ is given up. An example of such a structure is proposed in Fig. 6 of Ref. 4. The quantizing field due to the impurities in the n_1- and p_1 layers is nearly uniform within the (very wide) quantum well in between. If the average distance within the (xy)-plane between the impurity atoms is sufficiently large, the potential for the effective mass Schrödinger equation can be described appropriately by the superposition of a triangular potential $v_o(z)$, the Coulomb potential (49) and a vector potential

$$\mathbf{A}_{R_i} = (B/2)\,(y - y_i, -x + x_i, 0) \quad . \tag{50}$$

Such a system is of particular interest, as it is uniquely suited for the study of metal insulator transitions. This is due to the fact that it can be dynamically tuned

within a two-dimensional parameter space. The (two-dimensional) carrier density can be tuned from zero to "high" values such that not only the impurity band is occupied but also the Hubbard band, corresponding to doubly occupied impurities, by variation of optical excitation and/or external potential applied between selective contacts to the n_1- and p_1 - layers /4/. By variation of the magnetic field B_z on the other hand the overlap between neighbouring impurity wave functions can be tuned over a wide range. In particular, the (2-dimensional) doping density can be chosen such that the system is on the metallic side of the Mott-Hubbard metal/ insulator transition /10/ at $B_z = 0$, but goes through the transition with increasing B_z. The photoluminescence spectra due to recombination of electrons from the impurity- and Hubbard band with free holes in the uppermost hole subband monitor the density of states as a function of Fermi level position and bandwidth. Similarly, a somewhat differently designed system allows transport measurements above and below the Mott-Hubbard (or also the Mott-Anderson) transition /4/.

4. Conclusions

We have shown that the effects of a magnetic field on doping superlattices are quite dramatic. The band to band transition probabilities may *decrease* or *increase* in the presence of a magnetic field parallel to the layers by orders of magnitude, depending on the momentum of the carriers perpendicular to the magnetic field. By changing the direction of the field from parallel to normal to the layers the system changes its character from 2-dimensional and finally to 0-dimensional. In the case of states which are localized at B = 0 no increase of the transition probabilities is expected under finite B-fields, but only a more or less strong decrease. Magnetic field studies of n-i-p-i doping superlattices turn out to be a sensitive tool for the study of the wave functions and metal-insulator transitions.

References

1. G.H. Döhler: Phys. Stat. Sol. 52, 79 and 533 (1972); G.H. Döhler: J. Vac. Sci. Technol. 16, 851 (1979)
2. For a recent review see: G.H. Döhler: IEEE QE-22, 1682 (1986); or G.H. Döhler: CRC Review in Solid State and Material Sciences 13 (1986)
3. G.H. Döhler, G. Hasnain, and J.N. Miller: Appl. Phys. Lett. 49, 704 (1986)
4. G.H. Döhler: C.Y. Fong, ed., Plenum Publishing Company, N.Y., in press
5. J.C. Maan, Th. Englert, Ch. Uihlein, H. Künzel, A. Fischer, and K. Ploog: Solid State Commun. 47, 383 (1983)
6. G.H. Döhler and P.P. Ruden: Phys. Rev. B30, 59332 (1984)
7. G.H. Döhler and P.P. Ruden: Surface Science 142, 474 (1984)
8. D.L. Mitchell and R.F. Wallis: Phys. Rev. 151, 581 (1966); G. Martinez, M. Schlüter, and M.L. Cohen, Phys. Rev. B11, 651 (1975)
9. H.P. Hjalmarson: J. Vac. Sci. Technol. 21, 524 (1982); E.F. Schubert, Y. Horikoshi, and K. Ploog: Phys. Rev. B32, 1085 (1985)
10. Y. Yafet, R.W. Keyes, and E.N. Adams: J. Phys. Chem. Solids 1, 137 (1956)
11. N.F. Mott and E.A. Davis: Electronic Processes in Non-Crystalline Materials, Oxford (1979)

From: PROPERTIES OF IMPURITY STATES IN SUPERLATTICE SEMICONDUCTORS
Edited by C. Y. Fong, Inder P. Batra and S. Ciraci
(Plenum Publishing Corporation, 1988)

PROPERTIES OF IMPURITY STATES IN n-i-p-i SUPERLATTICE STRUCTURES

Gottfried H. Döhler

Institut für Technische Physik
Universität Erlangen
Erwin-Rommel-Str. 1, 8520 Erlangen, FRG

Abstract

The primary effect of the static potential of the impurity atoms in doping superlattices is the formation of space charge induced quantum wells. In most of our previous studies of n-i-p-i doping superlattices we have focussed our interest to the remarkable features which result from the spatial separation between electrons and holes, such as tunability of the electronic structure, electron-hole recombination lifetimes, increased by many orders of magnitude compared with those of bulk semiconductors, or huge optical non-linearities. In this lecture we will concentrate on the point defect aspects of impurities in doping superlattices. Topics to be discussed will include the impurity band formation by shallow (donor) and less shallow (acceptor) impurities over the whole concentration range from very low to high concentrations. We propose various n-i-p-i and hetero n-i-p-i structures which should be idealy suite for optical studies of impurity- and Hubbard bands, and for electrical investigations of the density of states of the conductivity in these bands as a function of (tunable) carrier and dopant density. In particular it is expected that these structures represent unique systems for investigations of the Mott-Hubbard transition in two dimensions.

I. Introduction

Since the first proposal of n-i-p-i doping superlattices as crystals with tunable electrical properties and their first theoretical investigation[1,2] a considerable amount of experimental work has been performed, which confirmed the theoretical predictions[3,4]. These results have stimulated further theoretical investigations and proposals for new experimental studies[5-13]. Although all the remarkable features of the n-i-p-i doping superlattices derive from impurities, almost no attention had been paid to the impurity states in these structures. We have almost all the time eliminated them from our discussion by replacing the random

distribution of the point charges within the two- or three-dimensional doping layers by a uniform two- or three-dimensional charge density. In this way a one-dimensional mesoscopic periodic potential is obtained and the well-known tunable electronic structure of n-i-p-i superlattices with tunable carrier concentration, band-gap, subband spacing, and lifetimes is obtained for this system with purely space-charge induced quantum wells. In fact, also some of the properties which are related to the impurity states and to their random distribution have at least qualitatively been discussed in the past[1, 5].

In this paper we first review some of the theoretical and experimental problems associated with the impurity atoms and their random distribution. In the following section we discuss possibilities to overcome these problems. In the last section, finally, we propose new hetero - n-i-p-i - structures, which appear ideally suited for experimental and theoretical investigations of impurity and Hubbard band formation and, in particular, of the Mott-Hubbard transition in two dimensions.

2. Problems associated with the point-charge character and the random distribution of impurities in doping superlatices

Fig. 1 shows an example of self-consistently calculated band-gap, subband energies, and electron and hole quasi Fermi-levels as a function of two-dimensional carrier density $n^{(2)}$ in a n-i-p-i crystal. As mentioned before, the space charge of the impurities has been assumed to be uniformly distributed within the respective layers. The quasi Fermi-level of the holes Φ_p has been taken as a constant reference energy. Formally, the impurity state associated with an additional impurity can be calculated. It is interesting to note, that for the present case of a three-dimensional doping layer, the energy of impurity states as a function of their position with the layer would approximately increase in parallel with the potential itself. Therefore, they would become resonant states of the subbands at relatively small distances from the center of the doping layer. This problem does not arise in the case of δ-doped layers. For this special case the energy of impurity levels in a n-i-p-i crystal and the increase in binding energy with increasing internal space charge fields had been discussed first in our original paper[1]. More detailed studies have been given by Crowne, Reinecke and Shanabrook[14].

In order to estimate the significance of these calculated impurity energies, one has to compare them with the potential fluctuations which are present in the layers as a result of the random distribution of impurity atoms. The fluctuations of this random potential, given by the expression

$$V_{rand}(r) = - \sum_{\substack{\text{all ionized}\\ \text{donors}}} e^2/(\kappa_0 |r-r_i|) + \sum_{\substack{\text{all ionized}\\ \text{acceptors}}} e^2/(\kappa_0 |r-r_j|) \qquad (1)$$

can become very large in the case of a compensated n-i-p-i

crystal in the ground state. With increasing population of the layers by electrons and holes, respectively, the amplitude of these fluctuations decreases rapidly.

It turns out, that the effect of increasing free carrier concentration is very strongly dependent on the effective mass of the charge carriers. The relatively large effective mass of holes in the valence bands of most crystals results in relatively large acceptor ionization energies and a relatively small effective Bohr radius. Thus, a treatment of the effect of increasing population in terms of step by step neutralization of the deepest lying states in this random potential is appropriate. From computer simulations[15] it follows that the potential fluctuations become smaller than the acceptor binding energy at a relatively low ratio of the (2-dimensional) hole to acceptor concentration $p^{(2)}/n_A^{(2)}$ even at rather high values of $n_A^{(2)}$. For the much lower effective masses of electrons in the conduction band of direct gap semiconductors the situation is substantially different. A considerably larger ratio of electron to

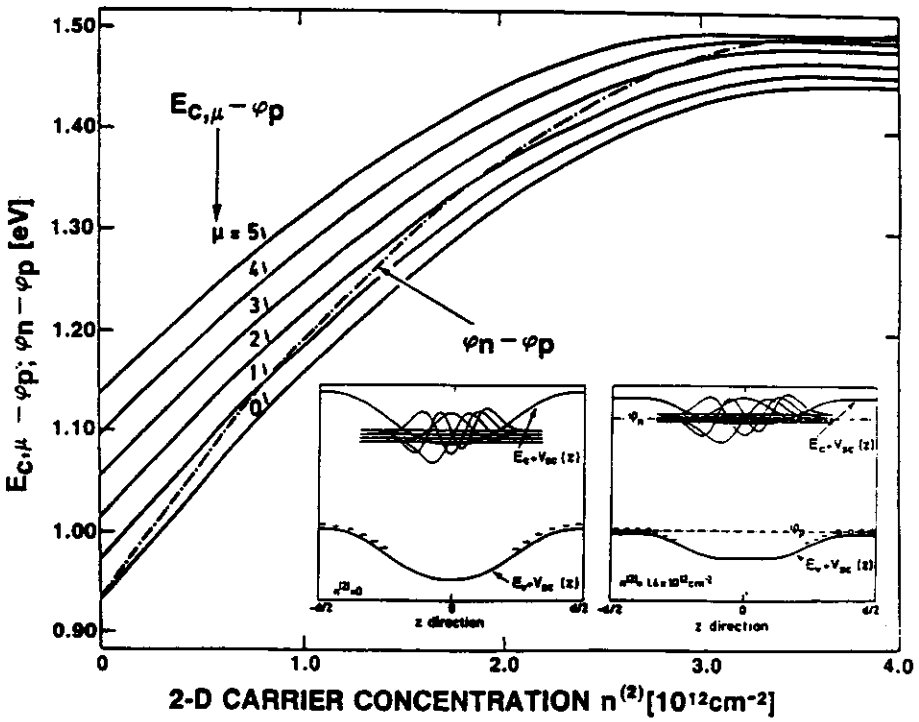

Fig. 1 Relation between (two-dimensional) carrier concentration in the layers and effective band gap and quasi Fermi level difference, calculated self-consistently for a GaAs doping superlattice with $n_D = n_A = 10^{18}cm^{-3}$ and $d_n = d_p = 40nm$. The inset shows the envelope wave functions $\zeta_{c\mu}(z)$ for the lowest subbands for the ground state and for an excited state with $n^{(2)} = 1.4 \times 10^{12}cm^{-2}$.

acceptor concentration $n^{(2)}/n_D^{(2)}$ is required in order to obtain an amplitude of the random potential (Eq. (1)) less than the donor binding energy at the corresponding donorconcentration $n_D^{(2)}$. It is found that at the typical donor concentrations used in n-i-p-i crystals the kinetic energy effects become already very important. The Fermi-energy of a two-dimensional electron gas

$$\varepsilon_F = (\hbar^2/2m_c)(2\pi n^{(2)}) \qquad (2)$$

becomes larger than the donor binding energy at these concentrations. This makes qualitatively plausible that the donor impurity potentials will no longer be strong enough for "condensation" of the electrons in an impurity band. Thus, impurity bands will no longer play a significant role in this case. The appropriate picture is a free electron gas which is screening the random potential of ionized donor potentials[5].

In contrast, the kinetic energy of heavy holes in the valence band becomes comparable to the acceptor ionization energy only at fairly high concentrations. It turns out, that, up to sheet carrier concentrations of $p^{(2)}$ of the order of about $10^{19}cm^{-3}$ the description in terms of an impurity band remains appropriate for acceptors.

From our previous discussion it becomes obvious, that all the energy levels observed in transitions between conduction subbands and the impurity band or some valence subbands exhibit significant broadening due to the imperfect screening of the space charge potential fluctuations. Also, it becomes understandable, that a correct treatment of these problems is quite complicated.

2.2 Acceptor impurity band wave functions

Transitions between conduction and valence subbands can be calculated straight forward by evaluation of the corresponding dipole matrix elements[16]. From our previous discussion, however, it follows that holes will populate not valence subbands, but rather the acceptor impurity band. A calculation of these transitions poses new problems. First of all, the wave function of an impurity band is not known. But even, if it is approximately replaced by a suitable superposition of acceptor wave functions, the following problem still remains unsolved. The maximum contribution to the dipole matrix element for valence to conduction band transitions comes from a rather narrow region somewhere between the centers of two adjacent doping layers. The exact position depends on the shape of the self-consitent potential and the effective masses of the electrons, light and heavy holes. Calculations of the bulk acceptor states have been performed by a variational method involving light and heavy hole states[17]. Although these calculations yield good values for the acceptor energies, it is questionable whether the wave functions obtained by this method are in a satisfactory manner describing their amplitude far away from the acceptor. This, however, is just the relevant range of distances, for a calculation of the transitions between the acceptor and the conduction subbands.

3. Possibilities to avoid impurity related problems in n-i-p-i doping superlattices

3.1 Weakly compensated δ-doped n-i-p-i - structure with low doping concentrations

In order to be specific, we consider a structure as shown in Fig. 2. This n-i-p-i design resembles the one considered in our original work[1,2]. We assume an acceptor concentration much lower than the donor concentration. All acceptors will be ionized in the ground state. The ionized donors will be those which are closest to the negatively charged acceptors.

In the following we will discuss this structure for the case of much lower doping levels than previously considered. In terms of tunable properties this structure becomes quite uninteresting. The intriguing aspects result from this structure representing an ordered version of the well-known donor acceptor pair luminescence[18]. The photon-energy emitted in a recombination between an electron on a donor and a hole on an acceptor is given by[18]

$$\hbar\omega = E_g^0 - E_D - E_A + e/\kappa_0 r_{DA} \qquad (3)$$

(this expression can be easily understood by considering the total energy difference between the initial state, characterized by a neutral acceptor and the electron sitting on a neutral donor, and the final state, characterized by the electron sitting on the acceptor and experiencing the negative electrostatic potential of the donor in the distance r_{DA}, given by $e^2/\kappa_0 r_{DA}$. The transition probability for this process is determined by the overlap between the donor and acceptor wave function.Therefore, it depends exponentially on the distance r_{DA},[18]

$$W(r_{DA}) = W_0 \exp-(r_{DA}/a^*). \qquad (4)$$

a^* is not much different from the effective Bohr radius of the less localized impurity involved.

In a uniform bulk crystal with a random distribution of donors and acceptors the photo-luminescence is determined by the capture and recombination of photo-excited electrons and holes. The Coulomb term in Eq. (3), of course, leads to a considerable broadening of the donor-acceptor pair luminescence spectra. The contribution of the pairs with low distance r_{DA} is, of course, particularly strong. These transitions also cannot easily be saturated because of the high transition probabilities at low distances (see Eq. (4)). The width of the luminescence line associated with donor-acceptor transitions can be estimated from the distribution function of donors neighbouring the acceptors (also for the bulk case we assume n_D much larger than n_A). The probability of finding the next nearest donor within a distance interval (r, r+dr) is given by

$$p(r)dr = 3(r^2/r_0^3) \exp-(r/r_0)^3 dr \qquad (5)$$

Two third of all nearest neighbours are found within the distance interval between r_- and r_+, with r_-, r_+ and r_0 given by

$$r_- = 0.567\ r_0 \tag{6a}$$
$$r_+ = 1.215\ r_0 \tag{6b}$$
$$r_0 = (4\pi n_D/3)^{-1/3} \tag{6c}$$

r_0 corresponds to the average nearest neighbour distance.

Inserting the values for r_- and r_+ into Eq. (3), we find that two thirds of all transitions are found within the energy interval

$$\Delta\hbar\omega^{(3)} = e^2/\kappa_0 r_- - e^2/\kappa_0 r_+ \tag{7}$$

For GaAs with a donor concentration of 10^{16} cm^3 we find

$$\Delta\hbar\omega = 7.1 - 3.3\text{meV} = 3.8\text{meV} \tag{8}$$

From Fig. 2 it is obvious that we suppress all the transitions at distances less than d_i by introducing our one-dimensional ordering. We can think of our n-i-p-i - structure as being obtained by a projection of all the impurities within a superlattice period $d = 2d_i$. This results onto planes separated by the distance d_i in sheet impurity concentrations of

$$n_D^{(2)} = n_D d \tag{9}$$

$$n_A^{(2)} = n_A d. \tag{10}$$

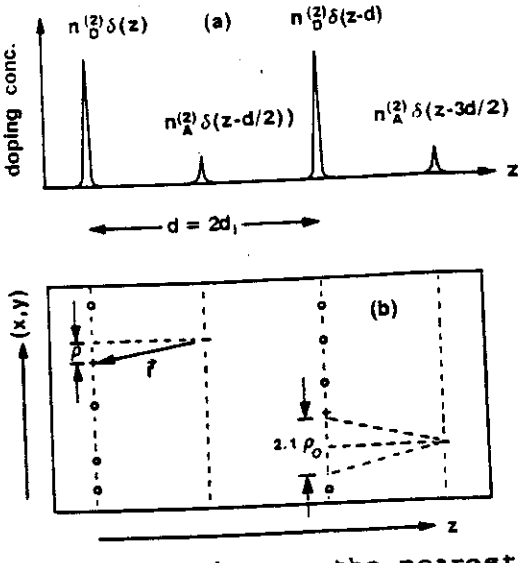

Fig. 2 n-i-p-i structure, as considered in our original work[1,2]. In the upper part the doping profile along the direction of growth, z, is shown. In the lower part a real space picture is shown schematically. The length of the vector r pointing from a (minority) acceptor state to its nearest (majority) donor neighbour is $r = (d_i^2+\varrho^2)^{1/2}$. Approximately 2/3 of all neighbouring donors are found within a circle of diameter $2.1\varrho_0$ centered at the normal projection of the acceptor position onto the neighbouring n-layers. In the ground state (depicted here) all acceptors are negatively charged, A^-, whereas the nearest donors are positive, D^+. In the fully excited state all the impurities are neutral.

Now the probability of finding the nearest donor within a

distance r (see Fig. 2) becomes strongly peaked near d_i. For the probability of finding the next donor within a distance interval (ϱ, $\varrho+d\varrho$) within the two-dimensional doping layer away from the nearest distance point is now

$$p(\varrho)d\varrho = 2(\varrho/\varrho_0{}^2)\exp-(\varrho/\varrho_0)^2 d\varrho \qquad (11)$$

with

$$\varrho_0 = (2\pi n_D{}^{(2)})^{-1/2} \qquad (12)$$

(the factor 2 in Eq. (12) results from the fact that each acceptor is facing two neighbouring donor layers). Quite analogous to our previous three-dimensional considerations we now define quantities $r_- = d_i$ and $r_+ = [d_i{}^2+(\varrho_{\frac{1}{3}})^2]^{\frac{1}{2}}$ such, that two thirds of all the nearest donors are found within this interval. Thus, we obtain $\varrho_{\frac{1}{3}} = 1.05\varrho_0$. For the luminescence linewidth we find therefore

$$\Delta\hbar\omega^{(2)} = e^2/\kappa_0 - e^2/\kappa_0[d_i{}^2 + (\varrho_{\frac{1}{3}})^2]^{1/2} \qquad (13)$$

For the n-i-p-i version of our previous example we find therefore

$$\Delta\hbar\omega^{(2)} = 2.34 - 2.26\text{meV} = 0.08\text{meV} \qquad (14)$$

Comparing the values from Eqs. (14) and (8), we observe a dramatic reduction in impurity pair luminescence linewidths. We believe that this strong narrowing of the linewidth, indeed, should be observable. The only energy in a luminescence experiment which could interfere with the donor acceptor pair luminescence could be due to excitons bound to neutral acceptors. This contribution to the luminescence would have a much faster decay after excitation compared with the donor acceptor pair luminescence, which is given by Eq.(4) with $r_{DA} = d_i$.

So far, we have neglected the Coulomb broadening of these lines due to other non-neutral donor-acceptor pairs. This broadening will be negligible if the donor acceptor transitions are saturated or almost saturated. Because of the uniform distribution of transition probabilities, which, at the same time are relatively small (for our present example they can be estimated to be of the order of 10^4 s^{-1}) saturation can be achieved with moderate excitation intensities quite easily.

Apart from the narrowing of the luminescence spectra, which is interesting by itself, this new system offers the exciting possibility to study the formation (of 2-dimensional) impurity bands. If we study a set of samples in which only the donor concentration in the n-layers differs, we expect a broadening of the luminescence spectra when the donor energy level distribution broadens due to the formation of an impurity band. The observed shape of the luminescence spectrum should reflect directly the density of state distribution $N(\varepsilon)$ of the impurity band. Note, that the acceptors are randomly distributed in the p-layers and, therefore, probe the impurity band independently on the special donor distribution within the n-layer.

A more elegant way of doing this study is probably to use one single samle with an impurity concentration higher than required for the impurity band formation. In this case, the impurity band formation can now be studied as a function of a magnetic field B_z applied perpendicular to the doping layers. The formation of the impurity band becomes now a function of the ratio ϱ_0/a_D with the effectice donor Bohr radius a_D now decreasing with increasing magnetic field[20,21].

We have discussed here only the case of donor band formation. Note, that similarly also the formation of an acceptor band can be studied. Instead of the GaAs system, which was discussed here as an example it seems attractive, or even advantageous, to study other systems like GaP, the classical example for donor-acceptor pair luminescence.

3.2. IV-VI n-i-p-i's.

The IV-VI compound semiconductors have a very large dielectric constant and very low (average) effective masses for both, electrons and holes. As a consequence, no bound impurity states exist in these crystals. Therefore, the properties of IV-VI compound n-i-p-i crystals are not unfavorably affected by impurity states. The intriguing properties of this class of n-i-p-i structures has been discussed in detail in Ref. 6.

3.3. Hetero - n-i-p-i - structures

A third possibility to get rid of the impurity states in doping superlattices is based on the hetero n-i-p-i concept.

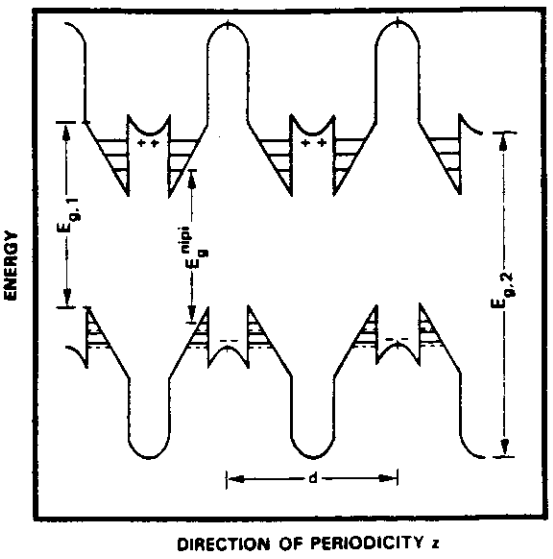

Fig. 3 Real space band diagram of a type-II hetero n-i-p-i. n- and p-doping is confined to the central part of the larger band gap material with band gap $E_{g,2}$. Electrons and holes are spatially separated from each other but also from their parent donors or acceptors, respectively.

A special version, a type-II hetero - n-i-p-i, is shown in Fig. 3. It is obvious that electrons and holes are now spatially separated, not only from each other but also from their parent donors and acceptors, respectively. The advantage is two-fold. First, the influence of potential fluctuations as a broadening mechanism for the subbands is now strongly reduced. Second, holes no longer populate acceptor impurity bands. Instead, they reside in hole subbands whose properties are readily accessible by the theory[22]. Recent photoluminescence and time-resolved luminescence measurements have, in fact, demonstrated much narrower luminescence lines[23]. Also distinct lines due to recombination from excited subbands could clearly be distinguished. In the next section we will discuss some specific properties of hetero - n-i-p-i - structures with very low doping concentrations which have not been considered previously.

4. Study of (2-dimensional) impurity- and Hubbard-bands in hetero - n-i-p-i's

In section 3.1 we discussed a new possibility to observe the density of states of impurity bands, $N(\varepsilon)$, for the special case of a completely or nearly completely filled impurity band. In this section we outline that hetero - n-i-p-i's provide a unique possibility to study impurity bands as a function of their population. This is, of course, a consequence of the tunability of the carrier concentration in n-i-p-i - structures. We will find that the situation in hetero - n-i-p-i's of appropriate design differs from that in the conventional n-i-p-i's by the fact that the tunability of the carrier density is not limited to the range between 0 and the density which just neutralizes all the impurities. We can increase the carrier density even beyond this limit. This implies the possibility to populate the "Hubbard-band"[lit z], formed by double occupancy of the impurity states. The most interesting aspect of this system is perhaps the possiblity to have a unique system for studying the Mott-Hubbard-transition[24] as a function of ϱ_0/a_D or ϱ_0/a_A, similar to the case of the simple impurity band formation in section 3.1. In this respect, our present system differs from any other system we are aware of. We do not see any possibility to design a similar bulk system in which the conductivity and the density of states could be investigated in the range of population higher than one carrier per impurity (we exclude the case of impurities which exist in a singly and doubly ionized state and which are separated by a large energy difference. The Mott-Hubbard transition can probably never be studied in such systems).

4.1. Hetero - n-i-p-i for the study of (2-dimensional) conduction in impurity and Hubbard-bands

Fig. 4 shows the band diagram for the conduction and valence bands of a hetero - n-i-p-i in the ground state (b), the excited state with neutral impurities (c), and with the Hubbard-band populated (d). The doping profile is indicated in part (a). The doping concentration in the p-layers is

assumed to be large enough to prevent carrier freeze-out at low temperatures. The width of the layer with the n-type δ-doping at its center is choosen such, that the quantized energy levels are well separated. The binding energy E_D^1 of the donors is enhanced compared to the pure bulk material by a factor between one and two, depending on the well width.

In the neutral donor state (c) the difference between the electron and hole quasi Fermi levels, Φ_n and Φ_p, at zero temperature is just

$$\Phi_{np}^0 \sim E_g^1 + E_{c,0} - E_D^1 - E_A. \qquad (15)$$

This state can be reached by applying an external potential

$$eU_{np}^0 = \Phi_{np}^0 \qquad (16)$$

between selective n- and p-type contacts to the hetero n-i-p-i[4,26,27]. We can avoid significant leakage currents between the n- and p-layer if we choose sufficiently large values of the superlattice period d and the barrier heights ΔE_c and ΔE_v, respectively. If U_{np} differs from the value determined by Eqs. (15) and (16), the sheet electron density in the layer varies according to

$$n^{(2)} = n^{(2)}_D + (U_{np} - U^0_{np})\,\kappa_0/\pi ed. \qquad (17)$$

For $n_D^{(2)} = 10^{11}$ cm^{-2} and d = 100nm, e.g., $n^{(2)}$ vanishes in AlGaAs/GaAs hetero n-i-p-i for

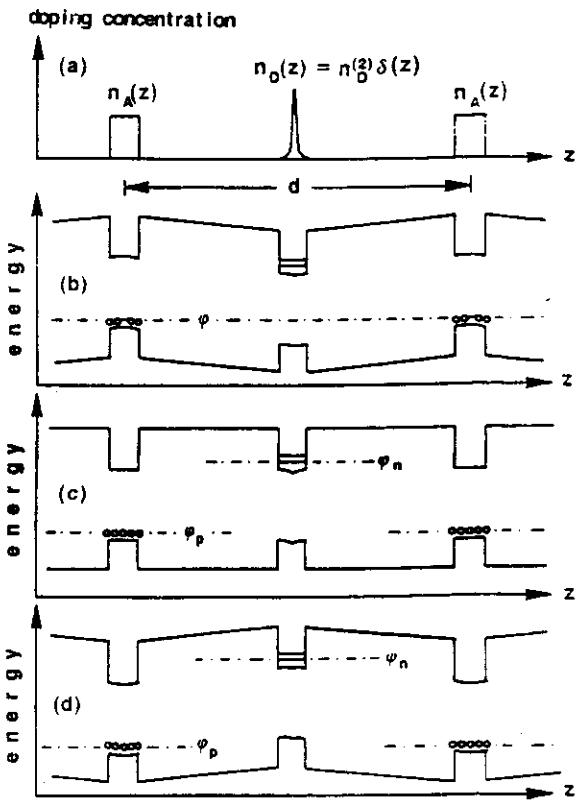

Fig. 4 Hetero n-i-p-i for the observation of (2-dimensional) impurity conduction in the neutral-impurity - and in the impurity - Hubbard-band as a function of sheet electron concentration $n^{(2)}$ in the interval $0 \lesssim n^{(2)} \lesssim 2n_D^{(2)}$. Part (a): doping profile. Parts (b) - (d): Schematic band profiles for different sheet electron concentration. (b): Ground state ($n^{(2)} = 0$); (c): Neutral-donor state ($n^{(2)} = n_D^{(2)}$): (d): Hubbard band completely filled ($n^{(2)} = 2n_D^{(2)}$). $n^{(2)}$ can be tuned by a bias U_{np} applied between selective n- and p-type contacts which inject cariers until $\Phi_n - \Phi_p = eU_{np}$ is satisfied. The conductivity in the n-layers will be measured by a small bias between two n-type contacts.

$$U_{np} - U^0_{np} < -35mV$$

At $U_{np} - U^0_{np} > 0$, on the other hand, D^- centers will be formed in the n-layers by the excess electrons, provided that $n_D^{(2)}$ is less than the critical density $n^{(2)}_{D,MH}$ for the Mott-Hubbard transition. These D^- centers form the Hubbard impurity band. The center of this band is shifted to higher energies, compared to the center of the D^0 impurity band by the repulsive correlation energy U_H.

For our example we find, that at a voltage

$$U_{np} = U^0_{np} + 35mev \qquad (19)$$

the number of electrons in the GaAs layers has increased up to $n^\infty = 2n_D^\infty$, which corresponds to a completely filled Hubbard band. This means, that we can shift the position of the electron quasi Fermi level from the lower edge of the D^0 impurity band up to the upper edge of the D^- Hubbard band by varying the voltage U_{np} between selective n- and p-contacts by a rather small amount (~ 70mV in our example). Over the whole range the leakage currents through the $Al_xGa_{1-x}As$ barriers are expected to be very low at very low temperatures.

In order to study the conduction processes in the D^0 and the D^- bands one has only to measure the current I_{nn} due to a small bias U_{nn} applied between two selective n-type contacts with the voltage U_{np} as a parameter[26,27]. A schematic picture of the density of states and the position of the electron quasi Fermi level Φ_n as a function of sheet electron density n^∞ is shown in Fig. 5.

At low temperatures we expect to observe the Mott-Anderson metal-insulator transition at low n^∞ provided that n_D^∞ is not too low. The most interesting tuning range, however, is $n^\infty \sim n_D^\infty$, i.e., from slightly below to slightly above this value. Depending on the doping level n_D^∞ and/or the strength of a magnetic field B_z perpendicular to the layers, the Mott-Hubbard metal-insulator transition due to the breakdown of the Hubbard gap at sufficiently strong interaction between neighbouring donor states, can be studied by conductivity measurements as a function of the position of Φ_n.

4.2 Hetero n-i-p-i for the optical investigation of the density of states in the impurity- and the Hubbard band

The structure shown schematically in Fig. 6 consists of weakly n-doped quantum wells with built-in electric space charge fields due to the space charge in the comparatively high doped n- and p-layers (see part (a) of Fig. 6 for the doping profile). In the ground state there are no carriers in the tilted quantum wells. Excitation with photons with an energy above the effective band gap, E_g^{eff} creates electron-hole pairs within the tilted quantum wells.

$$\hbar\omega > E_g^{eff,0} = E_g^1 + E_{c,0} - E_D^1 - eFd^1 + E_{vh,0} \qquad (20)$$

During the relaxation process the electron-hole pairs become spatially separated. The electrons fill up the donor impurity bands, first the D^0- impurity and subsequently the D^--Hubbard band until a steady state between generation and recombination processes is reached. The recombination processes of interest are the luminescent tunneling recombinations between the electrons in the donor bands and the holes in the uppermost heavy-hole subband. The shape of the luminescence lines reflects the density-of-states distribution $N(\varepsilon)$ of the D^0 and D^- donor bands, according to

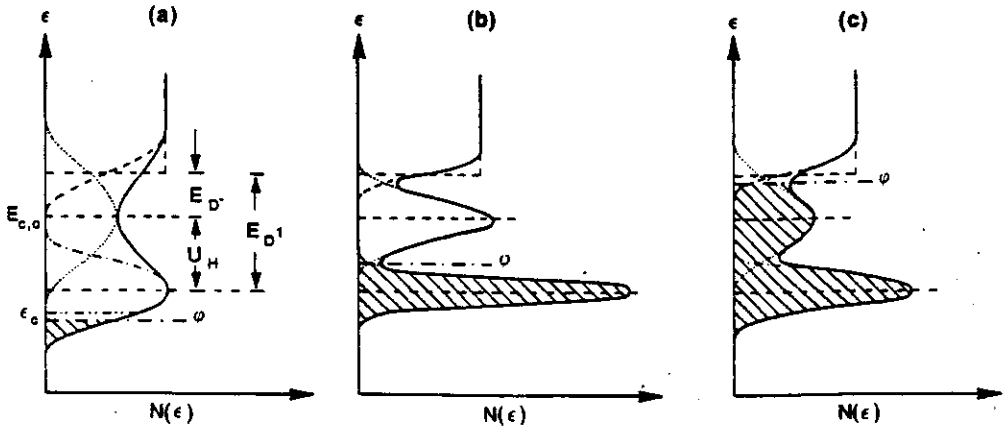

Fig. 5 Schematic diagram of the density of states of the lowest 2-dimensional subband with impurity bands due to neutral, singly occupied, and doubly occupied centers. Although the centers may be acceptors as well, the situation is shown for donors. Also, excited levels of the neutral and the doubly occupied donors are omitted. Part (a): Low sheet electron density ($n^{(2)} << n_D^{(2)}$). Only a small fraction of the donors is neutralized by electrons. Therefore, the conduction subband (dashed line), the neutral-donor impurity band (dash-dotted line), centered at about E_D^1 (the renormalized donor binding energy in the potential well) below the conduction subband, and the Hubbard band (dotted line), centered at the D^--energy, i.e. at the Hubbard correlation energy U_H above the D^1 level, they all are broadened due to the random potential of the ionized D^+- centers. The full line depicts the total density of states curve $N(\varepsilon)$. The Fermi level, Φ, is assumed to lie below the mobility edge, ε_c (which, in 2-dimensional systems, separates weakly localized states from strongly localized ones). The position of E_c depends on the product of effective Bohr radius, a_D, and sheet doping concentration, $n_D^{(2)}$. Part (b): Same, however, for $n^{(2)} = n_D^{(2)}$. Almost all donors are neutral. The bands are no longer broadened by the random Coulomb potential of D^+-centers. At high values of $a_D n_D^{(2)}$ the Mott-Hubbard insulator metal transition is expected to occur due to a collapse of the Hubbard gap[24]. Part (c): Same, however, for $n^{(2)} = 2n_D^{(2)}$. There is, again, Coulomb broadening present, due to the charged D^- centers. At intermediate sheet electron concentrations, $n^{(2)}$, upon tuning the Fermi level moves back and forth between regions of strong and weak localization, and, therefore, between regions of zero and finite conductivity at zero temperature[28,31].

their population, if the dispersion of holes populating the upper heavy-hole subband can be neglected. This requires a low hole concentration in the tilted quantum well even for the case that the D^0 and the D^- donor bands are filled with $2n_D^\infty$ electrons. To meet this goal the height of the barriers between the tilted quantum wells and the neighbouring n- and p-type quantum wells has to be chosen appropriately.

The probabilities for escaping from the tilted quantum wells by tunneling are proportional to exp $\{-4/3[m(\Delta E-E_0)^{3/2}/\hbar eF$, where the appropriate values for the effective mass, m, band edge of-set, ΔE and lowest bound state energy, E_0, have to be chosen for electrons and heavy holes, respectively. With the values for the system $Al_xGa_{1-x}As/GaAs$, $\Delta E_c/\Delta E_v = 65/35$, $m_c/m_{hh} = 0.168$ and $E_0 \alpha [(eF)^2/m]^{\frac{1}{3}}$ they turn out to be nearly identical for electrons and heavy holes, if the Al-content is the same in both types of barriers. It should be noted that the dependence on the ratio $\Delta E_c/\Delta E_v$ is very sensitive. It might even be useful for an accurate determination of Hetero junction band off-sets.

The design of the structure as shown in Fig. 6 allows for an external recombination of electrons and holes which have escaped from the tilted quantum wells via external selective contacts to the n- and p-type doped quantum wells. Moreover, the built-in electric field, F, can be modified by applying a

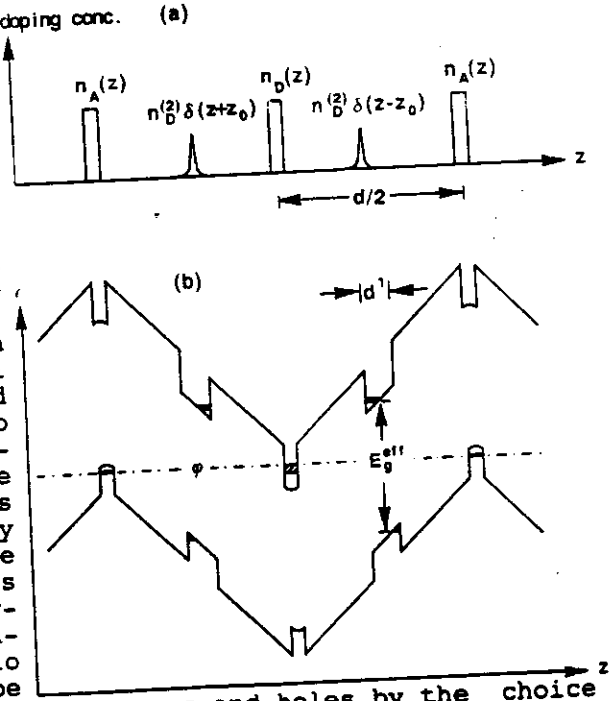

Fig. 6 Hetero n-i-p-i for the optical investigation of impurity and Hubbard bands in 2-diminsional systems. Part (a): Doping profile. $n_A(z)$ and $n_D(z)$ cause the built-in electric fields, F. The doping $n_D^{(2)}$ causes the impurity band which is subject to the optical investigations. Part (b): Band profile in the ground state (all donors in the tilted quantum well ionized, no holes in the valence subbands). The escape probability for electrons and holes generated by optical absorption in the tilted quantum wells determines the steady-state electron/hole concentration ratio $n^{(2)}/p^{(2)}$. It can be tailored independently for electrons and holes by the choice of the band gap in the neighbouring barrier regions. The escape probability can be made small by chosing large values of the superstructure period d. Moreover, it can be influenced strongly by variation of a bias U_{np} applied between selective n- and p- type contacts to the strongly doped n- and p-type quantum wells.

bias between these contacts. This allows to optimize the radiative lifetime within the tilted quantum wells by varying the overlap between the donor impurity band and the heavy hole subband envelope wave functions. Optimization means long enough to avoid broadening of the luminescence spectra by "hot" carriers, recombining before complete relaxation into the donor impurity bands. It also means short enough to observe strong enough luminescence intensity.

The design of the structure shown in Fig. 6 is also chosen such, that the luminescence spectra are not broadened by any close-by ionized impurities. With a thickness of the barriers of the order of 100nm the influence of the donors and acceptors in the n- and p-type quantum wells are negligible. This is true, in particular, as we assume strong enough doping levels in the n- and p-type quantum wells to guarantee screening by free carriers (moderate to high doping levels are required also in order to prevent carrier freeze out for a controlled application of external bias). Finally, we note that the luminescence can be restricted to the tilted quantum wells, if the excitation photon energy is chosen low enough and the width of the n- and p-doped quantum wells is small enough, such that their effective band gap becomes too large for absorption processes in these layers.

Similar to the case of the low doped ideal n-i-p-i structures discussed in section 3.1, the luminescence spectrum is expected to image the density of states distribution of the occupied states of the donor impurity band. Only, in the present case also the Hubbard- or D^--band is included. Thus, these luminescence experiments complete the information obtained from conductivity measurements as discussed in the previous section. In particular, it is expected, that the collapse of the Hubbard gap should be observable if, at a suitable donor density $n_D^{(2)}$ the Hubbard-Mott transition occurs due to a decreasing magnetic field perpendicular to the layers (or in a set of samples of varying $n_D^{(2)}$).

5. Conclusions

We have discussed problems which result from the random distribution of dopant atoms in n-i-p-i doping superlattices as well as those due to the unknown wavefunctions of the acceptor band states which are difficult to treat quantitatively. We have discussed possibilities to avoid those difficulties in weakly doped n-i-p-i's with 2-dimensional doping layers, IV-VI compound- and hetero n-i-p-i's. The first case is found to be an interesting special case of donor acceptor pair luminescence, which should provide valuable information about the impurity band formation (in two dimensions) as a function of impurity concentration. Finally we have proposed new hetero n-i-p-i structures which appear uniquely suited for the observation of both, the Mott-Anderson and the Mott-Hubbard transition. This can be done by investigating the conductivity and optical transitions as a function of the variable carrier density and of the product of 2-dimensional dopant concentration and effective Bohr radius (which can be tuned by a magnetic field perpendicular to the layers).

References

1. G.H. Döhler, Phys. Stat. Sol. 52, 79 (1972)

2. G.H. Döhler, Phys. Stat. Sol. (b) 52, 533 (1972)

3. For a review of the early work see, for instance: G.H. Döhler and K. Ploog, in: Synthetic Modulated Structure Materials, L.L. Chang and B.C. Giessen, Eds. (Academic Press, N.Y. 1985), 163, or, K. Ploog and G.H. Döhler, Advances in Physics 32, 285 (1983), or, G.H. Döhler, in: The Technology and Physics of Molecular Beam Epitaxy, E.H.C. Parker, Ed. (Plenum, N.Y., 1985) 233

4. For a review of the recent work see. for instance: G.H. Döhler, IEEE QE-22, 1682 (1986), or, G.H. Döhler, CRC Review in Solid State and Materials Sciences 13, 97 (1986)

5. P.P. Ruden and G.H. Döhler, Phys. Rev. B27, 3538 (1983)

6. G.H. Döhler and P.P. Ruden, Surface Science 142, 474 (1984)

7. P.P. Ruden and G.H. Döhler, Solid State Commun. 45, 23 (1983)

8. P.P. Ruden and G.H. Döhler, Phys. Rev. B27, 3547 (1983)

9. P.P. Ruden and G.H. Döhler, Proceedings of the 17th Intern. Conf. on the Physics of Semiconductors, J.D. Chadi and W.H. Harrison, Eds. (Springer, N.Y., 1985) 535

10. G.H. Döhler, Superlattices and Microstructures 1, 279 (1985)

11. G.H. Döhler, J. of Non-Crystalline Solids 77 & 78, 1041 (1985)

12. G.H. Döhler, R.A. Street, and P.P. Ruden, Surface Science 174, 240 (1986)

13. G.H. Döhler, NSF Workshop on Optical Nonlinearities, Fast Phenomena and Signal Processing, N. Peyghambarian, Ed. (Tucson, AZ, 1986) 292

14. F. Crowne, T.L. Reinecke, and B.V. Shanabrook, Proceedings of 17th Intern. C onf. on the Physics of Semiconductors, J.D. Chadi and W.H. Harrison, Eds. (Springer, N.Y., 1985) 363

15. G.H. Döhler, unpublished

16. W. Rehm, P. Ruden, G.H. Döhler, and K. Ploog, Phys. Rev. B 28, 5937 (1983)

17. Ref. für Akzeptor Welenflut (Bassani ?, P.R.'s Thesis), 18.Hopfield (DA Pair)

19. U. Heim, O. Röder, H.J. Queisser, and M. Pilkuhn, J. of Luminescence 1,2, 542 (1970)

20. A. Raymond, this workshop

21. J.L. Robert, A. Raymond. L. Konczewicz, C. Bousquet, W. Zawadzki, F. Alexandre, I.M. Masson, J.P. Andre, and P.M. Frijlink, Phys. Rev. B33, 5935 (1986)

22. The mixing of light- and heavy-hole subbands has been treated, for instance, by U. Ekenberg and M. Altarelli, Phys. Rev. B30, 3569 (1984); E. Bangert and G. Landwehr, Superlattices Microstruct. 1, 363 (1985); D.A. Broido and L.J. Sham, Phys. Rev. B31, 888 (1985); and Y.C. Chang and J.N. Schulman, Phys. Rev. B31, 2069 (1985)

23. R.A. Street, G.H. Döhler, J.N. Miller, and P.P. Ruden, Phys. Rev. B33, 7043 (1986)

24. N.F. Mott and E.A. Davis, Electronic Process in Non-Crystalline Materials, 2nd ed. (Oxford, 1979)

25. G.P. Srivastava, this workshop

26. G.D. Döhler, G. Hasnain, and J.N. Miller, Appl. Phys. Lett. 49, 704 (1986)

27. C.J. Chang-Hasnain, G. Hasnain, N.M. Johnson, G.H. Döhler, J.N. Miller, J.R. Whinnery, and A. Dienes, Appl. Phys. Letter 50, 915 (1987)

28. E. Abrahams, P.W. Anderson, D.C. Licciardello, and T.V. Ramakrishnan, Phys. Rev. Lett. 42, 673 (1979)

29. P.W. Anderson, Phys. Rev. 109, 1492 (1958)

30. See for instance: "Anderson Localization, Y. Nagaoka, Ed. (Springer, New York, 1982)

31. R.A. Davies, C.C. Dean, and M. Pepper, Surface Science 142, 25 (1984)